

Clinical validation of a wearable ultrasound sensor of blood pressure

Received: 6 January 2024

Accepted: 4 October 2024

Published online: 20 November 2024

 Check for updates

Sai Zhou ^{1,12}, Geonho Park ^{2,12}, Katherine Longardner ^{3,12}, Muyang Lin ^{2,12}, Baiyan Qi¹, Xinyi Yang¹, Xiaoxiang Gao², Hao Huang², Xiangjun Chen ¹, Yizhou Bian², Hongjie Hu ², Ray S. Wu ², Wentong Yue², Mohan Li⁴, Chengchangfeng Lu ⁴, Ruotao Wang², Siyu Qin ⁴, Esra Tasali⁵, Theodore Karrison⁶, Isac Thomas⁷, Benjamin Smarr^{8,9}, Erik B. Kistler^{8,10}, Belal Al Khiami⁷, Irene Litvan³ & Sheng Xu ^{1,2,4,8,11} ✉

Options for the continuous and non-invasive monitoring of blood pressure are limited. Cuff-based sphygmomanometers are widely available, yet provide only discrete measurements. The clinical gold-standard approach for the continuous monitoring of blood pressure requires an arterial line, which is too invasive for routine use. Wearable ultrasound for the continuous and non-invasive monitoring of blood pressure promises to elevate the quality of patient care, yet the isolated sonographic windows in the most advanced prototypes can lead to inaccurate or error-prone measurements, and the safety and performance of these devices have not been thoroughly evaluated. Here we describe validation studies, conducted during daily activities at home, in the outpatient clinic, in the cardiac catheterization laboratory and in the intensive care unit, of the safety and performance of a wearable ultrasound sensor for blood pressure monitoring. The sensor has closely connected sonographic windows and a backing layer that improves the sensor's accuracy and reliability to meet the highest requirements of clinical standards. The validation results support the clinical use of the sensor.

Blood pressure (BP) is a measure of the force that blood exerts against the vessel walls per unit area¹. Its changing characteristics reflect the status of the cardiovascular system in real time, making continuous BP monitoring essential for the optimal diagnosis and treatment of many cardiovascular conditions^{2,3}. Common methods for BP monitoring in the clinic provide accurate measurements but involve specific challenges (Supplementary Discussion 1). A cuff-based sphygmomanometer, typically comprising a stethoscope and an inflatable cuff

wrapped around the upper arm, is effective in measuring systolic blood pressure (SBP) and diastolic blood pressure (DBP). However, the time required for cuff inflation and deflation makes it unsuitable for continuous BP monitoring. Moreover, repetitive occlusion of the measured artery by the cuff causes irritation and interferes with daily activities, especially disturbing sleep when worn overnight⁴. The 'gold standard' for measuring BP, an arterial line (A-line), involves a catheter inserted into the artery to continuously monitor BP⁵. However, this

¹Materials Science and Engineering Program, University of California San Diego, La Jolla, CA, USA. ²Aiiso Yufeng Li Family Department of Chemical and Nano Engineering, University of California San Diego, La Jolla, CA, USA. ³Department of Neurosciences, University of California San Diego, La Jolla, CA, USA. ⁴Department of Electrical and Computer Engineering, University of California San Diego, La Jolla, CA, USA. ⁵Department of Medicine, The University of Chicago, Chicago, IL, USA. ⁶Department of Public Health Sciences, The University of Chicago, Chicago, IL, USA. ⁷Division of Cardiovascular Medicine, University of California San Diego, La Jolla, CA, USA. ⁸Shu Chien-Gene Lay Department of Bioengineering, University of California San Diego, La Jolla, CA, USA. ⁹Halicioğlu Institute for Data Science, University of California San Diego, La Jolla, CA, USA. ¹⁰Department of Anesthesiology and Critical Care, University of California San Diego, La Jolla, CA, USA. ¹¹Department of Radiology, University of California San Diego, La Jolla, CA, USA. ¹²These authors contributed equally: Sai Zhou, Geonho Park, Katherine Longardner, Muyang Lin. ✉e-mail: shengxu@ucsd.edu

invasive technique can be associated with pain upon insertion and serious complications (such as vascular occlusion, haematoma and infection)⁶, and thus is usually reserved for critical care settings.

Alternative approaches involve the derivation of BP from other haemodynamic parameters. Given their ability to estimate BP without disturbing the regular vascular system, marrying these approaches with wearable technology has the potential to enhance the patient's experience. For example, a wearable photoplethysmography device detects local changes in blood volume by measuring the light absorbed and scattered by red blood cells, which is correlated with BP⁷. Nonetheless, light can only penetrate <8 mm into tissue, which limits BP sensing to capillaries⁸. As blood propagates through the arterial tree, both the BP amplitude and waveform will change due to the different blood flow volumes and wall components of the vessels. Therefore, the parameters captured from capillaries by photoplethysmography are intrinsically different from those at clinical reference sites (such as brachial or radial arteries). Wearable mechanical sensors capture skin deflection above the peripheral arteries to estimate the BP^{9,10}, but those deflections are highly susceptible to internal factors (such as skin elasticity and subcutaneous fat) and external factors (such as temperature and humidity) that severely limit the accuracy and repeatability of the measurements. Wearable ultrasound sensors can sense clinically relevant arteries deep within the body due to the relative low attenuation of ultrasound waves through tissue⁸. Furthermore, ultrasound sensors, particularly high-frequency devices with high spatial resolution, focus directly on arterial pulsation rather than skin deformations. Therefore, their measurements are not affected by variations in skin characteristics, enhancing the accuracy and reliability of the readings¹¹.

Despite the advantages described above, several major challenges still affect the performance of today's most advanced wearable ultrasound sensors^{11–14}. This device was designed as a 4×5 isolated transducer array, with a $0.9 \times 0.9 \text{ mm}^2$ transducer element size and $\sim 3 \text{ mm}$ array pitch (that is, the distance between the centres of adjacent transducers) (Supplementary Fig. 1)¹¹. First, because it was designed for large central arteries, its large transducer element size and array pitch inevitably isolate the acoustic window of each element, making it difficult to align with smaller peripheral targets such as the brachial and radial arteries, which are more clinically relevant (Supplementary Fig. 2). Second, a backing layer (that is, a dampener to reduce redundant vibrations from the transducer) is needed to shorten the spatial pulse length of the received radio-frequency signals. The absence of this layer means that the prototype cannot accurately trace subtle dilations of arterial walls, particularly for stiff peripheral arteries with much less dilation than elastic central arteries. Third, the safety of the prototype has not been thoroughly assessed. Finally, its accuracy had not been rigorously validated to follow established standards¹⁵ (Supplementary Fig. 3 and Supplementary Discussion 2). A candidate device needs to have minimal biases (such as mean difference and standard deviation of the difference) when validated under strict conditions for the collection and statistical analysis of the data (Supplementary Fig. 4). Practical factors (such as white coat syndrome, daily activities and medications) can influence BP substantially, emphasizing the importance of comprehensive validation in diverse domestic and clinical settings¹⁶. Such considerations are often neglected during the development of wearable BP monitoring devices^{17–22}.

To address these challenges, we redesigned the transducer array and incorporated a backing layer to the transducers in a re-engineered wearable ultrasound sensor (Supplementary Fig. 1). We also validated its safety and accuracy by adhering closely to established BP validation standards. This new compact linear transducer array provides a closely connected $\sim 10 \text{ mm}$ wide acoustic window (the transducers are closely arranged with a minimal pitch), which minimizes device–artery misalignment, enhancing the reliability of measurements (Supplementary Fig. 5). Integrating a backing layer on each transducer substantially increases the accuracy of locating arterial walls. Using a hydrophone,

we comprehensively assessed the intensity of the wearable ultrasound sensor. Finally, we evaluated its accuracy following international standards in relevant use-case scenarios. The sensor showed good agreement with clinical reference methods, with biases well within the accepted thresholds. This validation study underscores the potential of this state-of-the-art wearable ultrasound technology for accurate, continuous and non-invasive BP monitoring, and establishes an effective framework for the evaluation of future wearable BP monitors, thereby benefiting the healthcare system at large.

Results

Re-engineering of the wearable ultrasound sensor

We adapted the wearable ultrasound sensor to target the brachial and radial arteries to comply with common BP measurement practices (Fig. 1a). Given the small size (2–5 mm in diameter) and shallow depth (3–20 mm) of these arteries^{23,24}, we used a linear transducer array with a central frequency of 7 MHz (Supplementary Fig. 6). This frequency provides a penetration depth of $\sim 25 \text{ mm}$ (Supplementary Fig. 7) that covers the brachial and radial arteries in almost all populations^{23,24}. The closely arranged 20-element array with a pitch of 0.5 mm yields a 10 mm wide combined acoustic window, providing full coverage of the target arteries and ample tolerance of device–artery misalignment (Supplementary Fig. 5). To enhance the accuracy of arterial wall tracking, a $500\text{-}\mu\text{m}$ -thick backing layer was used to reduce the transducer ringing effect (that is, redundant transducer vibrations after activation)²⁵, thus shortening the spatial pulse length and improving the tracking accuracy (Supplementary Fig. 8).

The re-engineered ultrasound sensor shows outstanding wearability. Serpentine copper patterns were used as both the top excitation and bottom ground electrodes to interconnect the bilayer stacking of the transducer element and backing layer^{26–28}. The re-engineered ultrasound sensor is only $\sim 800 \mu\text{m}$ in total thickness (including the elastomer encapsulation), enabling its conformal integration with curvilinear surfaces of phantoms (Supplementary Fig. 9) and various human skin morphologies (Fig. 1b). The device also shows excellent durability during various daily activities (Extended Data Fig. 1) and remains functional for re-use after sterilization, which supports its long-term monitoring capabilities.

Safety studies

All medical devices must comply with safety regulations (Supplementary Discussion 3). We activated the ultrasound transducers with a voltage $< 20 \text{ V}$ at a pulse repetition frequency of 1,000 Hz, ensuring that the maximum derated spatial peak temporal average intensity of all ultrasound transmissions was $< 5.76 \text{ mW cm}^{-2}$ and the maximum mechanical index was < 0.29 . These values are substantially lower than the maximum levels recommended by the Food and Drug Administration (FDA) Track 1 for diagnostic ultrasound applications (720 mW cm^{-2} and 1.9, respectively)²⁹.

We also conducted a thorough examination of thermal effects. Thermal imaging revealed a $< 1^\circ\text{C}$ increase in temperature when the device was attached to a human chest phantom for $> 48 \text{ h}$ (Supplementary Fig. 10 and Supplementary Discussion 3). In addition, we evaluated the impact of prolonged ultrasound exposure on the internal tissue temperature by calculating the thermal index, which is the ratio between the incident acoustic power and the power needed to increase the tissue temperature by 1°C (Supplementary Discussion 3)³⁰. The soft tissue thermal index was 0.17. The American Institute of Ultrasound in Medicine guidelines state that, for a thermal index ≤ 1.5 , there is no specified time limit for adult ultrasound because the thermal exposure will not generate any negative biological effects³¹.

Calibration

The ultrasound sensor monitors the vessel diameter and converts it into BP (Supplementary Discussion 4)¹¹. Considering the exponential

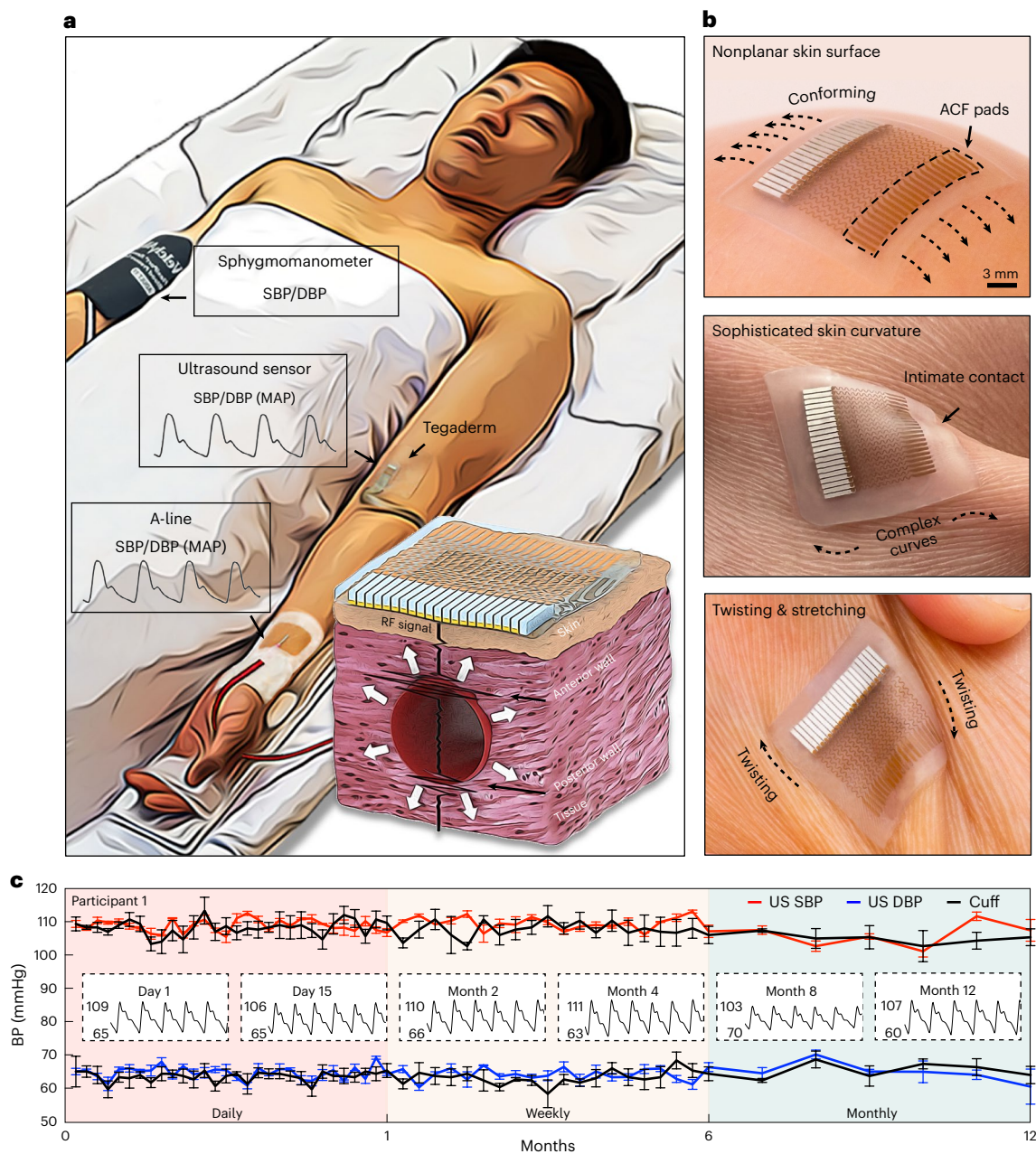


Fig. 1 | Wearable ultrasound sensor for BP measurement. **a**, Schematics of the testing setup and the working principle of the device. The ultrasound sensor attached to skin using Tegaderm is validated against an A-line on the ipsilateral arm, or a sphygmomanometer on the contralateral arm. The ultrasound beam penetrates deeply inside the human body to insonate the target artery. The anterior and posterior walls of the artery exhibit two peaks in the radiofrequency (RF) signals. The arterial wall pulsations are traced by the movements of the peaks to generate the arterial diameter waveforms. These waveforms are converted and calibrated as the BP waveforms. **b**, Optical images of the ultrasound sensor on

different skin surfaces, demonstrating its excellent mechanical compliance and robustness. An anisotropic conductive film (ACF) is used to connect the ultrasound sensor to the back-end control system. **c**, Ultrasound (US) sensor measurements of systolic blood pressure (SBP, red line) and diastolic blood pressure (DBP, blue line) with respective sphygmomanometer measurements (black lines) for 1 year in participant 1 (see Supplementary Fig. 13 for the other three participants). The measurements were repeated three times for each time point. Error bars indicate 1 s.d. of the measurements. The insets show representative BP waveforms of the ultrasound sensor on days 1 and 15, and months 2, 4, 8 and 12.

stress–strain relationship for biomaterials such as arterial walls (Supplementary Fig. 11 and Supplementary Discussion 5)³², the changes in arterial diameter can be correlated with the BP waveform using an arterial stiffness coefficient (Supplementary Fig. 12 and Supplementary Discussion 4)³¹. Deviation from the initial calibration, caused by physiological fluctuations such as changes in stiffness and the cross-sectional shape of the artery (Supplementary Discussion 6), can influence the stiffness coefficient, potentially compromising the accuracy of measurement. Frequent recalibrations may thus be necessary, which can

severely compromise the user experience³³. Therefore, the need to recalibrate the ultrasound sensor should be minimized while maintaining accurate measurements.

To evaluate the long-term viability of the calibration, BP measurements from the ultrasound sensor were tracked alongside a cuff-based auscultatory sphygmomanometer for 1 year in four participants (Methods, Extended Data Fig. 2 and Supplementary Table 1). On day 1, the ultrasound sensor was calibrated on the basis of average SBP and DBP values from three sphygmomanometer measurements. Daily BP

measurements were then taken three times repetitively using both the ultrasound sensor and sphygmomanometer during the first month (3×30 paired observations per participant, including the calibration data on day 1). This was followed by weekly measurements during the second to sixth months (3×20 paired observations per participant), and monthly measurements from the seventh to twelfth months (3×6 paired observations per participant) (Fig. 1c and Supplementary Fig. 13).

The aggregated data (all 3×55 paired readings from each of the four participants, excluding the first data point for calibration) were analysed using Bland–Altman plots to evaluate the agreement between the two devices (Supplementary Discussion 7). The mean differences and standard deviations between the ultrasound sensor and sphygmomanometer were 1.19 ± 3.10 mmHg in SBP and 0.91 ± 2.52 mmHg in DBP for participant 1, 1.85 ± 3.48 mmHg in SBP and 0.51 ± 3.02 mmHg in DBP for participant 2, -2.06 ± 4.16 mmHg in SBP and 1.56 ± 3.58 mmHg in DBP for participant 3, and 0.69 ± 3.56 mmHg in SBP and 0.60 ± 3.93 mmHg in DBP for participant 4 (Supplementary Fig. 14). The waveforms of the BP pulses for each participant showed similar contours throughout the measurement period (Fig. 1c and Supplementary Fig. 13). These observations suggest that a single calibration with a sphygmomanometer can maintain accurate BP measurements by the ultrasound sensor for a duration of at least 1 year.

Validation during various daily activities

BP changes dynamically in response to daily activities at home, so continuous BP monitoring can allow physicians to manage BP fluctuations more effectively³⁴, encourage patients to take an active role in adopting a healthier lifestyle, and provide critical insights relevant to the diagnosis and prognosis of cardiovascular diseases (Supplementary Fig. 15 and Supplementary Discussion 8).

To study the effects of daily activities on BP measurements, we used the ultrasound sensor alongside a cuff-based auscultatory sphygmomanometer to track BP changes from the brachial artery of seven participants. The ultrasound sensor was first calibrated using the sphygmomanometer while the participants were in a seated position (Methods). Then, the ultrasound sensor and sphygmomanometer were used to measure BP changes during various activities (Extended Data Fig. 2 and Supplementary Table 1).

Different postures induce physiological responses due to changes in hydrostatic pressure within the cardiovascular system³⁵. Specifically, compared with sitting, standing causes more blood to be pulled to the lower limbs due to gravity, causing a decrease in venous return and thus BP in the arm (Fig. 2a(i),(ii)). Conversely, in a supine position, the effect of gravity is reduced due to the minimal height difference of the blood across the entire body, which increases BP in the arm (Fig. 2a(iii)). Passive leg raising decreases the venous reservoir volume in the lower limbs, increasing the venous return and thus BP in the measured arm (Fig. 2a(iv))³⁶. Raising the measured arm, similar to standing, results in a larger gravitational venous return from the raised arm to the heart, substantially reducing BP (Fig. 2a(v)).

Pressor tests and cycling cause arterial vasoconstriction and cardiac output increase. Mental arithmetic provides a direct cerebral stimulus that increases sympathetic nervous activity and leads to an increase in BP compared with a relaxed seated position (Fig. 2a(i),(vi))³⁷. A local ice bath stimulates the peripheral vessels as well as pain and temperature receptors, also activating the sympathetic nervous system to increase BP (Fig. 2a(vii))³⁸. Similarly, during isometric handgrip, a sustained muscle contraction elicits a fight or flight response and thus increases BP (Fig. 2a(viii))³⁹. During cycling, to meet the demands of energy output, the growing cardiac output is the dominant factor causing a substantial BP increase (Fig. 2a(ix))⁴⁰.

In contrast, BP usually decreases during relaxation, such as deep breathing and meditation. Slow and controlled breathing augments vagal activity and relaxes peripheral smooth muscles, causing BP to fall (Fig. 2a(x))⁴¹. Similarly, meditation enhances baroreflex sensitivity

to reduce sympathetic and increase parasympathetic nervous system activities, thus reducing BP (Fig. 2a(xi))⁴².

Biochemical alterations can also influence BP. After a meal, carbohydrates are catabolized into monosaccharides, decreasing vasodilator nitric oxide levels and thus increasing BP⁴³. In addition, sodium triggers water retention, thereby increasing the total circulating blood volume and consequently the BP (Fig. 2a(xii))⁴⁴. Caffeine antagonizes the effects of adenosine receptors, increasing neuronal activity and stimulating the release of neural transmitters such as norepinephrine, which induces vasoconstriction, increasing BP (Fig. 2a(xiii))⁴⁵. Participant 3 showed no obvious BP changes (that is, ≤ 5 mmHg) in this context due to their habitual caffeine intake and thus relative caffeine insensitivity.

To evaluate the tracking capability of the wearable ultrasound sensor in comparison to the sphygmomanometer, the 12 daily activities (excluding sitting) described above were analysed on four-quadrant plots (Fig. 2b–d) to assess the concordance between the devices (Supplementary Discussion 9)^{46,47}. For both devices, the daily activities induced changes in both the direction and magnitude of BP relative to sitting. The four-quadrant plot provides a comprehensive representation of the agreement⁴⁶ (that is, the 1st and 3rd quadrants) and discrepancies (that is, the 2nd and 4th quadrants) between the BP measurements of the two devices (Supplementary Discussion 9). To ensure accurate and reliable statistical analysis, we removed measurement error, noise and clinically non-significant changes by applying an exclusion zone of 3 mmHg (Supplementary Discussion 9)⁴⁶. The calculated concordance rates were 95.8%, 98.5% and 93.2% for SBP, MAP (mean arterial pressure) and DBP, respectively. These results demonstrate that the ultrasound sensor and sphygmomanometer achieved similar tracking capabilities for both the direction and magnitude of BP changes during different daily activities.

Validation in the outpatient clinic

BP is routinely measured in the outpatient clinic with a cuff-based sphygmomanometer. In an outpatient setting, there is a need to evaluate the cardiovascular system's capability to maintain homeostasis under various conditions^{48,49}. To this end, interventions such as changing body postures can be implemented (such as supine or sitting or standing). By measuring fluctuations immediately after posture change, physicians can diagnose cardiovascular disorders that may be associated with autonomic disturbances, helping understand the body's haemodynamic responses^{49,50}.

We chose to validate the ultrasound sensor against the cuff-based auscultatory sphygmomanometer using the IEEE Std 1708a-2019 standard (Supplementary Discussion 2)^{51,52}. Its comprehensive, three-tier validation framework comprises initial calibration, a static test, a test with BP change and a test after a certain period of time from calibration. We segmented the validation into three tests: supine, standing and supine 30 min after the first test (Fig. 3a,b, Extended Data Fig. 2 and Supplementary Table 1). For each test, we collected three repeated measurements from both devices simultaneously. A cohort of 85 adult participants was recruited following the criteria stipulated by the IEEE standard, including age, sex, height, weight, arm circumference and BP ranges (Table 1 and Supplementary Fig. 4)^{51,52}.

The results are presented in histograms and scatterplots to display the broad distribution of variations in SBP and DBP under different magnitudes of BP changes across the three tests. Each dot represents a pair of BP measurements from both the sphygmomanometer and ultrasound sensor. The first test, conducted in supine positions after calibration, exhibited relatively small variations in BP (Fig. 3c). The second test showed a large fluctuation in BP following a change from supine to standing (Fig. 3d). A substantial BP drop from supine to standing typically manifests in patients with orthostatic hypotension, which could be due to medications, dehydration or an autonomic nervous system failure (Supplementary Discussion 8)⁵³. In the third test, the participants' BP tended to return to normal after 30 min supine, but the range of variations was notably wider than that in the first test

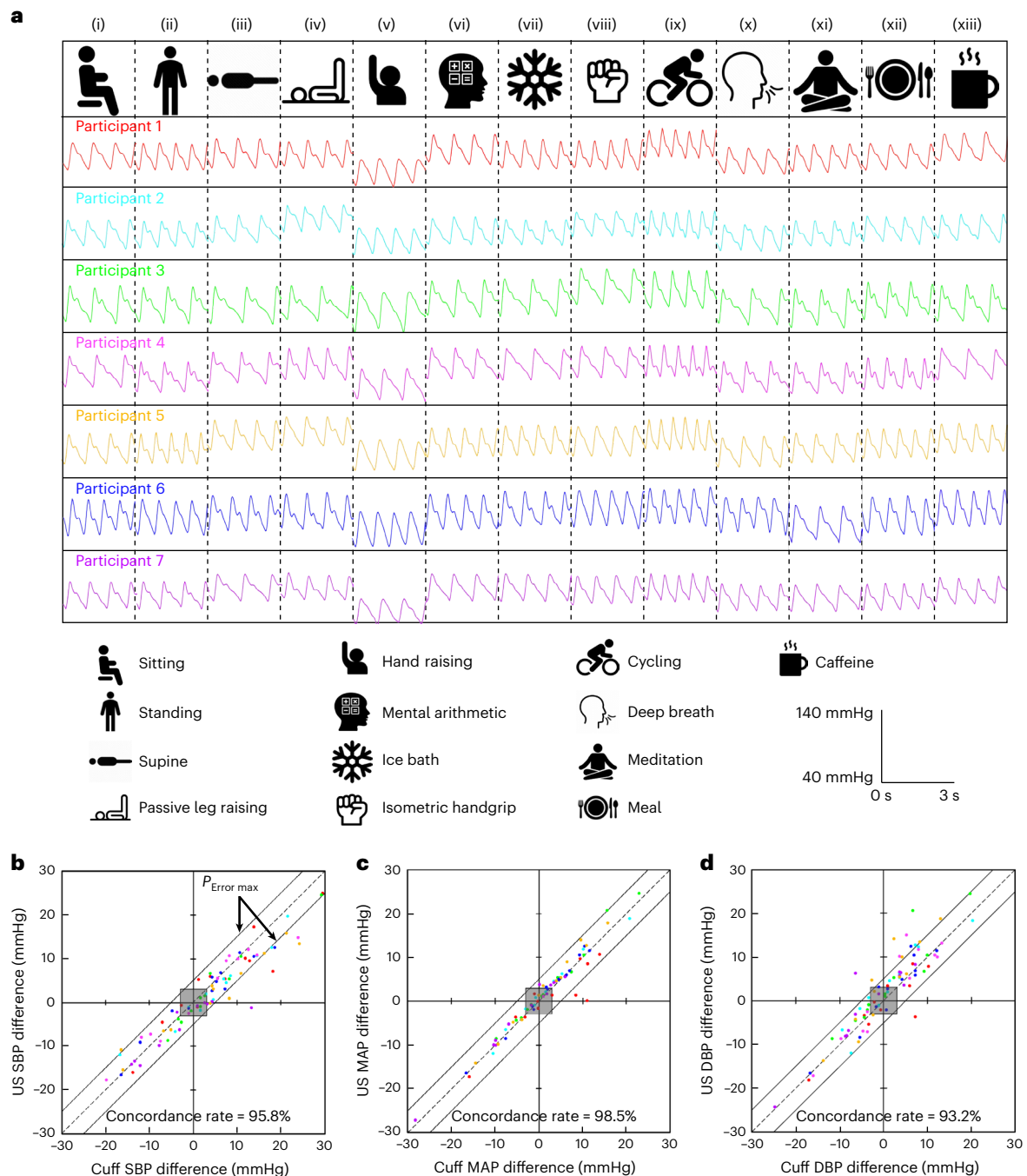


Fig. 2 | Validation across different daily activities. a, BP waveform recording during daily activities of seven participants. The waveforms share the same scale bar (bottom right). **b–d**, Four-quadrant plots and concordance rates comparing the BP measurements acquired from the ultrasound sensor and

sphygmomanometer on SBP (**b**), MAP (**c**) and DBP (**d**), respectively. The diagonal black lines represent an error bar of ± 5 mmHg ($P_{\text{Error max}}$). The grey area represents the exclusion zone of ± 3 mmHg, which was excluded for the calculation of the concordance rate. The colour codes in **b–d** are the same as those in **a**.

(Fig. 3e), suggesting that the cardiovascular systems of some participants may require additional time to recover from relative orthostatic hypotension, or some participants are just more relaxed after lying for 30 min. Bland–Altman plot results agreed broadly with the highest IEEE Std 1708a-2019 standard requirements across the three different tests (Fig. 3f–h). The mean differences and standard deviations in SBP were 1.89 ± 2.33 , 3.88 ± 4.47 and 2.37 ± 2.82 mmHg for the three tests, respectively (Extended Data Fig. 3). The corresponding mean differences and standard deviations in DBP were -1.26 ± 2.00 , 2.26 ± 3.10 and -1.17 ± 2.22 mmHg (Extended Data Fig. 3). When we took replicates of the same participant into account rather than assuming they are

independent measurements, the standard deviations were similar (Supplementary Fig. 16 and Supplementary Discussion 10)⁵⁴. These findings reveal small biases, underscoring the strong agreement between the ultrasound sensor and sphygmomanometer measurements.

The IEEE Std 1708a-2019 standard uses the mean absolute difference to grade the accuracy of a device⁵¹. This parameter weighs all intra-participant and inter-participant measurement differences equally⁵¹ and can be calculated as follows:

$$\left(\sum_{i=1}^n |p_i - y_i| \right) / n, \quad (1)$$

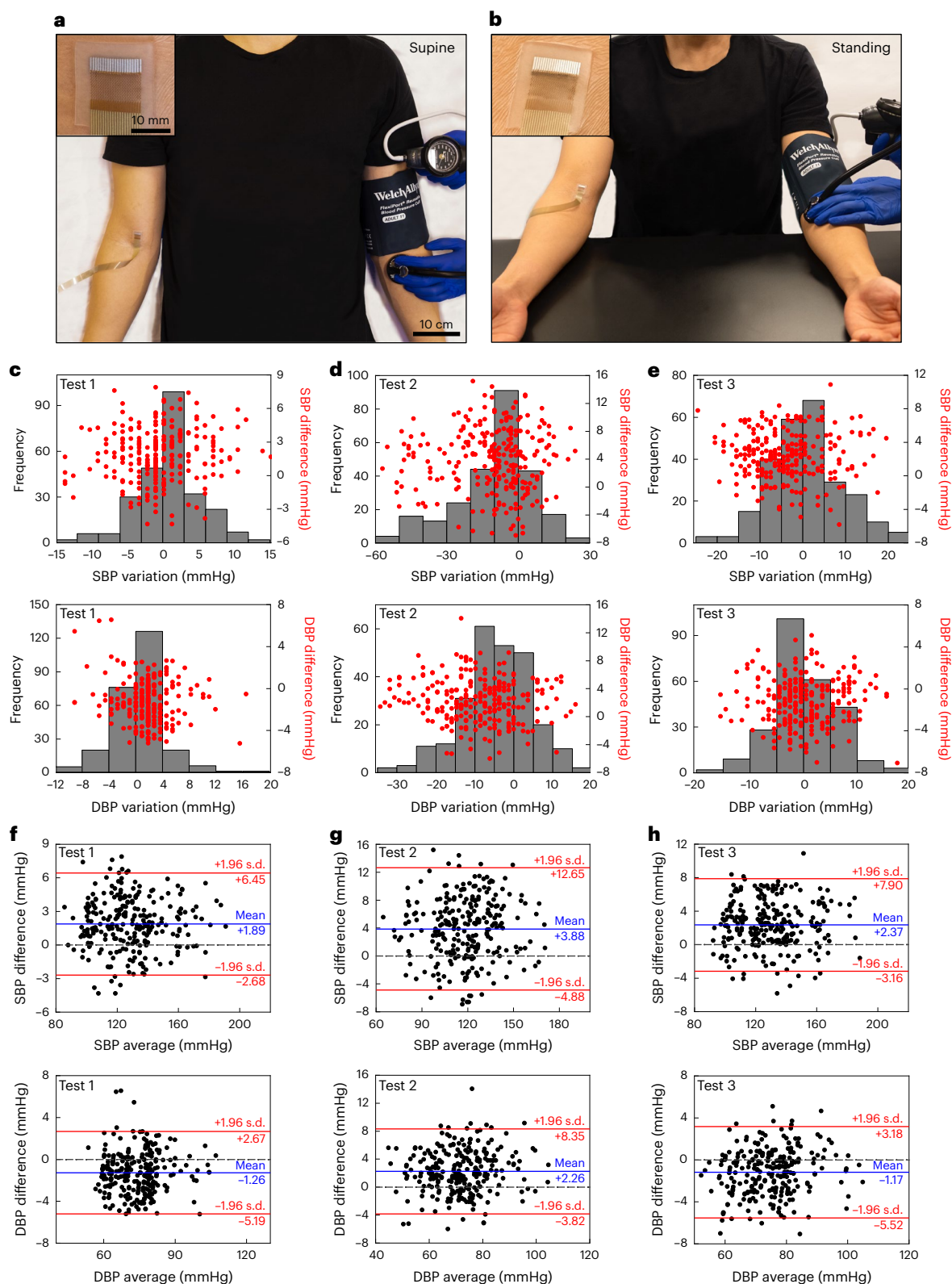


Fig. 3 | Validation of the device in the outpatient clinic. **a, b**, Optical images (same scale bar) depicting the setup for validating the ultrasound sensor with different postures (supine **(a)** and standing **(b)** in this study) against the reference sphygmomanometer. The inset images (same scale bar) show the zoomed-in view of the ultrasound sensor under test. **c–e**, Histograms and scatterplots representing the BP changes from the calibration point versus the frequency or the difference between the two devices for the three different tests (supine **(c)**, standing **(d)** and supine 30 min after the first test **(e)**). The approximate normal distribution of 255 measurements suggests that ~95% of measurements fall within

1.96 s.d. of the mean. **f–h**, Bland–Altman plots representing the biases in SBP and DBP measurements across the three tests ((supine **(f)**), standing **(g)** and supine 30 min after the first test **(h)**). Solid blue lines show the mean differences between the two devices, solid red lines show 95% limits of agreement (that is, 1.96 s.d. above and below the mean differences), and black dashed lines represent zero difference between the two devices. The small mean differences and standard deviations between the measurements from the two devices indicate a strong agreement, validating the accuracy and reliability of the ultrasound sensor.

Table 1 | Demographics and characteristics of the participants in the outpatient clinic

Sex	n (percentage)
Male	44 (51.76%)
Female	41 (48.24%)
At the time of study	Mean \pm s.d.
Age (years)	61.93 \pm 16.85
Height (cm)	169.18 \pm 16.99
Weight (kg)	76.04 \pm 18.05
Arm circumference (cm)	29.29 \pm 3.95
Baseline seated blood pressure	n (percentage)
Normal: SBP 90–119 mmHg and DBP 60–79 mmHg	27 (31.76%)
Prehypertension: SBP 120–139 mmHg or DBP 80–89 mmHg	33 (38.82%)
Stage 1 hypertension: SBP 140–160 mmHg or DBP 90–100 mmHg	18 (21.18%)
Stage 2 hypertension: SBP >160 mmHg or DBP >100 mmHg	7 (8.24%)

where i is the paired measurement number, ranging from 1 to n , p_i is the measurement from the ultrasound sensor and y_i is the measurement from the sphygmomanometer. For the ultrasound sensor, the mean absolute differences were 2.46, 4.90 and 3.01 in SBP and 1.92, 3.10 and 1.96 in DBP, for the three tests, which qualifies as grade A (the highest grade with a mean absolute difference ≤ 5 mmHg; Extended Data Fig. 3)⁵¹. There are three potential explanations for the relatively larger mean absolute difference when the participants changed to standing. First, the ultrasound sensor has a relatively larger bias in capturing such abrupt BP variations due to substantial variations in blood volume in the upper limbs, which can affect the relationship between arterial cross-sectional shape and BP⁵⁵. Second, the observed disparities could stem from inaccuracies in the sphygmomanometer measurements⁵⁶ because the sphygmomanometer presupposes a stable BP throughout the duration of measurement. However, in the context of postural changes, BP fluctuates continually, potentially leading to measurement errors. Third, many patients recruited from the Movement Disorders Center at the Altman Clinical and Translational Research Institute have Parkinson's disease and orthostatic hypotension—approximately 30% based on our experience. Orthostatic hypotension, defined as a drop in SBP of 20 mmHg or more or a drop in DBP of 10 mmHg or more when standing after 3 min, may contribute to the observed differences.

Validation in the cardiac catheterization laboratory

BP is one of the most important indicators used in the cardiac catheterization laboratory to monitor the patient's physiological status. During cardiac catheterization, BP can be monitored invasively by transducing the pressure from the tip of the A-line or the side port of an inserted femoral (or more commonly radial) arterial sheath. The acute effects of sedation, vasodilation, blood loss and haemodynamic fluctuations related to changes in cardiac output can be effectively recorded by the A-line system⁵⁷.

We selected the ISO 81060-2:2018 standard (<https://www.iso.org/standard/73339.html>) for validation in the cardiac catheterization laboratory for the following reasons. First, the ISO 81060-2:2018 standard uniquely allows validation using an invasive reference with a sample size exceeding 15, making it suitable for cardiac catheterization laboratories. Second, the ISO 81060-2:2018 standard is globally recognized and is the most recent to be endorsed by the FDA for BP

device validation, ensuring wider acceptability and rigorous compliance (old protocols from British Hypertension Society and European Society of Hypertension are also endorsed by the FDA; Extended Data Fig. 3). Finally, the IEEE Std 1708a-2019 standard requires notable BP fluctuations for validation^{51,52}, a perilous condition that is not consistently observed during procedures. The ISO 81060-2:2018 standard does not have such a mandate.

We enrolled 26 patients to participate in the validation study. The ISO 81060-2:2018 standard (<https://www.iso.org/standard/73339.html>) requires all participant data to be excluded if the invasive reference SBP variation range is >20 mmHg or if the invasive reference DBP variation range is >12 mmHg, so we excluded data from five patients (Supplementary Fig. 17 and Supplementary Discussion 11). The demographics of the remaining cohort of 21 participants satisfied the ISO 81060-2:2018 stipulations (<https://www.iso.org/standard/73339.html>), including age, sex, race, height, weight and BP distribution (Table 2 and Supplementary Fig. 4). We positioned the ultrasound sensor on the distal brachial artery of the ipsilateral arm with the radial A-line (Fig. 4a and Supplementary Table 1). The ultrasound sensor was calibrated using the A-line as a reference at the beginning of the procedure (Extended Data Fig. 2). We randomly sampled 10 consecutive cycles of the recorded BP waveforms from each patient following the ISO 81060-2:2018 standard (<https://www.iso.org/standard/73339.html>), resulting in a total of 210 cycles that were later subjected to statistical analysis.

Histograms were prepared to examine the frequency distribution of differences between BP measurements acquired using the A-line and ultrasound sensor in accordance with the ISO 81060-2:2018 standard (<https://www.iso.org/standard/73339.html>) (Fig. 4b). The approximate normal distribution indicated that ~95% of measurement differences were within 1.96 standard deviations of the mean, which helps to exclude the influence of participant-related variations (Supplementary Discussion 7)⁵⁴.

Bland–Altman plots revealed the agreement between the measurements from the two devices (Fig. 4c). The mean differences and standard deviations were 0.34 \pm 3.90, -0.18 \pm 2.20 and -0.43 \pm 2.66 mmHg, for SBP, MAP and DBP, respectively (Extended Data Fig. 3). Additionally, to avoid inter-subject factors, the measurement agreement between participants was evaluated using the average of repeated measurements from each participant. The mean differences and standard deviations were 0.34 \pm 1.94, -0.18 \pm 1.09 and -0.43 \pm 1.59 mmHg for SBP, MAP and DBP, respectively (Extended Data Fig. 3 and Supplementary Fig. 18). Given criterion 1 for general agreement (mean difference ≤ 5 mmHg, standard deviation <8 mmHg) and criterion 2 for agreement between participants defined by the ISO 81060-2:2018 standard (<https://www.iso.org/standard/73339.html>) (Extended Data Fig. 3), the results of these Bland–Altman plots indicated that the error ranges of the ultrasound sensor measurements were well within the specified boundaries. When taking replicates into account, the standard deviations become slightly smaller (Supplementary Fig. 19 and Supplementary Discussion 10)⁵⁴. The results remain compliant with the ISO 81060-2:2018 standard, confirming the strong agreement between the measurements from the A-line and ultrasound sensor.

The pulse waveform contour is rich in cardiovascular information. As the pulsation travels through the arterial tree, it encounters numerous reflection sites. Each of these sites contributes a reflected wave with a unique time delay and amplitude, resulting in a complex, deformed BP waveform with different contours at different recording sites (Supplementary Discussion 12). Despite this distortion throughout the arterial tree, the ultrasound sensor, placed on the brachial artery, still achieved high-fidelity waveform monitoring, comparable to the waveform measured by A-line in the radial artery (Fig. 4d and Supplementary Fig. 20). The degree of linear correlation between the BP waveforms captured by these two methods was evaluated using Pearson's correlation coefficient (r), resulting in an average value of 0.977 (Fig. 4e). The high degree of agreement between the paired BP

Table 2 | Demographics and characteristics of the participants in the cardiac catheterization laboratory

Sex	n (percentage)
Male	13 (61.90%)
Female	8 (38.10%)
Race	n (percentage)
White	14 (66.67%)
Asian	3 (14.29%)
Black/African American	2 (9.52%)
American Indian/Alaska Native	2 (9.52%)
At the time of study	Mean \pm s.d.
Age (years)	68.00 \pm 11.45
Height (cm)	172.61 \pm 11.79
Weight (kg)	81.45 \pm 22.10
Heart rate	76.14 \pm 9.13
Co-morbidities and habits	n (percentage)
Coronary artery disease	17 (80.95%)
Hypertension	16 (76.19%)
Cardiac arrhythmia	12 (57.14%)
Smoking	11 (52.38%)
Congestive heart failure	8 (38.10%)
Chronic kidney disease	8 (38.10%)
Diabetes	6 (28.57%)
Stroke	4 (19.05%)
Heart failure with a reduced ejection fraction	3 (14.29%)
Liver cirrhosis	3 (14.29%)
Valve disease	3 (14.29%)
Chronic obstructive pulmonary disease	2 (9.52%)
Blood pressure	n (percentage)
SBP <100 mmHg	3 (14.29%)
SBP 100–160 mmHg	15 (71.43%)
SBP >160 mmHg	3 (14.29%)
DBP <70 mmHg	15 (71.43%)
DBP 70–85 mmHg	3 (14.29%)
DBP >85 mmHg	3 (14.29%)

waveforms recorded by the two devices has been further confirmed by using the dynamic time warping method (Supplementary Fig. 21 and Supplementary Discussion 12).

Validation in the intensive care unit

A-line is the gold standard in the intensive care unit for the continuous monitoring of haemodynamic changes⁵⁸. However, a long-term indwelling A-line carries inherent risks, such as catheter-related thrombosis and associated tissue injury when the patient moves⁵⁹. A cuff-based sphygmomanometer is often used alongside the A-line on the contralateral arm to validate BP measurements⁶⁰. Repeated inflation and deflation on a single arm can be uncomfortable or even painful⁶¹. In addition, this dual system substantially limits patient mobility. Therefore, there is an unmet need in the intensive care unit for comfortable, non-invasive monitors that can track BP accurately over extended periods in response to different medical conditions^{62,63} or treatments^{64,65}.

We used the ultrasound sensor and an indwelling A-line to monitor BP simultaneously and continuously in four consenting patients who

were admitted to the intensive care unit for post-operative haemodynamic monitoring (Fig. 5a–d (top) and Methods). The patients were in Fowler's position (Supplementary Fig. 22)⁶⁶, with the ultrasound sensor placed on the radial artery contralateral to the radial A-line (Methods). The first minute of A-line data was used to calibrate the ultrasound sensor and both devices were subsequently used to record SBP, MAP and DBP for up to 12 h (Fig. 5a–d (top), Extended Data Fig. 2 and Supplementary Table 1).

MAP is usually the most relevant haemodynamic metric for critically ill patients and is non-stationary (its properties change with time) due to the complexity of human physiology (Supplementary Discussion 13)⁶⁷. To assess the correlations over time⁶⁸, we analysed minute-by-minute MAP data using wavelet coherence, which allows statistical analysis of periodic compositional agreement between two signals in the same time domain (Supplementary Discussion 13)^{69,70}. We found in-phase (as indicated by the rightward black arrows) and high magnitude-squared coherence within the high-period region of the wavelet coherence spectrogram (Fig. 5a–d (bottom) and Methods). The high coherence was consistent throughout the continuous monitoring session, indicating the successful detection of BP trends (Supplementary Discussion 13).

To evaluate the likelihood that the observed coherence levels occurred by chance, we estimated the confidence interval by bootstrapping (Supplementary Discussion 14)⁷¹. This technique generates random samples by replacing and shuffling data in the ultrasound sensor dataset (720 MAP values from the 12-h measurement) to construct a comparable new dataset. In this study, the ultrasound sensor dataset was bootstrapped 100 times while keeping the temporal resolution the same. Then, wavelet coherence was evaluated between the A-line and bootstrapped datasets for each participant (Methods and Supplementary Discussion 14). The results showed low magnitude-squared coherence and random phase difference (Supplementary Fig. 23). Maximum values of the magnitude-squared coherence were obtained for each minute for periods >60 min from both the ultrasound sensor and bootstrapped datasets (Supplementary Discussion 14). We excluded regions that might be susceptible to artefactual edge effects (that is, regions outside the white dashed lines; Methods and Supplementary Discussion 14). We calculated the mean maximum values of the magnitude-squared coherence of the ultrasound sensor and bootstrapped datasets over the entire duration of each measurement. Then, we calculated the z-scores (Methods and Supplementary Fig. 24). A z-score >2.58 corresponds to a confidence level >99%, indicating a significant difference between the ultrasound sensor and bootstrapped datasets. The mean maximum values of the magnitude-squared coherence obtained from the ultrasound sensor were consistently much higher than those from all bootstrap comparisons, resulting in z-scores of 11.02, 10.72, 8.11 and 11.81 for patients 1, 2, 3 and 4, respectively (Supplementary Fig. 24). These results suggest that the in-phase high magnitude-squared coherence within the high-period region was non-random.

Discussion

We present the first rigorous and comprehensive clinical validation of a wearable ultrasound BP sensor. In this re-engineered ultrasound sensor, we closely arranged 20-element transducer array, creating a closely connected 10-mm-wide acoustic window. This window not only ensures full coverage of the target arteries but also offers substantial tolerance for device–artery misalignment, addressing the challenge in previously published device^{11,12}. A 500- μ m-thick backing layer has been added to effectively reduce redundant vibrations and improve the arterial wall tracking capability of the transducers, thus substantially improving the accuracy of BP measurements. We evaluated the ultrasound intensity and safety of the device according to the FDA Track 1 guidelines²⁹ and the American Institute of Ultrasound in Medicine³¹.

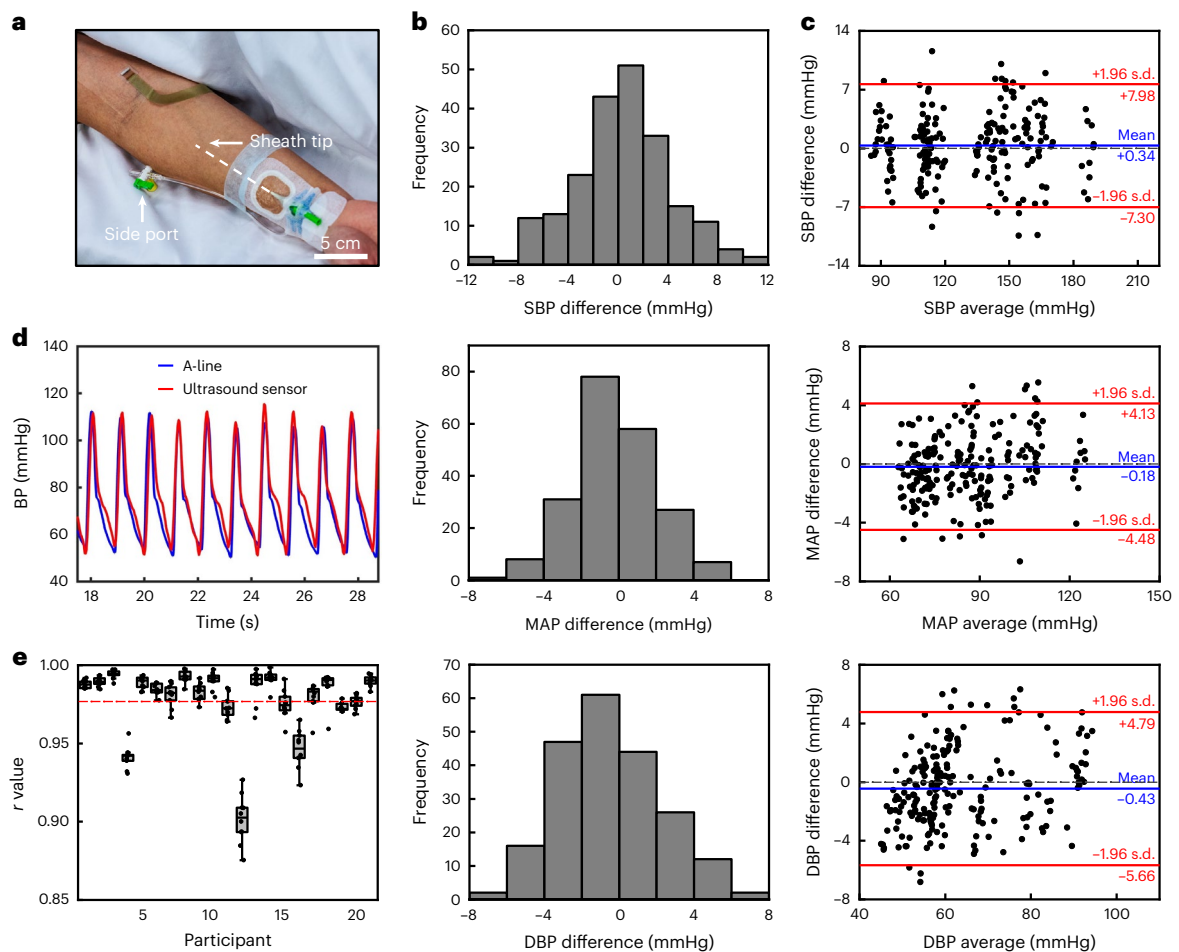


Fig. 4 | Validation of the device in the catheterization laboratory. **a**, Optical image depicting the setup for validating the ultrasound sensor against the reference A-line. The sheath is inserted into the radial artery and the side port is used to connect the transducer system for BP measurement. **b**, Histograms showing frequency distributions of measurement differences for SBP, MAP and DBP between the two devices. The 210 measurements approximately follow a normal distribution, implying that ~95% of measurements are within 1.96 s.d. of the mean. **c**, Bland–Altman plots representing the biases in SBP, MAP and DBP measurements. Solid blue lines show the mean differences between the two devices. The standard deviations in SBP, MAP and DBP are 3.90, 2.20 and 2.66, respectively. Solid red lines show the 95% limits of agreement (1.96 s.d. above and below the mean differences). The black dashed lines represent zero differences between the two devices. The small mean differences and standard deviations

between the measurements from the two devices indicate a strong agreement between them, validating the accuracy and reliability of the ultrasound sensor. **d**, A typical comparison of BP waveforms from patient 1 (see Supplementary Figs. 17 and 20 for comparison of waveforms across all patients). The BP waveforms from the A-line (blue line) and ultrasound sensor (red line) show a high degree of similarity. **e**, Boxplot representing Pearson's correlation coefficient (r) for BP waveforms collected by both devices. The centre line defines the median of each dataset. The upper and lower box ranges define the 75th and 25th percentiles of each dataset, respectively. The upper and lower whiskers define the $+1.5$ and -1.5 s.d. of each dataset, respectively. The dashed red line represents an average $r = 0.977$, suggesting a strong linear relationship between the BP waveforms from the two devices.

Multiple statistical analysis methods have been used in this study. The Bland–Altman plots were used to assess the agreement of BP measurements from the two devices. The Bland–Altman plot quantifies the agreement between each pair of measurements rather than a group of measurements. This provides a clear and quantifiable measure of bias between each pair of measurements (Supplementary Discussion 7). The Pearson correlation coefficient provides a quantitative measure of the strength and direction of the linear relationship between the two signals, effectively assessing how closely they match. Unlike other methods that require exact alignment of the time series data, dynamic time warping can align waveforms that may be out of phase, capturing the true essence of the BP waveform patterns. This makes dynamic time warping invaluable for accurately comparing BP waveforms, ensuring that differences in waveform patterns are carefully considered. Wavelet coherence analysis was utilized to assess the agreement between BP measurements from the two devices over time. Unlike traditional statistical methods that neglect

either temporal or frequency elements, wavelet coherence retains both local and global frequency information without compromising temporal information (Supplementary Discussion 13). This is particularly effective for analysing continuous measurements over extended periods.

Mean differences and standard deviations in BP measurements between the ultrasound sensor and standard clinical methods meet IEEE Std 1708a-2019 and ISO 81060-2:2018 standards. If the device is intended for use during periods of large BP fluctuations (that is, when the invasive reference systolic BP varies by >20 mmHg or the diastolic BP by >12 mmHg during or before the test, as outlined in ISO 81060-2:2018 6.2.4.d.1 (<https://www.iso.org/standard/71161.html>)), a specialized patient population—such as individuals with cardiovascular autonomic failure or critically ill patients—should be selected for validation. If not, all data from the participants shall be excluded. Adherence to this standard inherently promotes haemodynamic stability within the participant pool. Therefore, this stability is beneficial for validating

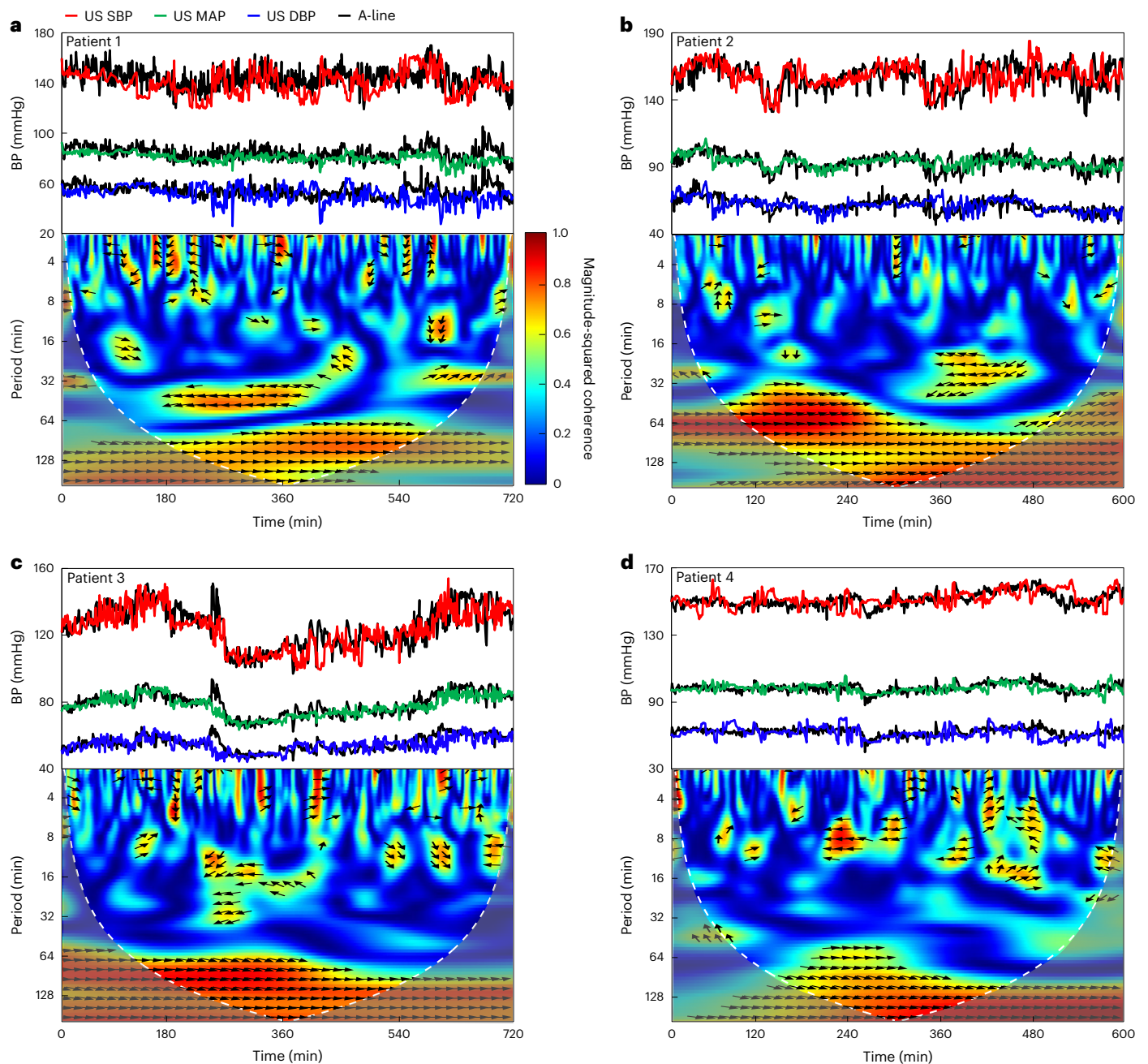


Fig. 5 | Validation of the device in the intensive care unit. a–d, Top: validation results of four different patients (patient 1 (a), patient 2 (b), patient 3 (c) and patient 4 (d)). SBP (red line), MAP (green line) and DBP (blue line) of the ultrasound (US) sensor with the A-line (black lines) for comparison for the duration of the measurement. Bottom: wavelet coherence spectrogram of MAP measurements between the ultrasound sensor and A-line on patient 1 (a), patient 2 (b), patient 3 (c) and patient 4 (d), respectively. The x axis represents the time of

measurement, the y axis represents the period, and the colour scale represents the magnitude-squared coherence. Black arrows represent the phase difference between the two device measurements, where rightward arrows indicate in-phase and leftward arrows indicate anti-phase. The white dashed line represents reliable statistical analysis regions, below which statistical analysis is unreliable due to artefactual edge effects. The wavelet coherence spectra share the same colour bar.

the wearable ultrasound sensor, because it ensures that the BP readings are within a controlled variability range.

The ultrasound and A-line waveform morphologies show a high linear relationship ($r = 0.977$) and degree of agreement. The sensor is physically robust during daily activities and calibration lasts for at least 1 year. The sensor performance is not influenced by the ageing skin (Supplementary Discussion 15). The user-friendly design of the sensor also encourages patient adherence to BP monitoring. The ultrasound sensor can reliably capture longitudinal BP trends over a period of 12 h in the intensive care unit. These collective features suggest

that the ultrasound sensor is accurate and reliable for eventual at-home use and common clinical settings.

The ultrasound sensor captures transient yet clinically important BP fluctuations, which can be early indicators of cardiovascular diseases or complications. For conditions such as autonomic dysfunction and paroxysmal hypertension, sphygmomanometers often fail to detect tell-tale BP fluctuations⁷². For nocturnal hypertension, an important predictor of cardiovascular events^{73,74}, BP may not dip as expected during sleep and might go unnoticed⁷⁵. In addition, this technology addresses challenges posed by traditional one-time BP

measurements, which can be influenced by factors such as white coat hypertension, where patients register abnormally high readings due to the anxiety induced by clinical settings⁷⁶, or masked hypertension, where patients show normal readings in the clinic but elevated BP elsewhere⁷⁷. By offering continuous and comprehensive BP monitoring, this device provides a more accurate and detailed representation of BP trends. Moreover, it reveals how BP responds to daily activities, potentially highlighting specific triggers or patterns of cardiovascular diseases that can be treated. Continuous, ambulatory monitoring facilitates the early detection of anomalies, ensuring timely interventions and a more holistic understanding of cardiovascular health. The ultrasound sensor may also help assess the effectiveness of therapy. Healthcare providers can evaluate the need to adjust medications or treatments on the basis of the continuous data stream, facilitating personalized treatments and optimal patient outcomes.

There are several promising directions for future improvements. First, in this study, we assumed a constant vessel stiffness coefficient on the basis of the initial calibration, but this coefficient can be affected by cardiovascular diseases. In the cardiac catheterization laboratory study, we observed less satisfactory comparative results between the A-line and ultrasound sensor on participant 12, with notable phase differences and variations in BP amplitude. These discrepancies can be attributed to the impact of severe irregular heart rhythms, which shift blood flow profiles from laminar to turbulent and cause stroke volume fluctuations. The viscoelastic properties of arterial walls during these irregular heart rhythms complicate measurements, because the stress–strain curve's hysteresis becomes more pronounced, potentially distorting BP readings. There is need for further research to understand arterial wall dynamics under irregular heart rhythms. Detailed studies of patient populations with specific arterial diseases (such as coronary artery disease, peripheral artery disease, or arterial aneurysm) are also needed to investigate and refine the diameter–pressure relationship⁷⁸. In addition, the physiological variances among different participant groups can influence the measurement results. The participants in the calibration duration studies comprised healthy individuals with stable haemodynamic profiles, which probably resulted in consistent vascular stiffness throughout the 1-year measurement period. In contrast, participants in the intensive care unit were recovering from surgical operations and thus more likely to experience haemodynamic instability, which might have led to vascular stiffness fluctuations. Therefore, while less frequent recalibration may suffice for the healthy cohort, the intensive care unit cohort may have benefited from more regular recalibrations to account for these variations for long-term monitoring. The pulse wave velocity can precisely reveal arterial stiffness in real time, and would help extend the calibration duration and potentially enable automatic calibration^{79,80}.

Second, the focus of this work is to validate the ultrasound sensor against the reference equipment (sphygmomanometer and A-line) and further iterate the device on the basis of the results and user feedback, but in future large-scale clinical trials, additional parameters such as intraclass correlation coefficient can be incorporated. The intraclass correlation coefficient would allow us to quantify the reproducibility of the measurements obtained by different operators (such as physicians, nurses and patients) using the ultrasound sensor, as well as the repeatability of the measurements made by the same operator. As the manufacturing process of the device becomes more industrialized and scaled up, conducting intraclass correlation coefficient analysis would be essential to assess its practicality and reliability in real-world clinical environments.

Third, integrating machine-learning pulse wave analysis could reveal the intricacies of waveform patterns and their link to subtle anomalies⁸¹, facilitating the early detection of cardiovascular diseases, offering insights into their progression and enabling personalized interventions.

Fourth, recent work has demonstrated a fully integrated wearable system¹⁴, which marks a notable advance towards more practical daily applications. However, the continuous operation of the system places large demands on the battery. Replacing commercial, off-the-shelf chips with application-specific integrated circuits could substantially reduce the power consumption of the system. Furthermore, integrating wearable power-harvesting components could extend the operational life of the system⁸².

Finally, seamless integration of the device with existing hospital systems to enable data uploading and synchronization is necessary to enhance patient care⁸³. Medical facilities rely on robust and cohesive electronic health record systems to maintain data accuracy and streamline medical operations. Direct, automated data transfer from the device to the hospital's electronic health records would eliminate manual data entry, which not only reduces the workload on healthcare professionals but also minimizes potential human errors. This is particularly beneficial for time-sensitive situations where immediate actions are needed.

Methods

Fabrication of the wearable ultrasound sensor

The wearable ultrasound sensor in this work was specifically designed for BP monitoring on clinical reference sites such as brachial and radial arteries (Supplementary Discussion 16). Fabrication consisted of three main processes: transducer dicing, electrode patterning and device assembly¹¹.

Transducer dicing. A 500- μm -thick backing layer made of silver epoxy (E-Solder 3022 Von Roll, EIS) was cured on a piece of 32.5 mm \times 32.5 mm \times 220 μm 1-3 composite 7 MHz ultrasound transducer (DL-53, Del Piezo Specialties) at 80 °C for 4 h. The ultrasound transducer with the backing layer was cut using a dicing machine (DAD3220, Disco) to a dimension of 3 mm \times 0.4 mm at a pitch of 0.5 mm.

Electrode patterning. The top and bottom electrode patterns were designed using AutoCAD 2020 (Autodesk). A thin layer of polyimide (PI2545, HD Microsystems) was spin coated on a 20- μm -thick copper foil (MicroThin). The polyimide-coated copper foil was soft baked on a hotplate at 110 °C for 3 min and 150 °C for 1 min, and then cured in a nitrogen oven at 300 °C for 1 h. A polydimethylsiloxane (184 silicone elastomer, Sylgard) coated glass slide served as the substrate to laminate the copper foil with the polyimide layer. The interface was activated by ultraviolet light (PSD series Digital UV Ozone System, Novascan) for 3 min to increase the bonding strength between the polyimide and polydimethylsiloxane. A laser system (Model 01-14, Laser Mark's) was used to pattern the high-resolution serpentine electrode on the copper foil. The pattern was then transferred by water-soluble tape (ASWT-2, Aquasol) to a 20- μm -thick Eco-flex (00-30, Smooth-On) substrate spin coated on a poly(methyl methacrylate)-coated glass slide.

Device assembly. The linear array with 20 diced transducers and one silver epoxy ground element was welded to the electrodes with silver epoxy and was fully cured at 80 °C for 2 h. A co-planar anisotropic conductive film was bonded to the electrodes at 140 °C for transferring signals and power. Finally, the device was encapsulated in Eco-flex and cured at room temperature for 2 h. The ultrasound sensor was then peeled off the glass slide.

Performance characterizations of the ultrasound sensor

The electrical impedance and phase angle were characterized using a network analyser (Hewlett Packard 4195A, HP) (Supplementary Fig. 6). The resonant and anti-resonant frequencies corresponded to the points of minimal and maximal electrical impedances, respectively. The associated phase angle close to 0 at the resonance frequency indicated the efficient energy conversion of the piezoelectric transducers.

The pulse-echo response was tested using an aluminum block in a water tank (Supplementary Fig. 6). A Verasonics Vantage 256 system was used to obtain the raw radiofrequency signals, which were then transformed into the frequency domain by using fast Fourier transform based on Matlab R2021a (Mathworks).

The two-dimensional (X-Z and Y-Z planes) and three-dimensional acoustic field simulations were performed using Field II, an open-source Matlab toolbox (Supplementary Fig. 7). The two-dimensional acoustic field was scanned using an ultrasonic mapping system (AIMS III hydrophone scanning system, Onda Corporation) (Supplementary Fig. 7).

Measurement of BP waveforms

The Verasonics system functioned as the host to control the device. The ultrasound sensor was attached to the skin using Tegaderm (1626W, 3M). A thin layer of ultrasound gel was used at the interface between the device and skin for the best acoustic coupling. The echo signal was then acquired at a sampling rate of 62.5 MHz, which allowed precise vessel wall tracking. Radiofrequency data collected from the ultrasound sensor were post processed using Matlab R2021a. The signals were analysed on the basis of the ultrasound time of flight, which could be used to calculate the propagation distance by multiplying the ultrasound speed in the media. We assumed a constant ultrasound speed in human tissues. Subsequently, the distance between the anterior and posterior walls of the target artery, representing the arterial diameter, was calculated and then converted to BP by using the equations in Supplementary Discussion 4. Initial calibration of the BP was provided by a sphygmomanometer or an A-line.

Calibration duration

Overview. The long-term accuracy of the calibrated ultrasound sensor was evaluated in four healthy consenting individuals with no previous history of cardiovascular conditions. The study was approved by the Institutional Review Board (IRB) of the University of California San Diego (IRB 804119).

Procedure. Due to environmental concerns in California, mercury sphygmomanometers are no longer used in clinical practice or research⁸⁴. A reference sphygmomanometer (DS58, Welch Allyn) compliant with ISO 81060-2:2013 was used instead.

To mitigate potential fluctuations in BP that could be attributed to dietary intake or inherent circadian rhythms, all BP measurements were consistently conducted within a narrow time window from 9:00 to 12:00, following a minimum fasting period of 12 h. In preparation for BP measurements, the participants were instructed to sit and rest quietly for 15 min before testing. This preparatory step was critical in ensuring the stabilization of haemodynamic parameters, thereby providing a more accurate reflection of the participant's baseline BP. To further enhance the consistency and comparability of the measurements throughout the 1-year period, we employed the same ultrasound sensor, which was affixed to the right brachial artery during testing, while the sphygmomanometer was positioned on the left brachial artery, facilitating concurrent BP measurements (Supplementary Table 1). We took three measurements from the sphygmomanometer interspersed with a 30 s interval to prevent potential venous congestion⁸⁵. For each sphygmomanometer measurement cycle, which included periods of both inflation and deflation, concurrent measurements from the ultrasound sensor were recorded. Then, the mean values of each beat over that cycle were averaged. Thus, three pairs of sphygmomanometer and ultrasound measurements were recorded.

On day 1, the ultrasound sensor was first calibrated. Then, BP measurements from the calibrated ultrasound sensor and reference sphygmomanometer were tracked for 1 year (daily measurements in the first month, weekly measurements in the second to sixth months, and monthly measurements from the seventh to twelfth months).

Data reporting. The average differences in SBP and DBP measurements from the ultrasound sensor and sphygmomanometer were calculated for each participant and measurement day.

Validation during daily activities

Overview. Normotensive participants with no previous history of cardiovascular conditions consented to participate in the study. All procedures complied strictly with the protocol approved by the IRB of the University of California San Diego (IRB 804119). In the interest of the participant's safety (following the suggestions of the IRB committee) and to maintain the integrity of the comparative analysis, the ultrasound sensor was compared to a sphygmomanometer. Human posture affects commercial sphygmomanometer BP measurements due to the hydrostatic pressure difference between the measurement arm and heart level⁸⁶. Thus, all measurements were obtained while the measurement arm was placed at the heart level except in the hand-raise test. Motion artefacts introduce noises that interfere with BP reading⁸⁷. Therefore, all experiments were performed and compared between the sphygmomanometer and ultrasound sensor with the measurement arm in a stationary position. All activities were executed in the identical order for all participants to maintain procedural consistency.

Procedure. The participants were instructed to fast for at least 12 h before the test and were asked to refrain from ingesting alcoholic and caffeinated beverages for 24 h. The test was performed in a lab environment. First, the participants sat and rested for 10 min to stabilize haemodynamic changes. Then, three reference BP measurements were recorded with the sphygmomanometer, each taken after waiting for 30 s. The average of the three reference measurements was used to calibrate the ultrasound sensor before it was placed above the brachial artery for recording. The placement of both the ultrasound sensor and sphygmomanometer was consistently on the right arm for the duration of all daily activities conducted (Supplementary Table 1)^{51,52}. Each participant performed sitting and 12 different daily activities, and BP measurements were acquired in a stationary position within 5 min after each activity.

Positional changes. First, after calibrating the ultrasound sensor in the seated position, the participant was asked to stand; the arm used for measurement was positioned at the heart level. After 5 min, BP was recorded. Subsequently, the participant transitioned into a supine position, utilizing a pillow to elevate the arm to the heart level, and waited 5 min for BP stabilization before measurements. Following this, the participant's legs were elevated for the passive leg-raise test; after 5-min stabilization, BP was measured. Finally, the participant returned to a seated position and waited for 10 min. Then, the participant raised the measurement arm for 5 min and BP was subsequently measured.

Pressor tests. The participant performed three different pressor tests (mental arithmetic, ice bath stimulus and isometric handgrip) in a seated position. Participants rested in a seated position for 10 min before each test to stabilize their BP. In the mental arithmetic test, participants were asked to solve 10 different mathematical calculations without a paper or a calculator within 10 min. BP was measured after the first question had been solved. For the ice bath stimulus test, the participants immersed their hands in an ice bath. After 1 min, BP was measured. Finally, a digital dynamometer (TL-LSC100, Trailite) was used to measure each participant's maximal voluntary contraction. Then, ~30% of the participant's maximal voluntary contraction was used to perform isometric handgrip with a handgrip strengthener (NIYIKOW), which offers an adjustable resistance, ranging from 5 to 60 kg⁸⁸. This method ensured that the participants maintained muscular contraction that was substantial enough to engage the muscles effectively, yet not so strenuous as to cause rapid muscle fatigue

or notable cardiovascular exertion. After 1 min of isometric handgrip, BP was measured.

Cycling. Before cycling, the participant was first in a seated position for 10 min. Then, participants performed 30 min of constant intensity exercise on a stationary bike. After 5-min cooling in a seated position¹², BP was obtained.

Deep breath. To minimize the effect of cycling, the participants rested in a seated position for 30 min. Then, the deep breathing exercise was guided by an audio recording according to a standardized approach (<https://www.youtube.com/watch?v=pWFaTxNOGnl>). The recording instructed the participants to adopt a rhythm of 6 s of controlled inhalation followed by 10 s of exhalation, creating a pattern that promotes parasympathetic activation and may contribute to cardiovascular relaxation. The participants were seated comfortably in a quiet environment, with their eyes closed and wearing noise-cancelling earphones (AirPods Pro, Apple) to minimize distractions. After an initial 5 min of deep breathing exercise, BP measurements were acquired.

Meditation. After 10 min of rest, meditation was performed in a sitting position according to a commercially available meditation session with music (<https://www.youtube.com/watch?v=O-6f5wQXSu8>). The participants followed instructions from the meditation session. BP was measured 10 min into the session.

Food intake. In Western diets, overconsumption of carbohydrates and sodium is a major cardiovascular risk factor and may cause spikes in BP. Thus, after 10 min of rest in the seated position, participants ate a Western meal and dessert (100 g of sugar-rich chocolate). After 30 min, BP was measured in a sitting position.

Caffeine intake. Caffeine in coffee, tea or energy drinks is the most widely consumed psychoactive substance. To minimize the effect of the meal intake, the participants rested for 120 min before the caffeine test. Then, the participants drank a sugar-free energy drink with 200 mg of caffeine. After 15 min, BP was measured in a sitting position.

Data reporting. With the ultrasound sensor calibrated from the sitting position, the BP measurements from the 12 activities were compared with those obtained from the reference sphygmomanometer. BP waveform changes were analysed and the four-quadrant plot was used to assess the trending ability of the ultrasound sensor compared to the reference measurements of all 12 activities. The concordance rate was defined as the percentage of measurements from the two devices that have the same directional change (1st and 3rd quadrants) to the sum of all changes (Supplementary Discussion 9).

Validation in the outpatient clinic

Overview. The ultrasound sensor and a reference sphygmomanometer were compared according to the IEEE Std 1708a-2019 standard⁵¹. The study was approved by the IRB of the University of California San Diego (IRB 191527). We recruited 85 consecutive outpatient participants from the community and from the Parkinson & Other Movement Disorders Center at the University of California San Diego. Study visits took place at the Altman Clinical and Translational Research Institute at the University of California San Diego (Table 1). All participants provided written informed consent for this study.

The actual effect of sphygmomanometer inflation and deflation on haemodynamics is unknown (Supplementary Video 1)⁸⁹. Studies have suggested that BP changes can be attributed to muscle activity, as well as the increased anxiety associated with the awareness of BP measurement⁹⁰. In addition, another factor to consider is the act of sphygmomanometer inflation itself, which, due to the potential discomfort it causes, may change the BP⁹¹.

Procedures. The validation was carried out using contralateral arms simultaneously by a team of three professional medical observers and a supervisor, who were trained and experienced in BP measurements (Supplementary Table 1).

After an initial 10-min rest period in a quiet, temperature-controlled outpatient clinic, BP was measured simultaneously at the heart level on both arms using the sphygmomanometer and ultrasound sensor. A reference BP value was given by the sphygmomanometer to calibrate the ultrasound sensor before the tests. Each participant underwent three tests (supine, standing and supine 30 min after the first test in this study), with three pairs of BP measurements taken for each condition.

Reference BP measurements were provided by two observers using the sphygmomanometer with a 'Y' connector. The cuff size was based on arm circumference measurement⁹². SBP and DBP measurements were captured using the Phase I and V Korotkoff sounds, respectively. If both measurements from the two observers were ≤ 4 mmHg apart, the mean value of the two measurements was used as the reference measurement. Otherwise, the BP measurement was repeated until the measurements were concordant within 4 mmHg. The third observer, a developer of the ultrasound sensor, was responsible for affixing the device to participants and ensuring correct alignment with the brachial artery. The ultrasound sensor was classified as a beat-to-beat BP measuring device. For each paired measurement, we calculated the mean value of all beats obtained from the ultrasound sensor during the measurement period of the sphygmomanometer. This period was specifically chosen to encompass the entire duration of sphygmomanometer inflation and deflation⁵¹. Three paired measurements were performed in this manner. The supervisor gave a verbal cue to the observers to initiate each measurement and record the results. A mandatory rest period of at least 30 s was given after each paired measurement to avoid venous congestion⁸⁵.

To maintain objectivity, observers were single blinded by calling out the BP readings throughout the entire study. The participants' involvement was concluded when the three test conditions were completed satisfactorily.

Data reporting. The report included a participant characteristic table (Table 1) and graphical representations for statistical analysis (Fig. 3c–h, Extended Data Fig. 3 and Supplementary Fig. 16). The characteristic table includes key demographic information such as age, sex, height, weight, arm circumference and BP. Charts (combined histogram and scatterplots, Bland–Altman plots) for statistical analysis were provided separately for the three tests. The mean absolute difference was calculated for each test to evaluate the ultrasound sensor.

Validation in the cardiac catheterization laboratory

Overview. This study compared the BP measurement from the A-line and ultrasound sensor according to ISO 81060-2:2018 guidelines (<https://www.iso.org/standard/73339.html>). The IRB of the University of California San Diego approved this study (IRB 191474). We recruited a cohort of 26 consenting participants but excluded data from five participants with BP fluctuations too large to meet the ISO 81060-2:2018 standard's criteria (<https://www.iso.org/standard/73339.html>) (Supplementary Fig. 17 and Supplementary Discussion 11). The final cohort of 21 participants had relatively stable BP throughout the measurement period. All participants were patients undergoing invasive cardiac catheterization to diagnose or treat cardiovascular conditions (such as invasive coronary angiography for the diagnosis and treatment of coronary artery disease; invasive haemodynamic assessment for the diagnosis and treatment of heart failure) in the Cardiac Catheterization Laboratory, Sulpizio Cardiovascular Center at the University of California San Diego.

Procedures. All procedures were conducted in accordance with the ISO 81060-2:2018 standard (<https://www.iso.org/standard/73339.html>)

using the same arm measure. The reference invasive BP monitoring equipment complied with the requirements of IEC 60601-2-34:2011. The arterial access sheath and transducer system (A-line) was flushed to remove air bubbles and thrombi before taking reference measurements. The transducer of the A-line system was examined for damping properties with a fast flush test and, if necessary, actions were taken to correct abnormal damping (Supplementary Discussion 1). The 6F Glidesheath slender arterial access sheath (Terumo Interventional Systems) was placed in the distal radial artery, and average BP readings from the initial three pulses were used to calibrate the ultrasound sensor. The sheath potentially affected flow in the radial artery lumen, which might increase arterial impedance and then distort in situ arterial wall dilation⁹³. Therefore, the ultrasound sensor was used to measure BP in the distal brachial artery in the same arm to minimize positional bias (Supplementary Table 1). For each patient, BP readings were collected from both devices for 30 s following calibration. Therefore, measurements were not subjected to the haemodynamic effects of medications given clinically as part of the procedure. Ten consecutive cycles of BP waveforms were randomly selected for analysis following the ISO 81060-2:2018 standard (<https://www.iso.org/standard/73339.html>).

Following these measurements, the arterial access was used to perform the clinically indicated diagnostic and/or therapeutic cardiac procedures and the patient's involvement in the study was concluded.

Data reporting. The report generated a patient characteristic table (Table 2) and graphical representations for waveform comparison (Supplementary Figs. 17, 20 and 21) as well as statistical analysis (Fig. 4b–d, Extended Data Fig. 3, and Supplementary Figs. 18–20). These components adhere to criteria 1 and 2 stipulated by the ISO 81060-2:2018 standard (<https://www.iso.org/standard/73339.html>). The characteristic table includes key demographic information as well as the co-morbidities or habit records of the patients. In accordance with criterion 1, each BP measurement obtained from the ultrasound sensor was compared with its corresponding A-line measurement. The biases between SBP, MAP and DBP readings from both devices were calculated, using the mean difference and standard deviation. Criterion 2 involved the average of 10 measurements from each patient, and the mean difference and standard deviation between measurements from both devices were calculated. Charts (histograms and Bland–Altman plots) for statistical analysis were provided to evaluate the measurements' distributions and agreement.

The timestamps from each cardiac cycle were identified for waveform analysis. A total of 210 pulse waveforms from 21 patients were statistically analysed (Supplementary Fig. 20). The degree of waveform similarity was assessed by computing Pearson's correlation coefficients for each pulse waveform.

Validation in the intensive care unit

Overview. This study aimed to use the ultrasound sensor for the continuous recording of BP changes in patients admitted to the intensive care unit for observation after planned surgical procedures at the Jacobs Medical Center at the University of California San Diego. All procedures in this clinical study were approved by the IRB of the University of California San Diego (IRB 805176). Patient 1 underwent lumbar decompression and instrumentation surgery, patient 2 received an endovascular aneurysm repair, patient 3 was admitted for neobladder reconstruction and patient 4 was admitted for a left subclavian-to-brachial artery graft. All patients gave written informed consent before the study.

Procedure. The ultrasound sensor measured the radial artery of the opposite arm from the indwelling radial A-line for simultaneous BP measurements (Supplementary Fig. 22). Although inter-arm BP differences may exist, it is typically a rare phenomenon⁹⁴. Contralateral BP measurements were employed due to the practical limitations imposed by the secured indwelling A-line, other sensors and wires

(such as electrocardiogram and pulse oximeter) with associated taping (Supplementary Table 1). The patients were in Fowler's position with the bed tilted between 30 and 60 degrees, the standard of care in the intensive care unit. The first measurement from the A-line was used to calibrate the ultrasound sensor. Both devices recorded SBP, MAP and DBP every minute for up to 12 h following the A-line sampling rate. Both devices remained in place throughout the duration of the test.

Data reporting. The minute-by-minute SBP, MAP and DBP data are presented for the duration of the test for each patient.

Because MAP is the primary parameter of interest in the intensive care unit, we further analysed the MAP data with wavelet coherence for time-period domain analysis. We used the Matlab toolbox for signal processing and applied the built-in function 'wcoherence' to perform the wavelet coherence of the BP measurements acquired from the ultrasound sensor and A-line. This statistical analysis method allows the decomposition of the non-stationary measurements from the ultrasound sensor and A-line into time-varying period distribution (Supplementary Discussion 13).

Further analysis was based on the magnitude-squared coherence of the high-period region in the wavelet coherence spectrogram (Supplementary Discussion 14). To consider the sampling frequency of both devices and differentiate the tracking ability over long periods from any measurement variances (such as contralateral arm differences and body motion), the high-period region was defined as periods longer than 1 h. Within this high-period region, we evaluated the probability of coherence that might have occurred randomly. First, the ultrasound sensor data were bootstrapped 100 times, maintaining the same temporal resolution as the experimental data. Second, wavelet coherence was analysed between the bootstrapped and A-line data. Third, we excluded the regions susceptible to artefactual edge effects and extracted the peak values of the magnitude-squared coherence for each minute in the high-period region. The mean of the peak magnitude-squared coherence values over the entire time window was calculated for both the experimental and bootstrapped data. Finally, the z-score was calculated for the experimental data in comparison to the 100 bootstrapped datasets using the following equation:

$$z\text{-score} = \frac{x - \mu}{\sigma}, \quad (2)$$

where x is the mean maximum value of the magnitude-squared coherence of the ultrasound dataset, μ is the mean maximum value of the magnitude-squared coherence of the bootstrapped dataset and σ is the standard deviation of the maximum values of the magnitude-squared coherence of the bootstrapped data. A z-score >2.58 demonstrates $>99\%$ confidence that the experimental coherence data were not random.

Reporting summary

Further information on research design is available in the Nature Portfolio Reporting Summary linked to this article.

Data availability

The main data supporting the results in this study are available within the paper and its Supplementary Information. Source data for the figures are available from figshare at <https://doi.org/10.6084/m9.figshare.25511761> (ref. 95).

References

- Vlachopoulos, C., O'Rourke, M. & Nichols, W. W. *McDonald's Blood Flow in Arteries: Theoretical, Experimental and Clinical Principles* (CRC Press, 2011).
- Turner, J. R., Viera, A. J. & Shimbo, D. Ambulatory blood pressure monitoring in clinical practice: a review. *Am. J. Med.* **128**, 14–20 (2015).

3. Huang, Q.-F. et al. Ambulatory blood pressure monitoring to diagnose and manage hypertension. *Hypertension* **77**, 254–264 (2021).
4. Pickering, T. G. What will replace the mercury sphygmomanometer? *Blood Press. Monit.* **8**, 23–25 (2003).
5. Pauca, A. L., O'Rourke, M. F. & Kon, N. D. Prospective evaluation of a method for estimating ascending aortic pressure from the radial artery pressure waveform. *Hypertension* **38**, 932–937 (2001).
6. Scheer, B. V., Perel, A. & Pfeiffer, U. J. Clinical review: complications and risk factors of peripheral arterial catheters used for haemodynamic monitoring in anaesthesia and intensive care medicine. *Crit. Care* **6**, 199–204 (2002).
7. Nachman, D. et al. Comparing blood pressure measurements between a photoplethysmography-based and a standard cuff-based manometry device. *Sci. Rep.* **10**, 16116 (2020).
8. Lin, M., Hu, H., Zhou, S. & Xu, S. Soft wearable devices for deep-tissue sensing. *Nat. Rev. Mater.* **7**, 850–869 (2022).
9. Boubouchairopoulou, N. et al. A novel cuffless device for self-measurement of blood pressure: concept, performance and clinical validation. *J. Hum. Hypertens.* **31**, 479–482 (2017).
10. Li, L. et al. Flexible pressure sensors for biomedical applications: from ex vivo to in vivo. *Adv. Mater. Interfaces* **7**, 2000743 (2020).
11. Wang, C. et al. Monitoring of the central blood pressure waveform via a conformal ultrasonic device. *Nat. Biomed. Eng.* **2**, 687–695 (2018).
12. Sempionatto, J. R. et al. An epidermal patch for the simultaneous monitoring of haemodynamic and metabolic biomarkers. *Nat. Biomed. Eng.* **5**, 737–748 (2021).
13. Wang, C. et al. Bioadhesive ultrasound for long-term continuous imaging of diverse organs. *Science* **377**, 517–523 (2022).
14. Lin, M. et al. A fully integrated wearable ultrasound system to monitor deep tissues in moving subjects. *Nat. Biotechnol.* **42**, 448–457 (2024).
15. Stergiou, G. S. et al. A universal standard for the validation of blood pressure measuring devices: Association for the Advancement of Medical Instrumentation/European Society of Hypertension/International Organization for Standardization (AAMI/ESH/ISO) Collaboration Statement. *Hypertension* **71**, 368–374 (2018).
16. Bailey, R. H. & Bauer, J. H. A review of common errors in the indirect measurement of blood pressure: sphygmomanometry. *Arch. Intern. Med.* **153**, 2741–2748 (1993).
17. Godai, K. et al. Validation of an automated home blood pressure measurement device in oldest-old populations. *Hypertens. Res.* **43**, 30–35 (2020).
18. Schoettker, P. et al. Blood pressure measurements with the OptiBP smartphone app validated against reference auscultatory measurements. *Sci. Rep.* **10**, 17827 (2020).
19. Sola, J. et al. Validation of the optical Aktiia bracelet in different body positions for the persistent monitoring of blood pressure. *Sci. Rep.* **11**, 20644 (2021).
20. Schwartz, C. L. et al. Validation of the Kinetik Blood Pressure Monitor-Series 1 for use in adults at home and in clinical settings, according to the 2002 European Society of Hypertension International Protocol on the validation of blood pressure devices. *J. Hum. Hypertens.* **35**, 1046–1050 (2021).
21. Fortin, J. et al. A novel art of continuous noninvasive blood pressure measurement. *Nat. Commun.* **12**, 1387 (2021).
22. Kireev, D. et al. Continuous cuffless monitoring of arterial blood pressure via graphene bioimpedance tattoos. *Nat. Nanotechnol.* **17**, 864–870 (2022).
23. Arnold, J. et al. Large artery function in patients with chronic heart failure. Studies of brachial artery diameter and hemodynamics. *Circulation* **84**, 2418–2425 (1991).
24. Madssen, E., Haere, P. & Wiseth, R. Radial artery diameter and vasodilatory properties after transradial coronary angiography. *Ann. Thorac. Surg.* **82**, 1698–1702 (2006).
25. Hu, H. J. et al. Stretchable ultrasonic transducer arrays for three-dimensional imaging on complex surfaces. *Sci. Adv.* **4**, eaar3979 (2018).
26. Wang, C. et al. Continuous monitoring of deep-tissue haemodynamics with stretchable ultrasonic phased arrays. *Nat. Biomed. Eng.* **5**, 749–758 (2021).
27. Hu, H. et al. Stretchable ultrasonic arrays for the three-dimensional mapping of the modulus of deep tissue. *Nat. Biomed. Eng.* **7**, 1321–1334 (2023).
28. Zhou, S. Transcranial volumetric imaging using a conformal ultrasound patch. *Nature* **629**, 810–818 (2024).
29. *Marketing Clearance of Diagnostic Ultrasound Systems and Transducers: Guidance for Industry and Food and Drug Administration Staff Report No. FDA-2017-D-5372* (Food and Drug Administration, 2023).
30. Bigelow, T. A. et al. The thermal index: its strengths, weaknesses, and proposed improvements. *J. Ultrasound Med.* **30**, 714–734 (2011).
31. Abramowicz, J. S. et al. AIUM official statement for recommended maximum scanning times for displayed thermal index values. *J. Ultrasound Med.* **42**, E74–E75 (2023).
32. Chandran, K. B., Rittgers, S. E. & Yoganathan, A. P. *Biofluid Mechanics: The Human Circulation* (CRC Press, 2012).
33. de Greeff, A. et al. Calibration accuracy of hospital-based non-invasive blood pressure measuring devices. *J. Hum. Hypertens.* **24**, 58–63 (2010).
34. Handler, J. The importance of accurate blood pressure measurement. *Perm. J.* **13**, 51–54 (2009).
35. Olufsen, M. S. et al. Blood pressure and blood flow variation during postural change from sitting to standing: model development and validation. *J. Appl. Physiol.* **99**, 1523–1537 (2005).
36. Monnet, X. & Teboul, J.-L. in *Applied Physiology in Intensive Care Medicine 2* 55–59 (Springer, 2012).
37. Sleight, P., Fox, P., Lopez, R. & Brooks, D. The effect of mental arithmetic on blood pressure variability and baroreflex sensitivity in man. *Clin. Mol. Med.* **55**, 381s–382s (1978).
38. Mouro, L., Bouhaddi, M. & Regnard, J. Effects of the cold pressor test on cardiac autonomic control in normal subjects. *Physiol. Res.* **58**, 83–91 (2009).
39. Kounoupis, A., Papadopoulos, S., Galanis, N., Dipla, K. & Zafeiridis, A. Are blood pressure and cardiovascular stress greater in isometric or in dynamic resistance exercise? *Sports* **8**, 41 (2020).
40. Halliwill, J. R. Mechanisms and clinical implications of post-exercise hypotension in humans. *Exerc. Sport Sci. Rev.* **29**, 65–70 (2001).
41. Grossman, E., Grossman, A., Schein, M., Zimlichman, R. & Gavish, B. Breathing-control lowers blood pressure. *J. Hum. Hypertens.* **15**, 263–269 (2001).
42. Goldstein, C. M., Josephson, R., Xie, S. & Hughes, J. W. Current perspectives on the use of meditation to reduce blood pressure. *Int. J. Hypertens.* **2012**, 578397 (2012).
43. Nguyen, S., Choi, H. K., Lustig, R. H. & Hsu, C.-Y. Sugar-sweetened beverages, serum uric acid, and blood pressure in adolescents. *J. Pediatr.* **154**, 807–813 (2009).
44. Fountain, J. H., Kaur, J. & Lappin, S. L. *Physiology, Renin Angiotensin System* (StatPearls Publishing, 2023).
45. Nurminen, M.-L., Niittynen, L., Korpela, R. & Vapaatalo, H. Coffee, caffeine and blood pressure: a critical review. *Eur. J. Clin. Nutr.* **53**, 831–839 (1999).
46. Saugel, B., Grothe, O. & Wagner, J. Y. Tracking changes in cardiac output: statistical considerations on the 4-quadrant plot and the polar plot methodology. *Anesth. Analg.* **121**, 514–524 (2015).

47. Nachman, D. et al. Wireless, non-invasive, wearable device for continuous remote monitoring of hemodynamic parameters in a swine model of controlled hemorrhagic shock. *Sci. Rep.* **10**, 17684 (2020).
48. Gupta, V. & Lipsitz, L. A. Orthostatic hypotension in the elderly: diagnosis and treatment. *Am. J. Med.* **120**, 841–847 (2007).
49. Gibbons, C. H. et al. The recommendations of a consensus panel for the screening, diagnosis, and treatment of neurogenic orthostatic hypotension and associated supine hypertension. *J. Neurol.* **264**, 1567–1582 (2017).
50. Sutton, R. & Bloomfield, D. M. Indications, methodology, and classification of results of tilt-table testing. *Am. J. Cardiol.* **84**, 10–19 (1999).
51. *IEEE Standard For Wearable Cuffless Blood Pressure Measuring Devices* IEEE Std 1708-2014 (IEEE, 2014).
52. *IEEE Standard for Wearable, Cuffless Blood Pressure Measuring Devices Amendment 1* (IEEE, 2019).
53. Dani, M. et al. New horizons in the ageing autonomic nervous system: orthostatic hypotension and supine hypertension. *Age Ageing* **51**, afac150 (2022).
54. Bland, J. M. & Altman, D. G. Measuring agreement in method comparison studies. *Stat. Methods Med. Res.* **8**, 135–160 (1999).
55. Papaioannou, T. G. & Stefanadis, C. Vascular wall shear stress: basic principles and methods. *Hellenic J. Cardiol.* **46**, 9–15 (2005).
56. Picone, D. S. et al. Accuracy of cuff-measured blood pressure: systematic reviews and meta-analyses. *J. Am. Coll. Cardiol.* **70**, 572–586 (2017).
57. Nishimura, R. A. & Carabello, B. A. Hemodynamics in the cardiac catheterization laboratory of the 21st century. *Circulation* **125**, 2138–2150 (2012).
58. Pierre, L., Pasrija, D. & Keenaghan, M. *Arterial Lines* (StatPearls, 2018).
59. Olsen, M. H., Riberholt, C. G., Capion, T., Berg, R. M. & Møller, K. Reliability of non-invasive arterial blood pressure measurement in patients with aneurysmal subarachnoid haemorrhage. *Physiol. Meas.* **43**, 07NT01 (2022).
60. Chatterjee, A., DePriest, K., Blair, R., Bowton, D. & Chin, R. Results of a survey of blood pressure monitoring by intensivists in critically ill patients: a preliminary study. *Crit. Care Med.* **38**, 2335–2338 (2010).
61. Kaufmann, T. et al. Non-invasive oscillometric versus invasive arterial blood pressure measurements in critically ill patients: a post hoc analysis of a prospective observational study. *J. Crit. Care* **57**, 118–123 (2020).
62. Gorcan, A. et al. A new risk factor for predicting stroke in patients with atrial fibrillation: morning blood pressure surge. *Blood Press. Monit.* **28**, 73–78 (2023).
63. Huart, J. et al. Pathophysiology of the nondipping blood pressure pattern. *Hypertension* **80**, 719–729 (2023).
64. Plange, N. et al. 24-h blood pressure monitoring in normal tension glaucoma: night-time blood pressure variability. *J. Hum. Hypertens.* **20**, 137–142 (2006).
65. Cortés-Ríos, J. & Rodríguez-Fernandez, M. Understanding the dosing-time-dependent antihypertensive effect of valsartan and aspirin through mathematical modeling. *Front. Endocrinol.* **14**, 1110459 (2023).
66. Kubota, S., Endo, Y., Kubota, M. & Shigemasa, T. Assessment of effects of differences in trunk posture during Fowler's position on hemodynamics and cardiovascular regulation in older and younger subjects. *Clin. Interv. Aging* **12**, 603–610 (2017).
67. Fage, N., Asfar, P., Radermacher, P. & Demiselle, J. Norepinephrine and vasopressin in hemorrhagic shock: a focus on renal hemodynamics. *Int. J. Mol. Sci.* **24**, 4103 (2023).
68. Tian, F., Tarumi, T., Liu, H., Zhang, R. & Chalack, L. Wavelet coherence analysis of dynamic cerebral autoregulation in neonatal hypoxic-ischemic encephalopathy. *NeuroImage Clin.* **11**, 124–132 (2016).
69. Grinsted, A., Moore, J. C. & Jevrejeva, S. Application of the cross wavelet transform and wavelet coherence to geophysical time series. *Nonlin. Process. Geophys.* **11**, 561–566 (2004).
70. Labat, D. Recent advances in wavelet analyses: Part 1. A review of concepts. *J. Hydrol.* **314**, 275–288 (2005).
71. Gonçalves, S. & Politis, D. Discussion: bootstrap methods for dependent data: a review. *J. Korean Stat. Soc.* **40**, 383–386 (2011).
72. Mann, S. J. Severe paroxysmal hypertension (pseudopheochromocytoma): understanding the cause and treatment. *Arch. Intern. Med.* **159**, 670–674 (1999).
73. Cappuccio, F. P. The role of nocturnal blood pressure and sleep quality in hypertension management. *Eur. Cardiol. Rev.* **15**, e60 (2020).
74. Thomas, S. J. et al. Association of sleep characteristics with nocturnal hypertension and nondipping blood pressure in the CARDIA study. *J. Am. Heart Assoc.* **9**, e015062 (2020).
75. Ejaz, A. A., Kazory, A. & Heinig, M. E. 24-hour blood pressure monitoring in the evaluation of supine hypertension and orthostatic hypotension. *J. Clin. Hypertens.* **9**, 952–955 (2007).
76. Pickering, T. G. et al. How common is white coat hypertension? *JAMA* **259**, 225–228 (1988).
77. Pandit, J. A., Lores, E. & Battle, D. Cuffless blood pressure monitoring: promises and challenges. *Clin. J. Am. Soc. Nephrol.* **15**, 1531–1538 (2020).
78. Oliver, J. J. & Webb, D. J. Noninvasive assessment of arterial stiffness and risk of atherosclerotic events. *Arterioscler. Thromb. Vasc. Biol.* **23**, 554–566 (2003).
79. Nabeel, P. M., Jayaraj, J., Srinivasa, K., Mohanasankar, S. & Chenniappan, M. Bi-modal arterial compliance probe for calibration-free cuffless blood pressure estimation. *IEEE Trans. Biomed. Eng.* **65**, 2392–2404 (2018).
80. Le, T. et al. Continuous non-invasive blood pressure monitoring: a methodological review on measurement techniques. *IEEE Access* **8**, 212478–212498 (2020).
81. Martínez-Ríos, E., Montesinos, L., Alfaro-Ponce, M. & Pecchia, L. A review of machine learning in hypertension detection and blood pressure estimation based on clinical and physiological data. *Biomed. Signal Process. Control* **68**, 102813 (2021).
82. Min, J. et al. An autonomous wearable biosensor powered by a perovskite solar cell. *Nat. Electron.* **6**, 630–641 (2023).
83. Pandit, J. A., Pawelek, J. B., Leff, B. & Topol, E. J. The hospital at home in the USA: current status and future prospects. *npj Digit. Med.* **7**, 48 (2024).
84. Beevers, G., Lip, G. Y. & O'Brien, E. Blood pressure measurement: Part I—sphygmomanometry: factors common to all techniques. *Brit. Med. J.* **322**, 981–985 (2001).
85. Ogedegbe, G. & Pickering, T. Principles and techniques of blood pressure measurement. *Cardiol. Clin.* **28**, 571–586 (2010).
86. Netea, R., Lenders, J., Smits, P. & Thien, T. Both body and arm position significantly influence blood pressure measurement. *J. Hum. Hypertens.* **17**, 459–462 (2003).
87. Alpert, B. S. et al. Evaluating the impact of motion artifact on noninvasive blood pressure devices. *J. Clin. Hypertens.* **22**, 585–589 (2020).
88. Mortimer, J. & McKune, A. J. Effect of short-term isometric handgrip training on blood pressure in middle-aged females. *Cardiovasc. J. Afr.* **22**, 257–260 (2011).
89. Sheshadri, V., Tiwari, A. K., Nagappa, M. & Venkatraghavan, L. Accuracy in blood pressure monitoring: the effect of noninvasive blood pressure cuff inflation on intra-arterial blood pressure values. *Anesth. Essays Res.* **11**, 169–173 (2017).

90. Veerman, D., van Montfrans, G. & Wieling, W. Effects of cuff inflation on self-recorded blood pressure. *Lancet* **335**, 451–453 (1990).
91. Charmoy, A. et al. Reactive rise in blood pressure upon cuff inflation: cuff inflation at the arm causes a greater rise in pressure than at the wrist in hypertensive patients. *Blood Press. Monit.* **12**, 275–280 (2007).
92. Pickering, T. G. et al. Recommendations for blood pressure measurement in humans: an AHA scientific statement from the Council on High Blood Pressure Research Professional and Public Education Subcommittee. *J. Clin. Hypertens.* **7**, 102–109 (2005).
93. Getliffe, K. Catheter blockage in community patients. *Nurs. Stand.* **5**, 33–36 (1990).
94. Eguchi, K. et al. Consistency of blood pressure differences between the left and right arms. *Arch. Intern. Med.* **167**, 388–393 (2007).
95. Zhou, S. Clinical validation of a wearable ultrasound blood pressure sensor (version 1). *figshare* <https://doi.org/10.6084/m9.figshare.25511761> (2024).

Acknowledgements

We thank H. Ghodsi, R. Thompson, M. Skipworth, C. Addington, M. Suarez, P. Chavez and K. West for assistance with participant recruitment, as well as A. Mishra, A. Rao, P. Bheemreddy and L. Stanton for sensor fabrication. S.X. was supported for the research described in this study by the Wellcome Trust Innovator Award (grant number WT215841/Z/19/Z) and the National Institutes of Health (grant number 1 R01 EB03346401). The content is solely the responsibility of the authors and does not necessarily represent the official views of the National Institutes of Health. All bio-experiments were conducted in accordance with the ethics guidelines of the National Institutes of Health and with the approval of the Institutional Review Board of the University of California San Diego. The mention of commercial products, their sources or their use in connection with material reported herein is not to be construed as actual or implied endorsement of such products by the Department of Health and Human Services.

Author contributions

S.Z. and S.X. conceived the project. S.Z., G.P., K.L. and M. Lin performed the experiments. S.Z. and G.P. processed the data. S.Z. and

G.P. analysed the data. S.Z., G.P. and S.X. wrote the paper. All authors provided constructive and valuable feedback on the paper.

Competing interests

S.X. discloses support for the research described in this study from Wellcome Trust Innovator Award (grant number WT215841/Z/19/Z) and the National Institutes of Health (grant number 1 R01 EB03346401). The other authors declare no competing interests.

Additional information

Extended data is available for this paper at <https://doi.org/10.1038/s41551-024-01279-3>.

Supplementary information The online version contains supplementary material available at <https://doi.org/10.1038/s41551-024-01279-3>.

Correspondence and requests for materials should be addressed to Sheng Xu.

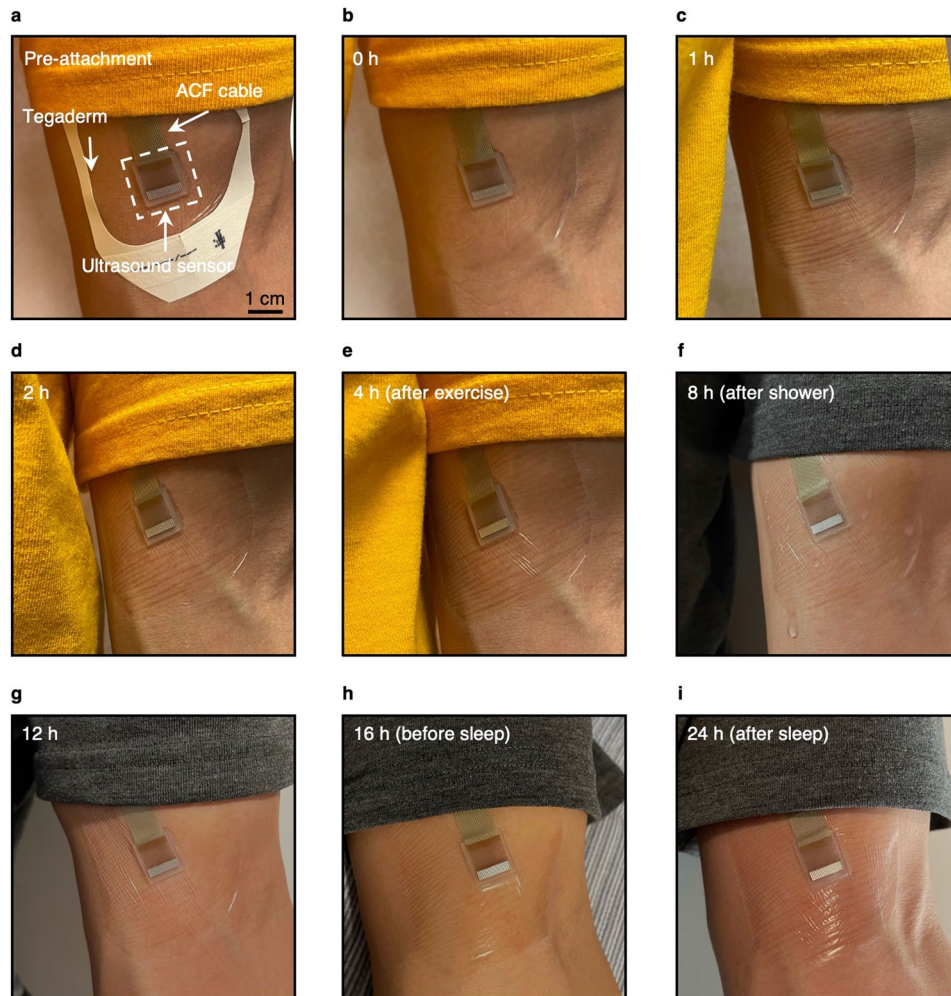
Peer review information *Nature Biomedical Engineering* thanks Andrew Lowe and the other, anonymous, reviewer(s) for their contribution to the peer review of this work.

Reprints and permissions information is available at www.nature.com/reprints.

Publisher's note Springer Nature remains neutral with regard to jurisdictional claims in published maps and institutional affiliations.

Springer Nature or its licensor (e.g. a society or other partner) holds exclusive rights to this article under a publishing agreement with the author(s) or other rightsholder(s); author self-archiving of the accepted manuscript version of this article is solely governed by the terms of such publishing agreement and applicable law.

© The Author(s), under exclusive licence to Springer Nature Limited 2024



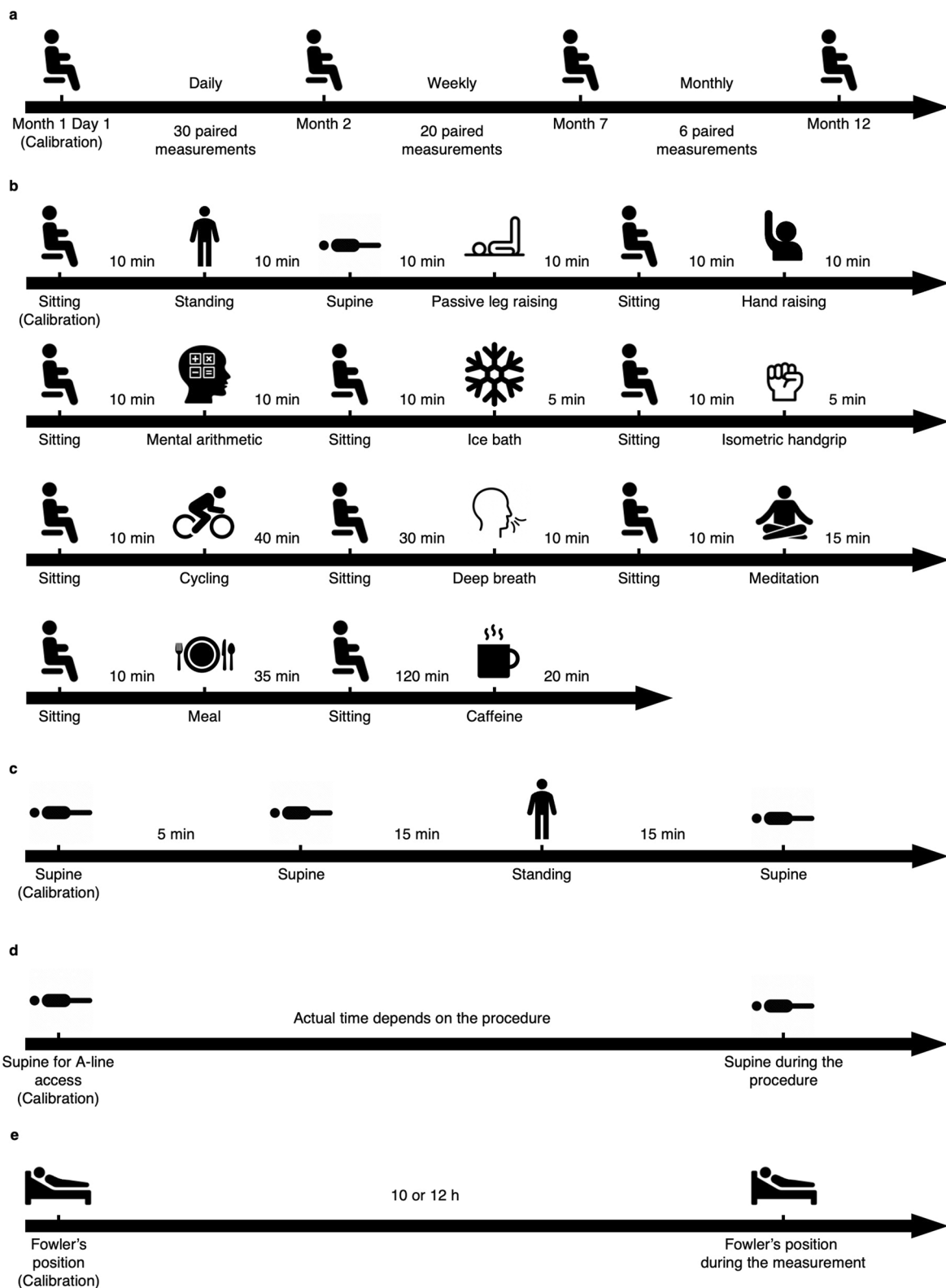
Extended Data Fig. 1 | Longevity and robustness of the ultrasound sensor.

a, Ultrasound sensor pre-attachment with Tegaderm (1626 W, 3 M).

b, immediately after attachment. **c**, 1 h, and **d**, 2 h after attachment and performing various daily activities. **e**, 4 h after attachment and after 1 h of exercise with repeated movements that induce deformation and stretching to the

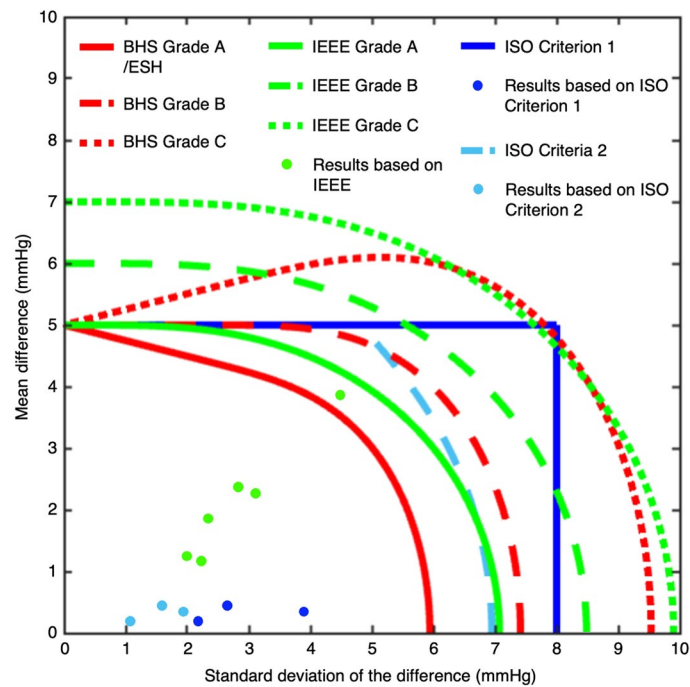
sensor. **f**, 8 h after attachment and after shower. **g**, 12 h after attachment.

h, 16 h after attachment and before going to sleep. **i**, 24 h after attachment and after 8 h of sleep. This sequence demonstrates the sensor's outstanding durability and adaptability through a comprehensive set of common daily activities and routines. The images share the same scale bar. ACF, anisotropic conductive film.



Extended Data Fig. 2 | Timeline of the validation protocol. **a**, Protocol for the calibration duration study. On day 1, the ultrasound sensor was calibrated. Then, BP measurements were tracked for 1-year (daily measurements in the first month, weekly measurements from the second to sixth months, and monthly measurements from the seventh to twelfth months). **b**, Protocol for the daily activity intervention study. The tests were performed in order in one day. Sitting was performed in between different activities to stabilize hemodynamic changes from previous activities. **c**, Protocol for the outpatient clinic study.

The ultrasound sensor was calibrated at the supine position before the testing. After 5 min, the subjects underwent three tests (that is, supine, standing, and supine again) in sequence. **d**, Protocol for the cardiac catheterization laboratory study. The ultrasound sensor was calibrated when the subject was supine for A-line access. The BP measurements were taken during the procedure. **e**, Protocol for the intensive care unit study. The subjects were in Fowler's position during the measurement. The ultrasound sensor was placed on the radial artery contralateral to the radial A-line, and BP measurements were taken for 10 or 12 h.



Extended Data Fig. 3 | Accuracy criteria of different standards. Different standards require different mean differences and standard deviations of the differences for device grading. The ISO 81060–2:2018 criterion 1 is the most widely utilized one. The blue, light blue, and green dots label the ultrasound sensor grades issued by the ISO 81060–2:2018 criterion 1, ISO 81060–2:2018 criterion 2,

and IEEE Std 1708a–2019, respectively. All biases in the ultrasound sensor measurements are significantly below the corresponding requirements, signifying its potential for precise BP measurements. BHS, British Hypertension Society; ESH, European Society of Hypertension; IEEE, Institute of Electrical and Electronics Engineers; ISO, International Organization for Standardization.

Reporting Summary

Nature Portfolio wishes to improve the reproducibility of the work that we publish. This form provides structure for consistency and transparency in reporting. For further information on Nature Portfolio policies, see our [Editorial Policies](#) and the [Editorial Policy Checklist](#).

Statistics

For all statistical analyses, confirm that the following items are present in the figure legend, table legend, main text, or Methods section.

n/a Confirmed

- The exact sample size (n) for each experimental group/condition, given as a discrete number and unit of measurement
- A statement on whether measurements were taken from distinct samples or whether the same sample was measured repeatedly
- The statistical test(s) used AND whether they are one- or two-sided
Only common tests should be described solely by name; describe more complex techniques in the Methods section.
- A description of all covariates tested
- A description of any assumptions or corrections, such as tests of normality and adjustment for multiple comparisons
- A full description of the statistical parameters including central tendency (e.g. means) or other basic estimates (e.g. regression coefficient) AND variation (e.g. standard deviation) or associated estimates of uncertainty (e.g. confidence intervals)
- For null hypothesis testing, the test statistic (e.g. F , t , r) with confidence intervals, effect sizes, degrees of freedom and P value noted
Give P values as exact values whenever suitable.
- For Bayesian analysis, information on the choice of priors and Markov chain Monte Carlo settings
- For hierarchical and complex designs, identification of the appropriate level for tests and full reporting of outcomes
- Estimates of effect sizes (e.g. Cohen's d , Pearson's r), indicating how they were calculated

Our web collection on [statistics for biologists](#) contains articles on many of the points above.

Software and code

Policy information about [availability of computer code](#)

Data collection

Data analysis

For manuscripts utilizing custom algorithms or software that are central to the research but not yet described in published literature, software must be made available to editors and reviewers. We strongly encourage code deposition in a community repository (e.g. GitHub). See the Nature Portfolio [guidelines for submitting code & software](#) for further information.

Data

Policy information about [availability of data](#)

All manuscripts must include a [data availability statement](#). This statement should provide the following information, where applicable:

- Accession codes, unique identifiers, or web links for publicly available datasets
- A description of any restrictions on data availability
- For clinical datasets or third party data, please ensure that the statement adheres to our [policy](#)

The main data supporting the results in this study are available within the paper and its Supplementary Information. Source data for the figures are available from figshare via the identifier <https://doi.org/10.6084/m9.figshare.25511761>.

Research involving human participants, their data, or biological material

Policy information about studies with [human participants or human data](#). See also policy information about [sex, gender \(identity/presentation\), and sexual orientation](#) and [race, ethnicity and racism](#).

Reporting on sex and gender	Information on sex and gender was collected and is reported in the paper.
Reporting on race, ethnicity, or other socially relevant groupings	Information on race was collected and is reported in the paper.
Population characteristics	118 participants, aged 18 or older.
Recruitment	The consented participants were recruited randomly.
Ethics oversight	All studies on the human participants were approved by the Institutional Review Board at the University of California, San Diego (IRB #804119, #191527, #191474, #805176).

Note that full information on the approval of the study protocol must also be provided in the manuscript.

Field-specific reporting

Please select the one below that is the best fit for your research. If you are not sure, read the appropriate sections before making your selection.

Life sciences Behavioural & social sciences Ecological, evolutionary & environmental sciences

For a reference copy of the document with all sections, see [nature.com/documents/nr-reporting-summary-flat.pdf](https://www.nature.com/documents/nr-reporting-summary-flat.pdf)

Life sciences study design

All studies must disclose on these points even when the disclosure is negative.

Sample size	A total of 118 consenting subjects were recruited.
Data exclusions	Data from 5 participants were excluded according to the requirements of the ISO 81060–2:2018 standard and their significant blood-pressure fluctuations during the measurement.
Replication	All attempts at data replication were successful.
Randomization	The participants were randomly selected.
Blinding	No blinding measures were taken deliberately, and all data were processed together by multiple authors.

Reporting for specific materials, systems and methods

We require information from authors about some types of materials, experimental systems and methods used in many studies. Here, indicate whether each material, system or method listed is relevant to your study. If you are not sure if a list item applies to your research, read the appropriate section before selecting a response.

Materials & experimental systems

n/a	Involved in the study
<input checked="" type="checkbox"/>	<input type="checkbox"/> Antibodies
<input checked="" type="checkbox"/>	<input type="checkbox"/> Eukaryotic cell lines
<input checked="" type="checkbox"/>	<input type="checkbox"/> Palaeontology and archaeology
<input checked="" type="checkbox"/>	<input type="checkbox"/> Animals and other organisms
<input type="checkbox"/>	<input checked="" type="checkbox"/> Clinical data
<input checked="" type="checkbox"/>	<input type="checkbox"/> Dual use research of concern
<input checked="" type="checkbox"/>	<input type="checkbox"/> Plants

Methods

n/a	Involved in the study
<input checked="" type="checkbox"/>	<input type="checkbox"/> ChIP-seq
<input checked="" type="checkbox"/>	<input type="checkbox"/> Flow cytometry
<input checked="" type="checkbox"/>	<input type="checkbox"/> MRI-based neuroimaging

Clinical data

Policy information about [clinical studies](#)

All manuscripts should comply with the ICMJE [guidelines for publication of clinical research](#) and a completed [CONSORT checklist](#) must be included with all submissions.

Clinical trial registration	Clinicaltrial.gov registration number: NCT05909605
Study protocol	The full study protocol can be accessed via the Institutional Review Board of The University of California, San Diego.
Data collection	Detailed information of data collection can be found in Methods.
Outcomes	The primary outcome measures involved blood-pressure measurements obtained from the ultrasound sensor. The secondary outcome measures included a calibration process of the ultrasound sensor. These were assessed by using statistical analyses.

Clinical validation of a wearable ultrasound sensor of blood pressure

In the format provided by the
authors and unedited

Contents

Supplementary Discussion 1 Approaches for measuring blood pressure (BP) in clinical settings.....	3
Supplementary Discussion 2 Summary of different standards.	6
Supplementary Discussion 3 Device safety evaluation.	7
Supplementary Discussion 4 Comparison of different simulation models for BP.....	10
Supplementary Discussion 5 Arterial wall components analysis.....	13
Supplementary Discussion 6 Factors affecting calibrated BP.	14
Supplementary Discussion 7 Statistical methods for agreement evaluation.	14
Supplementary Discussion 8 BP changes throughout the day due to various activities.	16
Supplementary Discussion 9 Four–quadrant plot and concordance rate.	17
Supplementary Discussion 10 Bland–Altman analysis for repeated measurements.	18
Supplementary Discussion 11 BP monitoring in patients with large BP fluctuations...	19
Supplementary Discussion 12 BP waveform analysis.....	20
Supplementary Discussion 13 Wavelet coherence analysis.....	21
Supplementary Discussion 14 Bootstrapping.....	23
Supplementary Discussion 15 BP measurement in participants with aging skin.	24
Supplementary Discussion 16 Design of the wearable ultrasound sensors.	24
Supplementary Fig. 1 Device re–engineering.....	25
Supplementary Fig. 2 Critical device–artery alignment in existing prototypes.....	26
Supplementary Fig. 3 Timeline of BP monitoring standards.	27
Supplementary Fig. 4 Criteria for selecting participants of different standards.....	28
Supplementary Fig. 5 Connected device–artery alignment in this work.....	29
Supplementary Fig. 6 Piezoelectric property characterizations.....	30
Supplementary Fig. 7 Simulated and scanned device acoustic fields.....	31
Supplementary Fig. 8 Pulse–echo responses of a transducer element with and without a backing layer.	32
Supplementary Fig. 9 Optical images of the re–engineered ultrasound sensor.....	33
Supplementary Fig. 10 Thermal characterization of the ultrasound sensor.....	34
Supplementary Fig. 11 Arterial wall distension mechanism.....	35

Supplementary Fig. 12 Comparison of pressure waveforms and diameter waveforms.	36
Supplementary Fig. 13 Calibration duration of the ultrasound sensor for participants #2, #3, and #4.	37
Supplementary Fig. 14 Bland–Altman plots of calibration results for each participant.	38
Supplementary Fig. 15 Summarized effects of different daily activities on cardiovascular parameters.	39
Supplementary Fig. 16 Bland–Altman plots of repeated measurements in the outpatient clinic study.	40
Supplementary Fig. 17 Waveform comparison on excluded patients in the catheterization laboratory study.	41
Supplementary Fig. 18 Bland–Altman plots of BP distribution between participants in the cardiac catheterization laboratory study.	42
Supplementary Fig. 19 Bland–Altman plots of repeated measurements in the cardiac catheterization laboratory study.	43
Supplementary Fig. 20 Waveform comparison on included patients in the catheterization laboratory study.	45
Supplementary Fig. 21 Dynamic time warping analysis.	46
Supplementary Fig. 22 Fowler’s position.	48
Supplementary Fig. 23 Wavelet coherence spectrogram between the bootstrapped dataset and A–line dataset.	49
Supplementary Fig. 24 Comparison of average of maximum magnitude–squared coherence for bootstrapped data and experimental data.	50
Supplementary Table 1 Testing methods for each validation study.	51
Supplementary Video 1 BP waveforms recorded during sphygmomanometer inflation and deflation.	52

Supplementary Discussion 1 | Approaches for measuring blood pressure (BP) in clinical settings.

BP is a vital sign routinely monitored in clinical settings due to its importance in diagnosing and managing various cardiovascular conditions. The approach for measuring BP has been improved over time with advancements in medical technology, and currently, several techniques are employed clinically with their unique advantages and drawbacks.

(1) Auscultation. Auscultation is one of the traditional and most commonly used methods for BP measurement in the clinic¹. This technique utilizes a manually inflated sphygmomanometer, a stethoscope, and an inflatable cuff wrapped around the participant's upper arm.

The key component is the hearing of Korotkoff sounds, which are a series of distinct, progressively changing sounds that correspond to different phases of the arterial blood flow². The process begins by inflating the cuff to a pressure higher than the systolic blood pressure (SBP), which temporarily halts blood flow. As the pressure in the cuff gradually reduces, the first appearance of faint, tapping sounds (Phase I Korotkoff) indicates the SBP, which represents the point at which the arterial pressure is just sufficient to force blood past the occluded area. These sounds continue as the pressure in the cuff drops until the sounds eventually disappear at a certain point (Phase V Korotkoff), marking the diastolic blood pressure (DBP). This signifies the point at which the artery is no longer constricted, and blood is flowing freely.

While the mercury sphygmomanometer is traditionally considered the gold standard for in-office BP measurement, global restrictions (particularly in California) on mercury use have led to a decline in its application¹. Aneroid sphygmomanometers have emerged as the prevalent alternative. Instead of transferring pressure to a mercury column, they are designed to transfer the detected pressure via an elastic expansion chamber into gauge needle movement³. While these devices offer environmental advantages, their accuracy may deteriorate over time during clinical usage due to wear and tear of mechanical components, potential misalignment, and the effects of repeated stress and eventual fatigue on the internal parts. Consequently, only aneroid sphygmomanometers that undergo routine technical inspection, including recalibration approximately every six months, can assure reliable measurement accuracy².

Although auscultation can provide overall accurate results, it still faces multiple challenges in clinical practices. The inflation and deflation processes of the cuff take approximately a minute, thus constraining the temporal resolution of the readings. This can be an impediment, especially in situations where continuous or frequent monitoring of BP is required. Further, some patients may experience physical discomfort associated with the use of sphygmomanometers. Repetitive inflation of the cuff can cause soreness or even bruising in the upper arm. For patients who require frequent or prolonged monitoring, this can cause discomfort and may interfere with their daily activities.

(2) *Doppler ultrasound*. Devices incorporating this technique replace the stethoscope with an operator-held continuous wave Doppler probe placed over the brachial artery underneath the cuff. As the cuff continuously deflates, the arterial wall starts to dilate at SBP, causing a Doppler phase shift in the reflected ultrasound waves. The DBP is identified when this arterial dilation ceases (no flow signal from the Doppler probe)⁴. Using the Doppler probe can assist in identifying the BP especially for patients with faint Korotkoff sounds, such as those with muscular atrophy⁵.

(3) *Oscillometry*. Oscillometric monitoring captures the pressure pulses utilizing a cuff that can be automatically inflated and deflated⁶. The oscillometer first inflates the cuff to a pressure above the expected SBP to occlude the artery. As the oscillometer gradually deflates the cuff, it measures the oscillation amplitude in the arterial wall caused by the pulsatile arterial pressure and generates an oscillometric envelope, which represents the variation in oscillation amplitude. The pressure in the cuff counteracts the pressure in the artery. When the cuff pressure is much higher than the SBP, the cuff completely occludes the artery, preventing blood flow. Because the artery is fully compressed, there are minimal to no oscillations detected by the oscillometer. On the other side, when the cuff pressure is much lower than DBP, the artery is almost in its fully open state during the entire cardiac cycle. As a result, the amplitude of these oscillations is minimal. Therefore, the amplitude of these oscillations typically forms a spindle-like shape, and the amplitude is at its maximum when the cuff pressure is approximately equal to the mean arterial pressure (MAP)². SBP and DBP will then be indirectly estimated via empirically derived algorithms⁷.

A major advantage of oscillometric monitoring lies in its design, which does not necessitate a stethoscope placed over the brachial artery. This makes it less prone to external noise interference⁵. Moreover, its automated process is particularly suited for at-home BP measurement, helping to minimize the “white-coat” effect (e.g., a phenomenon where BP readings are higher when taken by a healthcare professional due to patient anxiety)⁸. However, the interplay of both physiological and technical factors must be meticulously accounted for when using algorithms to transfer the sensor’s readings into accurate BP values⁷. Therefore, the accuracy of oscillometric measurements necessitates a comprehensive validation process against established standards before it can be employed.

(4) *Finger cuff*. This method utilizes an inflatable cuff wrapped around the middle phalanx to monitor BP⁹. This technique employs a built-in photoplethysmographer and automatic algorithms to maintain the pulsating finger artery at a constant volume throughout cardiac cycles by adjusting the cuff pressure. The varying cuff pressure then equals the dynamic finger arterial pressure. The derived finger arterial pressure is subsequently related to a brachial artery pressure using transfer functions⁹. This approach effectively estimates the fluctuations of the pulse pressure⁵. However, it does not yet meet the necessary criteria for clinical interchangeability with currently used invasive devices, limiting its application to specific

clinical contexts only⁹. Furthermore, it can be impractical to wear throughout the day as its placement on the hand can interfere with day-to-day activities.

(5) *Intra-arterial cannula.* The arterial line (A-line) represents the gold standard in BP measurement, providing accurate, beat-to-beat information. This method involves the insertion of a Teflon or polyurethane cannula into an artery, ideally a non-end artery (i.e., an artery that is not a sole or terminal source of blood to its target tissue and has potential collateral pathways) like the radial artery, which ensures blood supply through collateral arteries even in the event of thrombosis. The hand's collateral supply can be assessed using Allen's test¹⁰. If cannulation of the radial artery proves challenging, end arteries such as the brachial or femoral may be used with due caution regarding distal arterial sufficiency. The cannula connects to a disposable tubing system, which delivers a constant infusion of either plain or heparinized 0.9% saline at a rate of 2~4 mL/h. This continuous infusion helps avert cannula occlusion by thrombus². The tubing system must maintain pressurization to ensure consistent flow into the arterial system. The infusion fluid in the tubing contacts a diaphragm that moves in sync with the transmitted pressure waveform. A transducer then converts this movement into an electrical signal.

The accuracy of A-line monitoring is paramount in critical care settings. The damping effect in the A-line system refers to a distortion of the measured arterial waveform, preventing it from truly representing the intra-arterial pressure. This discrepancy can arise when the arterial pulse frequency aligns with the natural resonance frequency of the arterial catheter and its tubing, amplifying (i.e., under-damping) the pressure waveform. On the contrary, an over-damped system poorly transmits pressure waves, resulting in a blunted waveform. This may be caused by the presence of small clots or air bubbles, extended line lengths or additional connectors, and improperly calibrated pressure transducers¹¹. To evaluate the system's damping, a fast flush test is typically conducted by swiftly introducing a saline bolus¹². An under-damped system will exhibit oscillations post-flush, while an over-damped one will show a gradual waveform return. In contrast, an optimally damped system displays a swift upstroke and downstroke with limited oscillations. Besides checking the damping effect of the A-line, the transducer must be held at the same elevation level as the patient, traditionally at the right atrium. Zeroing the system is also critical and is achieved by exposing the transducer to atmospheric pressure before the cannulation.

A-lines are particularly valuable when anticipating rapid BP fluctuations due to cardiovascular instability, large fluid shifts, or pharmacological effects. They are also useful when non-invasive BP monitoring is either impossible or likely inaccurate, such as in patients with obese body habitus, cardiac arrhythmias, or non-pulsatile blood flow during cardiopulmonary bypass². In addition, A-lines facilitate continuous long-term measurements in critically ill patients, avoiding the localized tissue damage caused by repeated cuff inflation and enabling regular sampling for blood gases and laboratory analysis.

Despite being the gold standard, A-lines are uncomfortable and carry potential risks due to their invasive nature^{13,14}. Complications may include vascular occlusion, where the blood vessel becomes blocked, and thrombosis, a condition of clot formation that can interrupt blood flow. Ischemia, or inadequate blood supply to an organ or tissue, is also a risk. Hematoma formation, or blood pooling outside of a vessel, can lead to inflammation and further complications. Moreover, there is the possibility of catheter-related infections, ranging from localized to systemic, and can even cause severe sepsis.

Supplementary Discussion 2 | Summary of different standards.

The procedures for validating BP measuring devices date back to the 1980s (Supplementary Fig. 3). In 1987, the United States Association for the Advancement of Medical Instrumentation published the first comprehensive standard for evaluating the accuracy of BP monitors¹⁵. A minimal sample size of 85 participants was required in this standard. This standard was further revised in 1992, 1994, 1996, 2002, 2003, 2006, and 2008 to expand the scope of applications to the latest BP measuring devices.

In 1990, the British Hypertension Society developed a protocol for evaluating BP measurement devices¹⁶, also with a sample size requirement of 85 participants. The British Hypertension Society working party subsequently revised its protocol in 1993 in the interest of providing a comprehensive procedure for the evaluation of all BP measuring devices, including those for intermittent 24 hrs BP measurement¹⁷.

In 1999, the German Hypertension League (Deutsche Hochdruckliga) developed the Quality Seal Protocol for BP measuring devices¹⁸. This protocol was based on the requirements according to EN 540:1993¹⁹, with additional requirements for the sample size ($N \geq 96$).

The European Society of Hypertension working group on BP monitoring introduced the European Society of Hypertension International Protocol in 2002²⁰. The European Society of Hypertension International Protocol for validation of BP measuring devices was published based on the Association for the Advancement of Medical Instrumentation and British Hypertension Society protocols but permitted a rationalization and simplification of validation procedures. The major difference was a smaller sample size requirement ($N \geq 33$). After analyzing reported studies since 2002, the European Society of Hypertension working group modified the participants' range, simplified the validation process, and updated their protocol in 2010²¹.

In 2004, the European Committee for Standardization published its standard (EN 1060–4:2004) for BP measuring devices. It is different from the validation process of other standards but has similar requirements for sample size ($N \geq 85$).

In 2009, the International Organization for Standardization developed another standard (ANSI/AAMI/ISO 81060–2:2009), which adopted aspects of the AAMI SP:10 (e.g., sample

size and validation criteria) and has been recognized by the Association for the Advancement of Medical Instrumentation Sphygmomanometer Committee²². A revised version of the ANSI/AAMI/ISO standard was released in 2013²³.

In 2014, the Institute of Electrical and Electronics Engineers standard committee published the IEEE Std 1708–2014, which established a normative definition of wearable cuffless BP measuring devices and the objective performance evaluation of these kinds of devices²⁴. It required two phases of the validation process with a smaller sample size ($N \geq 45$). It is worth noting that IEEE Std 1708–2014 was not approved by the Food and Drug Administration²⁵. Therefore, the Institute of Electrical and Electronics Engineers working group updated the amendment (IEEE Std 1708a–2019) in 2019 to increase the requirements of sample size to 85²⁶.

Different groups (e.g., patients, consumers, manufacturers, and scientists) would be best served if all BP measuring devices were assessed for accuracy according to an agreed single validation protocol that had global acceptance. Therefore, an international initiative was taken by the Association for the Advancement of Medical Instrumentation, the European Society of Hypertension, and the International Organization for Standardization to develop a universal standard for device validation. In 2018, the AAMI/ESH/ISO standard (AAMI/ESH/ISO, ISO 81060–2:2018) was published and is now regarded as the single universal standard to replace all other previous standards/protocols²⁵.

In response to the growing prevalence of wearable BP sensors, the International Organization for Standardization introduced a new standard, ISO 81060–3:2022 in 2022, specifically to validate these devices²⁷.

The main standards implemented in validating BP measuring devices in the United States are EHS–IP 2010, ISO 81060–2:2018, BHS 1993, and IEEE Std 1708a–2019. They have similar requirements for sample selection and accuracy. Except for the $N \geq 33$ requirement from the EHS–IP 2010, other standards require that the sample size is at least 85 participants (ISO 81060–2:2018 has an $N \geq 15$ requirement for using an invasive reference method). Given the expected 5 mmHg mean difference and 8 mmHg standard deviation, a 95% confidence interval ($\alpha = 0.05$) and a statistical power of 98% ($\beta = 0.02$) yield a sample size of 85 participants²⁵. The British Hypertension Society has no clear requirements as to the sex distribution of the sample, whereas other standards require more than ~30% of males and females. Similarly, the British Hypertension Society lacks explicit age distribution criteria, but other standards set distinct age parameters for adult groups. Given that the distribution of BP is a pivotal factor influencing device accuracy, each standard outlines its unique specifications for this aspect (Supplementary Fig. 4).

Supplementary Discussion 3 | Device safety evaluation.

We characterized mechanical and thermal safety based on guidelines from the Food and Drug Administration²⁸ and the American Institute of Ultrasound in Medicine²⁹.

(1) *Mechanical safety.* Quantitative characterization of the acoustic field is imperative for the development and pre-clinical validation of ultrasound devices, as well as in the planning of clinical procedures. We have confirmed the acoustic intensity of the ultrasound sensor by hydrophone measurement. In the experiment, we used a hydrophone mounted on a 3D linear motor in a water tank to measure the signal from the ultrasound sensor.

Each individual element of the ultrasound sensor is transmitted simultaneously to form a plane wave beamforming strategy. Thus, the highest beam intensity was near the ultrasound sensor (Supplementary Fig. 7). Therefore, we characterized the beam intensity near the aperture by scanning X–Y plane at depth of 1 mm.

To perform accurate voltage to pressure conversion, the hydrophone system loaded sensitivity $M_L(f)$ could be calculated:

$$M_L(f) = G(f)M_c(f)\frac{C_H}{C_H+C_A+C_c}, \quad (1)$$

where the preamplifier gain $G(f)$ was 20 dB, hydrophone end-of-cable open circuit sensitivity $M_c(f)$ was $2.512 \times 10^{-8} \text{ V}\cdot\text{Pa}^{-1}$ at 7 MHz, capacitance of hydrophone C_H was 70 pF, capacitance of preamplifier C_A was 7 pF, and the capacitance of connector C_c was zero because the preamplifier was connected directly to the hydrophone³⁰.

Using this hydrophone system loaded sensitivity, we could calculate the pressure variable $p(z)$:

$$p(z) = \frac{V_{output}(z)}{M_L(f)}, \quad (2)$$

where $V_{output}(z)$ was the output voltage, and z was the depth of 1 mm in this study. Then, the attenuated pressure could be calculated as:

$$p_\alpha(z) = p(z)10^{(-\alpha z f_{awf}/20\text{dB})}, \quad (3)$$

where α was the attenuation coefficient ($0.3 \text{ dB}\cdot\text{cm}^{-1}\cdot\text{MHz}^{-1}$)²⁸ and f_{awf} was the acoustic working frequency 7 MHz³¹. The attenuated pulse pressure squared integral $ppsi_\alpha(z)$ could be estimated:

$$ppsi_\alpha(z) = \int p_\alpha^2(z, t)dt, \quad (4)$$

The attenuated pulse intensity integral $pui_\alpha(z)$ was defined as:

$$pui_\alpha(z) = \frac{1}{\rho c} ppsi_\alpha(z), \quad (5)$$

where ρ was the density of water $997 \text{ kg}\cdot\text{m}^{-3}$ and c was the speed of sound in water $1480 \text{ m}\cdot\text{s}^{-1}$. Finally, the attenuated spatial peak pulse average intensity could be calculated as:

$$I_{SPPA,\alpha}(z) = \frac{1}{t_d(z)} pui_\alpha(z), \quad (6)$$

where $t_d(z)$ was the pulse duration, which was 1.25 multiplied by the interval between the time when the time integral of the square of the instantaneous acoustic pressure reached 10% and 90% of its final value³². And the attenuated spatial peak temporal average intensity could also be calculated as:

$$I_{SPTA,\alpha}(z) = PRF \text{ } p_{r,\alpha}(z), \quad (7)$$

where PRF was the pulse repetition frequency 1000 Hz.

The mechanical index MI measured cavitation–related problems due to the mechanical waves of ultrasound^{28,33}. The derated MI was defined as:

$$MI = \frac{p_{r,\alpha}(z)}{\sqrt{f_{awf}}}, \quad (8)$$

where $p_{r,\alpha}$ was the attenuated peak rarefactional pressure (i.e., the maximum negative acoustic pressure in the waveform) in MPa.

The Food and Drug Administration imposes several application–specific exposure limits, including limits for the peripheral vessel, cardiac, fetal, and ophthalmic ultrasonics³⁴. Considering the ultrasound sensor focuses on peripheral arteries (e.g., brachial and radial artery) monitoring, the acoustic exposure level on the peripheral vessel has been chosen ($I_{SPPA} \leq 190$ W/cm², $I_{SPTA} \leq 720$ mW/cm², $MI < 1.9$). The I_{SPPA} , I_{SPTA} , and MI of the ultrasound sensor were 23.00 W/cm², 5.76 mW/cm², and 0.29, respectively, which were all much lower than the Food and Drug Administration–allowed intensity for medical applications.

(2) *Thermal safety*. We characterized the thermal safety by thermal imaging and thermal index calculation.

First, the heat generated from the ultrasound sensor was characterized by thermal imaging. The sensor was attached to a human chest phantom that has a heat transfer coefficient similar to skin. A Verasonics system excited the transducers for 48 hrs to simulate long–term monitoring of the human body. The device had a slight temperature increase (< 1 °C), and the temperature remained at around 22 °C during the testing period (Supplementary Fig. 11).

Second, the thermal index (TI) was calculated based on hydrophone measurements. There are three types of TI : soft tissue TI (TIS), bone TI (TIB), and cranium TI (TIC)³⁵. Because there was no bone in the scanning plane of interest in this study and the beam intensity was highest at the surface (Supplementary Fig. 7), we only calculated the TIS at surface (TIS_{as}):

$$TIS_{as} = \frac{P_{1 \times 1} \cdot f_{awf}}{210 \text{ mW MHz}}, \quad (9)$$

where $P_{1 \times 1}$ is the bounded–square output power over an one square centimeter area in mW. $P_{1 \times 1}$ can be measured by the hydrophone transverse plane scan and integrating over the beam cross–section with an intensity boundary of –26.2 dB of the maximum value. $P_{1 \times 1}$ was measured to be 5.13 mW, so the TIS was calculated to be 0.17, which was far below the threshold recommended by the American Institute of Ultrasound in Medicine for long–term monitoring (i.e., $TIS \leq 1.5$)²⁹.

Supplementary Discussion 4 | Comparison of different simulation models for BP.

An appropriate mathematical model is the key to measuring the BP via wearable technologies. There are four major models that have been widely used, as summarized in the following.

(1) *Linear relationship model.* Among the various models available for BP monitoring, the linear relationship model stands out for its simplicity and clarity. This model is based on the concept that the difference between MAP and DBP remains constant across the arterial tree³⁶, which can be used to calculate the pulse pressure at the target artery based on the pulse pressure at the reference artery³⁷.

This model employs a straightforward linear conversion that translates the diameter waveform, $D(t)$, to the pressure waveform. Calibration of the end diastolic and mean arterial diameter, D_d and $\bar{D}(t)$, to the DBP and MAP respectively, results in the derivation of the conversion factor k ³⁸:

$$k = \frac{MAP - DBP}{\bar{D}(t) - D_d}, \quad (10)$$

The diameter waveform is transformed into the BP waveform through the application of the conversion factor k , and the slope–intercept b is measured at the DBP:

$$P(t) = D(t) \cdot k + b, \quad (11)$$

While the diameter of elastic arteries, such as the carotid artery, changes almost linearly with pressure in participants with normal BP³⁹, stiffer peripheral arteries like the radial artery present distinct characteristics. Due to their reduced compliance and potential arterial remodeling, this linear relationship can potentially display overfitting³⁸. Given that these peripheral arteries are commonly used for BP measurements in clinics, the applicability of the linear relationship model in clinical scenarios has been constrained.

(2) *Pulse wave analysis.* This model analyzes the pulse contour to quantify BP values⁴⁰. When blood is ejected from the heart, it generates a pressure wave that travels along the arterial walls. Due to varying hydraulic impedance at each arterial bifurcation or site of arterial impedance discontinuity, a portion of this pressure wave is reflected⁴¹. The resulting pressure waveform is thus a superposition of a forward wave from the heart to the periphery and reflected waves from the systemic periphery back to the heart (Supplementary Discussion 12). This analysis method helps quantify the temporal and amplitude characteristics of pulse contours, establishing a framework to correlate recorded waveform to the actual BP values.

Pulse wave analysis is advantageous for diagnosing masked hypertension by examining the pulse contour during the systole phase⁴². Masked hypertension is characterized by BP readings that appear normal in clinical environments but are elevated in other settings. While the actual BP values might fluctuate over time, the waveform contour for patients with masked hypertension remains relatively consistent. Consequently, attributes such as the timing, magnitude, and morphology of the BP waveform linked with masked hypertension can be effectively detected using pulse wave analysis. However, it may induce larger errors when

applied to participants during interventions, such as daily activities or vasodilating drug therapy^{42,43}. Another challenge associated with the pulse wave analysis is its inter-participant variability. The observed diameter or volume change waveforms are highly dependent on the individual's physiological and anatomical characteristics. It is challenging to adapt this analysis method to the specificities of the participant, especially for patients with various arterial diseases⁴³.

(3) *Pulse wave velocity*. Pulse wave velocity and its reciprocal, pulse arrival time and pulse transit time, have recently emerged as promising models for BP measurement⁴⁴. The pulse transit time, a measure of the time delay in the propagation of pressure waves through the vascular system, can be computed from pulse waveforms measured on different spots through the arterial tree. Another notable parameter, pulse arrival time, gauges the time difference between the R-peak of the electrocardiography and a specific point of the pulse waveform. It encompasses both the pulse transit time and the pre-ejection period delay, represented by:

$$PAT = PTT + PEP, (12)$$

where PAT is the pulse arrival time, PTT is the pulse transit time, and PEP is the pre-ejection period, during which the electrical signal is converted into a mechanical pumping force for isovolumetric contraction to open the aortic valve⁴⁵. Pulse transit time is a measure of arterial stiffness because this duration is influenced by the elasticity or stiffness of those arteries. As arteries become stiffer, the pulse wave travels faster, leading to a shorter pulse transit time and vice versa.

Pulse wave velocity can be calculated using the pulse transit time over a certain distance between proximal and distal arterial sites in the arterial tree:

$$PWV = L/PTT, (13)$$

where PWV stands for the pulse wave velocity and L is the distance between the proximal and distal arterial sites.

The measured pulse wave velocity can be translated into arterial pressure by using two key equations. The first one is Hughes equation that relates Young's modulus (a parameter that quantifies a material's stiffness by relating stress to strain) to arterial pressure⁴⁶:

$$E = E_0 e^{aP}, (14)$$

where E is Young's modulus at a specific pressure, E_0 is Young's modulus at zero pressure, P is the arterial pressure, and a is a parameter related to the vessel's mechanical properties.

The other one is the Moens-Korteweg equation in which the elasticity of vessels determines the pulse wave velocity⁴⁷:

$$PWV = \sqrt{\frac{Eh_0}{2\rho R_0}}, (15)$$

where h_0 and R_0 are the vessel thickness and the lumen diameter at a typical pressure (e.g., MAP or DBP), and ρ is the blood density.

Combining equations (14) and (15), the relationship between pressure and pulse wave velocity can be derived as:

$$PWV = \sqrt{\frac{h_0 E_0 e^{aP}}{2\rho R_0}}, \quad (16)$$

These equations indicate that a rise in BP correlates with an increase in PWV. Nonetheless, the Moens–Korteweg equation is founded upon two principal assumptions: firstly, the arterial wall is sufficiently thin, resembling a delicate shell; and secondly, the arterial thickness and radius remain unchanged irrespective of variations in BP. In the context of human arteries, the veracity of these assumptions is questionable⁴⁶. In addition, the Hughes equation is rooted in empirical observation and lacks a theoretical framework⁴⁶. Consequently, a range of mathematical and empirical models have been developed to simplify the association between BP and PWV:

$$BP = \alpha \times \ln(PWV) + \beta, \quad (17)^{45}$$

$$BP = \alpha \times PWV + \beta, \quad (18)^{48}$$

$$BP = \alpha \times PWV^2 + \beta, \quad (19)^{46}$$

where α and β are considered constants that depend on the material properties, geometry of the artery, and demographic data of the participant⁴⁵.

Pulse wave velocity is considered one of the most important clinical parameters for evaluating cardiovascular risk, vascular adaptation, and therapeutic efficacy⁴⁹. However, there are several pitfalls of pulse wave velocity related models. First, those models assume a constant relationship between BP and pulse wave velocity. While other factors related to cardiovascular activities can be added to enhance the reliability of the model, different vascular diseases are impossible to be thoroughly considered. Therefore, its performance cannot be guaranteed for patients with different diseases. Second, requiring two sensors at different body sites limits its applicability. Although a long distance between two sensors is suggested to obtain a larger pulse transit time or pulse arrival time, and thus a more precise BP value, accurate assessment of travel distance remains ambiguous, especially for two distant sensors.

(4) Exponential relationship model. The exponential relationship model between artery cross-section and BP suggests that as BP increases, the cross-sectional area of the artery expands exponentially.

Assuming that the target arteries are rotationally symmetrical, $A(t)$ can then be calculated as:

$$A(t) = \frac{\pi d^2(t)}{4}, \quad (20)$$

where $d^2(t)$ equals to the square of the diameter waveform from the target arteries. The BP waveform can be derived as:

$$P(t) = P_d \cdot e^{\alpha \left(\frac{A(t)}{A_d} - 1 \right)}, \quad (21)$$

where P_d is diastolic pressure, A_d is the diastolic arterial cross-section, and α is the vessel stiffness coefficient, which can be calculated by:

$$\alpha = \frac{A_d \ln(P_s/P_d)}{A_s - A_d}, \quad (22)$$

where A_s is the systolic arterial cross-section, P_s is the SBP. Since equation (20) is valid over a pressure range⁵⁰, α is considered pressure independent and constant within that range. If there is a substantial variation of blood volume and flow, the BP may move outside of this range. In this case, the relationship between arterial cross-section and BP would change, and a new α is needed. To accurately determine α , it is worth noting that P_s and P_d must be obtained at the same position as $A(t)$.

The conversion from arterial cross-section to BP using the exponential relationship model exhibits a high consistency to the experimental data^{51,52}. Unlike the linear relationship model, which assumes constant vessel elasticity across varying BP, the exponential model considers the distinct elastic properties of the various components of the vessel, such as collagen fibers, elastic fibers, and smooth muscles (Supplementary Discussion 5). These elements model the vessels with pressure-dependent elasticity, leading to different Young's modulus under various pressure conditions (Supplementary Fig. 12)⁵³. This aligns with the observed exponential relationship between vessel diameter and BP, making the exponential relationship model more practical and accurate for BP measurements. Compared to the pulse wave velocity model, the exponential relationship model only requires a sensor at the targeted site and a simple derivation process, enhancing its use convenience, and making it more suitable for continuous BP monitoring across diverse settings. Additionally, interventions that may alter the morphology of the BP waveform have minimal impact on the accuracy of the measurements, making this model more robust than the pulse wave analysis model. Consequently, we chose the exponential relationship model for this study.

Supplementary Discussion 5 | Arterial wall components analysis.

The arterial wall is a composite of three layers, which contain varying amounts of elastin, collagen, and vascular smooth muscle cells that dominate the mechanical behaviors of the arteries⁵³. The *intima*, or inner layer, of the artery is made up of a single layer of endothelial cells and an extremely thin lamina of elastin, which provides a smooth wall and selective permeability to substances between the bloodstream and the tissues. The middle *media* layer is made up of elastin, collagen, and vascular smooth muscle that are embedded in an extracellular matrix. The *adventitia*, or outside layer, is made up of connective tissue that merges with the surroundings.

Compared to elastin fibers that have low Young's modulus, collagen fibers, which form a network in both the media and the adventitia, are much stiffer. Usually, the unloaded collagen fibers possess a degree of slackness. Therefore, their full stiffness is not obvious until the vessels are stretched to the extent where the slackness is gone. For a combination of elastin and collagen fibers, the effect of increasing distension where the collagen fiber becomes taut and reacts to the load will result in a nonlinear behavior. An exponential stress-strain curve will emerge from the constant recruitment of additional collagen fibers as the load increases

(Supplementary Fig. 12)⁵³. The purpose of the elastin and collagen fibers is to maintain a relatively stable strain within the arteries to counteract the transmural pressure.

The smooth muscle cells, on the other hand, provide active tension by contraction or relaxation under physiological control. Their behavior can be modulated by various external stimuli, including neurological signals⁵⁴, endocrine factors⁵⁵, physical forces⁵⁶, and metabolic elements⁵⁷. These influences can result in the contraction or relaxation of these cells, thus affecting arterial stiffness. Importantly, peripheral arteries exhibit a higher concentration of smooth muscle content compared to central arteries, enabling more precise control of vascular resistance by modulating the tension or relaxation of these muscle cells.

Supplementary Discussion 6 | Factors affecting calibrated BP.

The exponential model derives BP from the arterial diameter with the assumption that the stress–strain curve of the arteries is exponential. Nevertheless, several factors may influence this relationship and thus the calibration accuracy. First are chronic or acute changes in arterial stiffness during the BP measurement⁵⁸. Pathological states, including hypertension or atherosclerosis, can substantially modulate the complex hemodynamics of blood flow (e.g., laminar or turbulence) and blood rheology. This can increase the shear stress of the vessel wall⁵⁹. Age–induced arterial stiffness can occur through elastin loss or arterial collagen deposition⁶⁰. Furthermore, acute alterations in vascular tone, manifesting as vasoconstriction or vasodilation, regulate blood transport for optimal metabolic supply across tissues in the body. Second, in this work, the artery is assumed to be rotationally symmetrical to calculate the arterial area, which is converted into BP (Supplementary Discussion 4). However, arteries seldom exhibit perfect circularity⁶¹. Consequently, with arterial deformation induced by variations in muscle composition or limb orientation, diameter measurements may be affected. As a result, it is imperative to undertake a comprehensive and longitudinal study of BP accuracy to monitor potential deviations after the initial calibration.

Supplementary Discussion 7 | Statistical methods for agreement evaluation.

To adopt a new BP sensing device, it is important to ensure that the device can provide measurements as accurate as reference devices. Various statistical methods have been used to quantitatively interpret the agreement. The first method that has been widely used is the Pearson correlation coefficient⁶². However, this is inappropriate because it only measures the strength of linear association between variables.

A paired t–test is also commonly used to test the significance of differences between the means of two sets of measurements⁶³. Non–significant results have been misunderstood as implying no differences. However, valid interpretation depends on the sample size, and the mean can be affected by the extremely large or extremely small values. Moreover, the mean difference only indicates whether there is any systematic bias. In an agreement study, we are not only interested in the mean difference (i.e., bias), but also the variability in the differences, because high variability indicates that individual differences can be substantial in an unacceptable fraction

of the participants. What matters is that each measurement from the standard device should be comparable to the new device.

Another method used for assessing agreement is the intra-class correlation coefficient⁶³, which was initially devised to assess reliability. Reliability denotes the extent to which measurements can be replicated⁶². However, it does not directly reflect the actual error (i.e., bias) between pairs of measurements using different devices⁶⁴. Therefore, relying solely on the intra-class correlation coefficient may not provide a comprehensive assessment of agreement.

The Bland–Altman method evaluates how close each pair of measurements are⁶⁵. One assumption of the Bland–Altman method is that the distribution of the differences approximately follows a normal distribution⁶⁵. Histograms are usually used to examine the distribution of the differences. When the data follow a normal distribution, approximately 95% of the differences will fall within the mean difference ± 1.96 times the standard deviation of the differences. These limits are therefore referred to as the 95% limits of agreement. If these limits are sufficiently narrow, the agreement between the devices is deemed small. The Bland–Altman method employs a scatter plot, graphing the difference between two measurements against their average. While this approach defines the limits of agreement, it doesn't dictate whether these limits are acceptable. The best way to use it would be to define a priori acceptable differences (e.g., limits of agreement or standard deviation of difference) based on biologically or analytically relevant criteria, and then to obtain the statistics to see if these limits are exceeded. This method has been used by most of the standards to validate BP measurement devices^{24,25,66}. When there are repeated measurements in the same participant, a more complicated analysis can be performed (Supplementary Discussion 10).

We incorporated dynamic time warping to evaluate the agreement between BP waveforms recorded by the ultrasound sensor and A-line. In dynamic time warping, each pixel in the analyzed results denotes the distance between the pair of two points in the two time series data, with the darkness indicating the different distance between the two points (Supplementary Fig. 24). The red line shows the best match with minimal distance. The more skewing or curving of this line, the more warped or shifted are the two time series data against each other. This approach is particularly advantageous for this study because it does not require the time series data to be exactly aligned. For example, in the catheterization laboratory study, all patients included in the study exhibited almost straight diagonal lines in their dynamic time warping analyses. The small zig-zag patterns indicate the mismatch of each pulse measured by the A-line on the radial artery and those by the ultrasound sensor on the brachial. Specifically, this indicates that the phase of the waveform captured by the ultrasound sensor alternates between being ahead of and being lagging behind the waveform recorded by the A-line. The patients excluded in the study represent different degrees of skewing and curving patterns, which correspond to the distinct difference between the BP waveforms recorded by the A-line and the ultrasound sensor (Supplementary Fig. 24b).

However, the dynamic time warping also has its limitations. The larger the relative value of each plot, the larger the average distance is between the two time series data. For example, participant #12 with notable BP value differences between the two recorded waveforms represents the maximum value in dynamic time warping. However, even though all patients included in the study exhibited almost straight diagonal lines in their dynamic time warping analyses, their relative values were largely different, which was influenced by their mean difference of the BP waveforms and pulse pressure range (i.e., the difference between systolic BP and diastolic BP) measured by the ultrasound sensor and the A-line. Despite this limitation, dynamic time warping remains essential for comparing the BP waveform patterns and provides reliable agreement evaluation.

Supplementary Discussion 8 | BP changes throughout the day due to various activities.

Various daily activities can affect BP. This study examined 12 different daily activities in comparison to seated position in a small sample size of healthy volunteers to understand their impact on BP. The effects of these activities on BP can be generally categorized into three distinct categories of alterations in the cardiovascular system: modifications in cardiac output, vascular tone, and blood volume (Supplementary Fig. 17).

Cardiac output is defined as the blood flow from the heart through the left ventricle and equals the stroke volume times heart rate⁶⁷. While stroke volume remains relatively consistent in the absence of notable cardiac anomalies, heart rate exhibits diurnal fluctuations due to myriad stimuli. Predominantly, these stimuli modulate the central nervous system, affecting both the sympathetic and parasympathetic nervous systems, which exert opposing influences on heart rate and BP⁶⁸. Specifically, the sympathetic response elevates during stress or fight-or-flight situations, leading to the release of catecholamines (e.g., norepinephrine and epinephrine), which increase the heart rate and contractility, activating the β_1 -adrenoreceptors. These effects are countered by the parasympathetic nervous system, which decreases heart rate by releasing acetylcholine via the vagus nerve to the heart. Collectively, these systems orchestrate BP homeostasis, with heart rate alterations directly affecting cardiac output.

Vascular tone, characterized by the dynamic interplay of vasoconstriction and vasodilation, is regulated by a multifaceted network of factors⁶⁹. Most importantly, the endothelial factors of the vessel walls contract and relax the surrounding smooth muscle to change vascular tone. The initiation of vasoconstriction is predominantly mediated by several factors: an increase in intracellular calcium concentration, augmented levels of norepinephrine from the sympathetic nervous system, and a surge in angiotensin II hormones from the renin-angiotensin-aldosterone system^{70,71}. An increase in norepinephrine level activates the smooth muscle α_1 -adrenoreceptors, contributing to local smooth muscle contraction. On the other hand, nitric oxide, an endothelium-derived relaxing factor, directly induces vasodilation. Acetylcholine neurotransmitters are released from the parasympathetic nervous system, which triggers the production of nitric oxide by the endothelial cells in the blood vessel walls⁷² and thus provides local vasodilation of the blood vessel.

Lastly, blood volume changes occur due to gravitational transfer–induced hydrostatic pressure changes and total blood volume circulating in the entire cardiovascular system⁷³. First, during postural changes, such as supine, sitting, standing, passive leg raising, and hand raising, there is a gravitational transfer of blood volume among different areas of the peripheral vessels. The alterations in venous return lead to changes in BP and subsequently are sensed by vascular pressure sensors, known as baroreceptors, within the arteries, chiefly the carotid sinus and the aortic arch. In response to the BP change detected by the baroreceptors, the central nervous system releases norepinephrine from the sympathetic nervous system or acetylcholine from the parasympathetic nervous system to increase or decrease cardiac output, respectively, by adjusting the heart rate⁷⁴. All these compensatory mechanisms help in restoring the BP to maintain homeostasis in response to BP changes. Because BP is usually measured in the brachial or radial artery, it is essential to factor in the relative vertical displacement of the brachial or radial artery to the whole body. Second, there may also be a change in total circulating blood volume. In most cases, this has minimal effect throughout the day unless there is an acute hemorrhage or overconsumption of exogenous chemicals such as alcohol or salt, which can affect the renin–angiotensin–aldosterone system⁷⁰ and thus BP through the secretion of renin from the kidney to catabolize angiotensinogen. Then, catabolized angiotensinogen creates angiotensin I that binds with an angiotensin–converting enzyme to become angiotensin II. Angiotensin II triggers the release of aldosterone hormone from the adrenal glands to retain sodium, which increases the total circulating blood volume and thus BP. We excluded alcohol testing in this study due to inconclusive results in the literature^{75,76}.

Supplementary Discussion 9 | Four–quadrant plot and concordance rate.

The four–quadrant plot provides a visual method for tracking the capabilities of the study device compared to the reference device⁷⁷. One main advantage of the four–quadrant plot, compared to Bland–Altman plot, is its ability to observe the direction of changes of the study device (y–axis) in comparison with the direction of changes of the reference device (x–axis). Specifically, the calculated data points are plotted in one of the four quadrants in the plot to visualize the positive or negative changes of the two devices.

When both devices have an increase in the measurement values, the point is plotted in the 1st quadrant (upper right). Similarly, when both devices have a decrease in the measurement values, the point is plotted in the 3rd quadrant (lower left). In the 1st and 3rd quadrants, there is a concordance in the measured changes for the study device and the reference device. On the other hand, when the reference device has a decrease in the measured value while the study device has an increase in the measured value, the point is plotted in the 2nd quadrant (upper left). Similarly, when the reference device has an increase in the measured value while the study device has a decrease in the measured value, the point is plotted in the 4th quadrant (lower right). In the 2nd and 4th quadrants, the direction of change of the study device is not in concordance with the direction of change of the reference device.

A comparison of the number of points in the 1st and 3rd quadrants to the number of total points indicates the concordance rate of the four–quadrant plot. Thus, the concordance rate shows the ability of the study device to agree to the positive or negative changes to the reference device. Note that an exclusion zone is defined in the four–quadrant plot to calculate the concordance rate. An exclusion zone removes possible measurement errors, noise, and clinically insignificant changes from the analysis; a typical acceptable range is set as 10~15% of the maximum value in the four–quadrant plot⁷⁸.

The four–quadrant plot can intuitively and quantitatively distinguish when both devices have the same magnitude and direction of changes. Thus, in this study, the 12 daily activities induce dynamic BP changes compared to the sitting position, making the directionality of these changes an important aspect to visualize and investigate.

Supplementary Discussion 10 | Bland–Altman analysis for repeated measurements.

In standard Bland–Altman analysis, we often treat repeated measurements from each participant to be independent, as suggested by the standard guidelines^{24,66}. However, these repeated measurements originate from the same individual and are therefore correlated.

The approach to address this issue is to take repeated measurements into account rather than assuming these replicates are independent measurements. One approach is to assume that each participant’s true value does not change between repeated measurements. However, given that BP is a dynamic metric that fluctuates over time, the true values tend to vary across repeated measurements, such as those observed in replicates during the clinical outpatient clinic and cardiac catheterization laboratory study. We can avoid the assumption of constant true values and ascertain the limits of agreement using a variance components analysis⁷⁹, which utilizes the differences between each pair of measurements. For instance, the difference for a pair of measurements j on participant i can be represented by:

$$D_{ij} = B + I_i + E_{ij}, \quad (23)$$

where B denotes a constant bias, I_i is the interaction term that captures how the participant's BP response varies with the measurement method, and E_{ij} represents the random error within the participant for that specific pair of measurements.

The variance of D_{ij} (i.e., s_d^2) can be broken down into two components:

$$\text{Var}(D_{ij}) = s_d^2 = s_{dI}^2 + s_{dw}^2, \quad (24)$$

where s_{dI}^2 is the method times participant interaction term, and s_{dw}^2 is the within–participant variance. If there are m_i pairs of observations for n participants, the components of variance are then estimated by:

$$s_{dI}^2 = \frac{(n-1)\sum m_i}{(\sum m_i)^2 - \sum m_i^2} (MS_b - MS_w), \quad (25)$$

$$s_{dw}^2 = MS_w, \quad (26)$$

where MS_b and MS_w are the between-participants mean square and the within-participant mean square, respectively, obtained via the one-way analysis of variance in SPSS (28.0, IBM). The Bland-Altman limits of agreement are then given by:

$$LOA = \bar{d} \pm 1.96 * s_d, (27)$$

where \bar{d} is the grand mean taken over all observations. After taking the repeated measurements into account, the updated Bland-Altman plots involve the method times participant interaction, which shall be more reasonable and closer to the realistic cases (Supplementary Figs 19 and 22)⁷⁹.

Supplementary Discussion 11 | BP monitoring in patients with large BP fluctuations.

Large BP fluctuations in participants with irregular heart rhythms undoubtedly pose challenges to BP measurements. Compared to the sinus heart rhythm (also known as regular heart rhythm), an irregular heart rhythm is simply defined as a variation from the normal heart rate or rhythm that is not physiologically justified. The hemodynamics in person with irregular heart rhythm participants obviously differ from those with normal sinus heart rhythm. In participants with normal sinus rhythm, the beat-to-beat BP is generally stable, which is the premise for BP measurement. On the contrary, in participants with irregular heart rhythms, the beat-to-beat BP level is unstable. The beat that follows a longer R-R interval in an electrocardiogram has higher BP, but that follows a shorter R-R interval has lower BP. When the R-R interval of the previous pulse is very short, the following BP may be even too low to be detected⁸⁰.

The auscultatory device relies on Korotkoff sounds to measure BP, which can face challenges in participants with irregular heart rhythms. The irregular beats can introduce inconsistent silent gaps between beats or cause the tapping sounds of one beat to overlap with the subsequent beat. These can confuse or mask the clear sequence of Korotkoff phases, complicating the determination of SBP and DBP⁸¹. In irregular rhythm conditions, the characteristic spindle-like profile of the oscillometric pulse pressure in the automatic cuff becomes notably distorted. The peak oscillometric pulse pressure, traditionally linked to the MAP, may manifest unpredictably during the measurement, disrupting its usual correlation (Supplementary Discussion 1). Consequently, the estimations of SBP and DBP derived from standard oscillometric algorithms lose their accuracy⁸². Some standards also intentionally separate the cardiac arrhythmia population from the general hypertensive population^{25,66}, which indicates that some commercial devices are not applicable to participants with cardiac arrhythmia. Given these challenges, the A-line, with its high temporal resolution (> 200 Hz), becomes invaluable for capturing precise BP changes, especially in individuals with irregular heart rhythms.

In the cardiac catheterization laboratory study, data from participants #12, #14, #20, #21, and #24 were excluded according to the requirements of ISO 81060-2:2018 standard and their notable BP fluctuations⁶⁶. While the primary focus of this study was not on BP measurement

during pronounced BP fluctuations, BP waveforms from these five participants, as measured by the ultrasound sensor, were compared against A–line results to assess the sensor's potential to record considerable BP fluctuations (Supplementary Fig. 20).

In the case of participants with severe irregular heart rhythms, such as participant #12, the comparative results are less satisfactory. There are noticeable phase differences between the results from the A–line and ultrasound sensor, and the beats that follow a longer R–R interval give a much larger BP amplitude recorded by the ultrasound sensor. Irregular heart rhythms can induce marked variations in blood velocity due to the inconsistent force and timing of heart contractions. This inconsistency can alternate the flow profile within vessels from a primarily laminar to a more turbulent pattern. The resultant blood volume can fluctuate substantially with each heartbeat. Such a confluence of varied velocity, altered flow profile, and unpredictable ejection volumes directly impact arterial wall dilation and BP. This contributes to the observed discrepancies in BP measurements during irregular rhythms. A plausible explanation for the temporal discrepancies may be the pronounced viscoelastic properties of arteries during disordered rhythmic instances. The hysteresis of the stress–strain curve becomes more obvious⁸³. The shape of the stress–strain curve might be distorted by the abnormal blood flow patterns⁸⁴, which may explain the difference in BP amplitude. However, using arterial wall pulsations to derive BP is relatively new, and thus the dynamics data and understanding of arterial walls during irregular heart rhythms are limited. The potential mechanisms to account for such temporal and amplitudinal errors remains the participant of further investigations.

Participant #14 showed mild irregular heart rhythm, and BP waveforms from some of the pulses were missed by the A–line, which might be because the changes in the blood volume in these pulses are too low to be detected by the A–line. However, those pulses were recorded by the ultrasound sensor, indicating that pressure waves still existed on the arterial walls.

The artifacts recorded from the A–line in participant #20 may result from the accidental pressure transducer movement, as the ultrasound sensor continued to provide a stable recording of BP waveform. The findings from participants #21 and #24 demonstrate a strong consistency between the BP waveforms captured by the A–line and the ultrasound sensor. Throughout all episodes of irregular heart rhythms, the two BP waveforms exhibited similar patterns, which substantiates the capability of the ultrasound sensor for monitoring patients under such conditions.

Supplementary Discussion 12 | BP waveform analysis.

The complex structure of the arterial tree, with its hierarchical branches and non–uniform nature, necessitates careful consideration when analyzing BP waveforms. Such complexity is primarily attributed to the presence of reflected waves. A traveling pressure wave will be reflected to some extent wherever there is a mechanical discontinuity in the system. Possible reflecting sites include branching points, and areas of alteration in arterial stiffness such as the interface between small arteries and high resistance arterioles⁸⁵. The reflected waves from

those sites throughout the body will be combined to exhibit a cumulative backward wave to the heart.

Considering the reflection waves are mechanical waves along the arterial wall, their velocity (i.e., pulse wave velocity) is primarily dictated by the mechanical properties of the arterial walls (e.g., geometry and stiffness). The pulse wave velocity⁴¹ typically ranges from 5 to 15 m/s, considerably greater than the blood flow velocity, which is around 0.5~1.5 m/s. This suggests that within a single cardiac cycle, reflection waves may be reflected multiple times between the heart and distal reflection sites. Moreover, the amplitude of the reflected waves and re-reflected waves are less than that of the incident wave because of energy dissipation along the traveling wavefront. Consequently, the observed BP waveform is the result of the superimposition of a powerful incident wave produced by left ventricular ejection, and the diminished reflected and re-reflected waves, generated by mechanical discontinuity within the cardiovascular system.

Those different components contribute to modifying the BP waveform as it travels from central to peripheral arteries. The shape of the systolic peak, for instance, is largely influenced by reflected waves returning from the arterial tree. As the pressure wave travels further down to the peripheral sites, the influence of the reflected wave intensifies. The peak of the combined reflection waves moves further into systole and merges with the peak of the incident systolic wave to provide a higher systolic peak pressure, which is called distal systolic pulse amplification⁶⁹. As a result, the BP waveform exhibits a steeper slope during systole and an overall lower pressure during diastole as it moves from central to peripheral arteries. This pattern has been widely observed in most waveform comparison results between brachial waveforms from the ultrasound sensor and the radial waveform from the A-line (Supplementary Fig. 23).

Supplementary Discussion 13 | Wavelet coherence analysis.

BP measurements over extended periods of time exhibit non-stationary characteristics, meaning that their statistical properties change with time due to various physiological complexities (e.g., movement, circadian rhythms, stress, emotion, food, and medicine). Traditional Fourier transform methods, which assume time stationarity and periodicity of the measurement, are unable to adequately decompose these dynamic changes^{86,87}. This means that distinct peaks cannot be obtained by Fourier transform, making it difficult to evaluate the statistical differences. However, wavelet transform offers a robust time-frequency analysis tool that can effectively decompose the signal's frequency components over the measurement duration^{86,88}.

To compare BP measurements from the ultrasound sensor and A-line, wavelet coherence analysis based on the Morlet wavelet transform of the two BP measurements provides cross-correlation within the time-frequency domain to construct a wavelet coherence spectrogram^{87,89}. Wavelet transform is defined as:

$$W_x(a, b) = \int x(t)\psi_{a,b}^*(t)dt, (28)$$

where $W_x(a, b)$ is the wavelet transform of signal $x(t)$, which is the MAP measurement from the A–line in this study. $\psi_{a,b}^*(t)$ is the complex conjugate of $\psi_{a,b}(t)$, the generalized form of wavelet, which is defined as:

$$\psi_{a,b}(t) = a^{-\frac{1}{2}}\psi\left(\frac{t-b}{a}\right), (29)$$

where $a^{-\frac{1}{2}}$ is the normalization factor, a is the wavelet frequency scale, b is the wavelet position in time, and the ψ term is the Morlet wavelet:

$$\psi(t) = \pi^{-\frac{1}{4}}e^{6ti}e^{-\frac{t^2}{2}}, (30)$$

where $\pi^{-\frac{1}{4}}$ is the normalization factor, which ensures the Morlet wavelet has consistent energy across all scales, e^{6ti} is the complex sinusoid, and $e^{-\frac{t^2}{2}}$ is the Gaussian envelope.

$$W_y(a, b) = \int y(t)\psi_{a,b}^*(t)dt, (31)$$

where $W_y(a, b)$ is the wavelet transform of signal $y(t)$, MAP measurement from the ultrasound sensor in this study.

$$W_y^*(a, b) = \int y(t)\psi_{a,b}(t)dt, (32)$$

where $W_y^*(a, b)$ is the conjugate wavelet transform of signal $y(t)$.

The magnitude–squared coherence $R^2(a, b)$ is defined as:

$$R^2(a, b) = \frac{|S(W_x(a,b) \times W_y^*(a,b))|^2}{S(|W_x(a,b)|^2) \times S(|W_y(a,b)|^2)}, (33)$$

where S is the smoothing operator in time and scale.

The phase difference $\Delta\phi(a, b)$ is defined by:

$$\Delta\phi(a, b) = \arg(W_x(a, b) \times W_y^*(a, b)), (34)$$

where \arg is the argument of the complex number, which is the angle between the positive real axis and the complex number in the complex plane.

The wavelet coherence spectrogram provides a visually intuitive representation of regions with high correlation in both the frequency and time domains between the two signals (Fig. 5a–d, bottom panels)⁸⁷. Specifically, in the wavelet coherence spectrogram, the x–axis represents the measurement time window, which was calculated based on changes in b in equation (34), and the y–axis represents the period (i.e., shown in period rather than frequency to maintain intuitive consistency with the x–axis in terms of time), which was calculated based on changes in a in equation (34). The color scale denotes the magnitude–squared coherence, serving as an indicator of the correlation strength between the BP measurements from the two devices (i.e.,

higher values indicate stronger correlation and vice versa). In addition, the black arrows pointing rightwards signify in-phase coherence, indicating minimal phase difference between the BP measurements from the two devices, while the black arrows pointing leftwards signify anti-phase coherence. BP measurements from the two devices should demonstrate both high magnitude-squared coherence and in-phase characteristics for areas of interest in the spectrogram. Finally, below the white dashed lines mark areas for unreliable statistical analysis due to artifactual edge effects. The wavelet cannot be entirely localized in time at the edges. The width of such edges varies, depending on the scale of the wavelet: the larger the scale, the wider the edge. Consequently, areas outside the white dashed lines should be disregarded for accurate statistical analysis purposes.

Supplementary Discussion 14 | Bootstrapping.

We used the *z*-scoring method and bootstrapping to identify any randomness of the coherence between the BP measurements from the ultrasound sensor and A-line⁹⁰. Bootstrapping is a random sampling technique that ensures each selected data point to be independent from the subsequent data point⁹⁰. This means that the sampled dataset by bootstrapping has higher variability because each individual sample is independent of each other. The ultrasound sensor data were bootstrapped 100 times, generating 100 randomly sampled datasets with the same temporal resolution as the experimental ultrasound sensor data. This ensures that the 100 datasets are randomized with respect to time.

With the experimental and 100 bootstrapped datasets, these 101 datasets underwent wavelet coherence analysis with the same A-line data. Given that the objective of this study was to observe the changes in longitudinal BP trend between the two devices, we defined the low-frequency region as periods exceeding 60 min to minimize the statistical discrepancies arising from the sensor sampling frequency and measurement variance (e.g., contralateral arm differences, body motion). The regions outside the white dashed lines in the spectrogram were excluded (Supplementary Discussion 13). Subsequently, we extracted the highest magnitude-squared coherence values for each time point within the high period region. Then, we computed the mean of the highest magnitude-squared coherence values for each dataset (Supplementary Fig. 26).

To assess the statistical significance, we calculated the *z*-score for the experimental dataset and all bootstrapped datasets, identifying the statistical difference between the bootstrapped data and the experimental data. A *z*-score of 1.65 corresponds to a 90% confidence level, 1.96 to a 95% confidence level, and 2.58 to a 99% confidence level⁹¹. All *z*-scores in this study are higher than 2.58, indicating a statistically significant difference between the bootstrapped data and the experimental data, thereby demonstrating the non-random nature of the ultrasound sensor measurements.

Supplementary Discussion 15 | BP measurement in participants with aging skin.

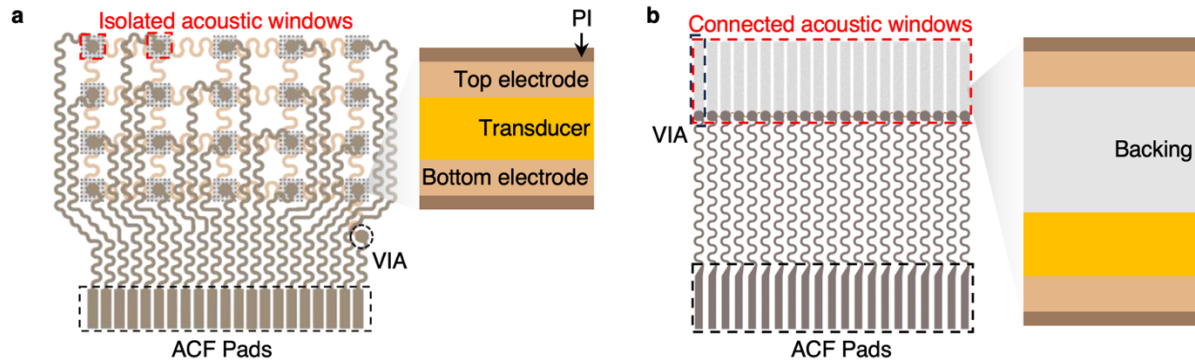
We have taken the aging skin into consideration while using the wearable ultrasound sensor for BP measurement. First, it is noteworthy that the sensor captures arterial wall pulsations directly, rather than relying on skin deformations. This approach reduces the impact of variations in skin stiffness on the accuracy of BP measurements. Second, attaching the sensor to aging skin might lead to misalignment issues. To mitigate this issue, the sensor in this study incorporates a closely arranged transducer array, forming a 10–mm wide acoustic window, which substantially increases the tolerance for misalignment. Third, the wearable ultrasound sensor is designed to be highly conformable to the skin. And the optional use of a thin layer of ultrasound gel as a coupling agent between the sensor and the skin further minimizes the potential of skin wrinkles to affect the accuracy of BP measurements. Last but not least, in the outpatient clinic (Table 1) and catheterization laboratory studies (Table 2), a substantial portion of the participants were senior patients with aging skin. The outcomes of these studies demonstrated the sensor's effectiveness and reliability for BP measurement in those senior participants.

Supplementary Discussion 16 | Design of the wearable ultrasound sensors.

In the literature, three primary ultrasound transducer structures are commonly discussed⁹²: piezoelectric ceramics, capacitive micromachined ultrasound transducers, and piezoelectric micromachined ultrasound transducers. Among these, piezoelectric ceramics are the most prevalent, and they have been the primary focus of our research efforts thus far. Consequently, the patch structures in our publications typically share a certain degree of similarities.

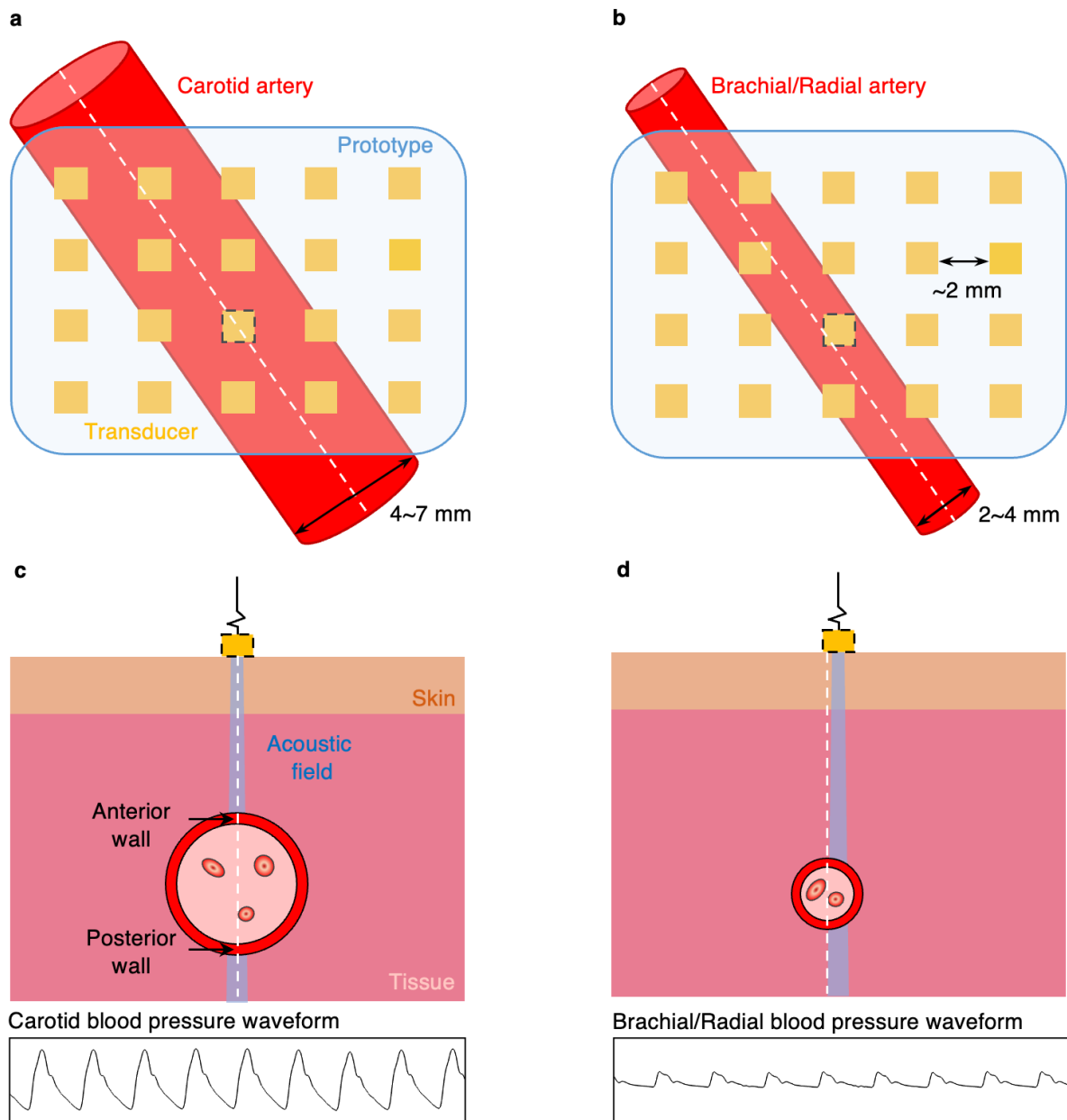
The major contribution in our Nature paper (Nature 613, 667-675, 2023)⁹³ is the successful demonstration of imaging capabilities using a wearable patch. Similarly, the Nature Biotechnology paper (Nature Biotechnology, 42, 448-457, 2023)⁵⁸ underscores a major breakthrough: the presentation of a circuit enabling wireless control of the ultrasound patch, alongside an algorithm designed to automatically select the transducer element for tracking moving targets. In the context of this study, our key contribution lies in demonstrating the efficacy and safety compliance of wearable ultrasound devices through clinical validation, aligning with established standards for the first time.

Additionally, in this study, we specifically re–engineered the device to enhance its efficacy in targeting the more clinically relevant brachial and radial arteries for BP monitoring. Given the unique challenges associated with the small sizes of these two arteries^{94,95}, we closely arranged the 20–element array to form a connected 10 mm wide acoustic window. This design ensures comprehensive coverage of the target arteries and accommodates potential misalignments between the device and the artery, which is critical for BP monitoring in practical uses.



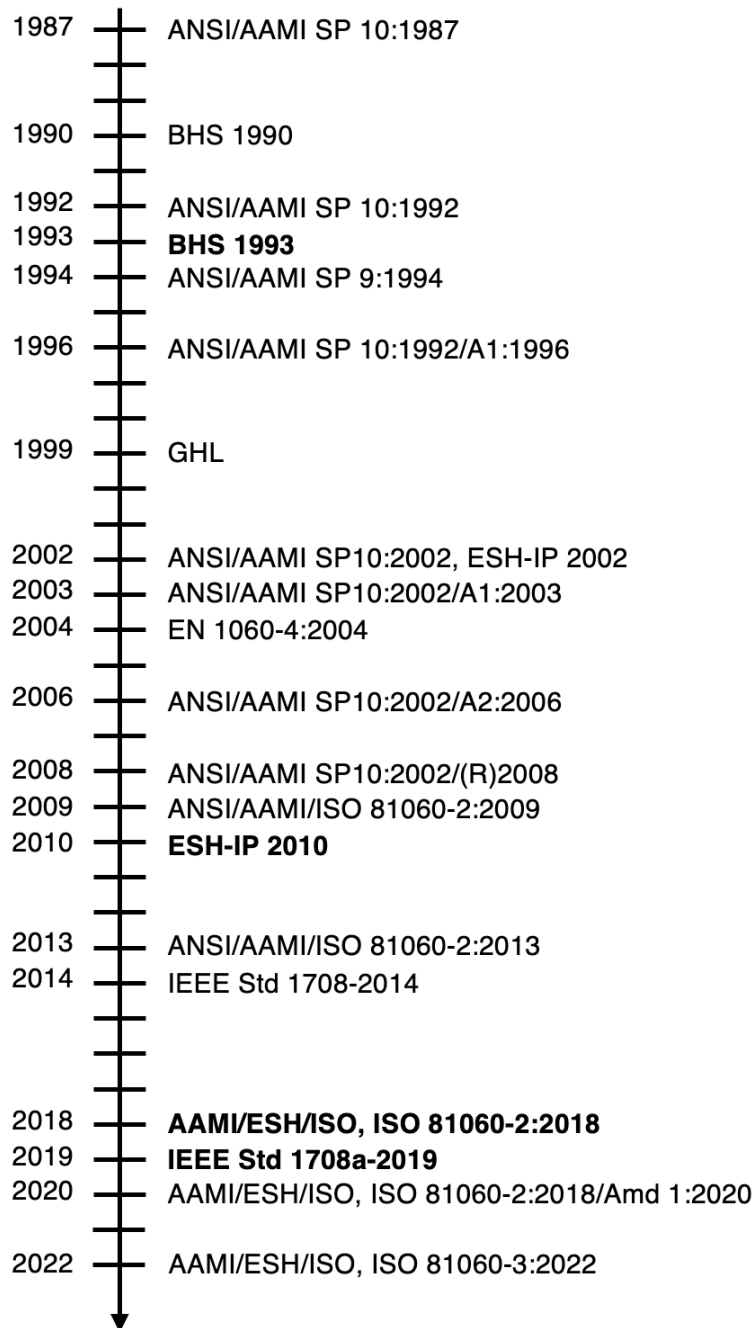
Supplementary Fig. 1 | Device re-engineering.

a, Published prototype design with isolated acoustic windows⁹⁶. The transducers are connected by polyimide coated copper electrodes (i.e., top and bottom electrodes). **b**, Re-engineered device design with a connected wide acoustic window in this study. The transducers within the re-engineered device have backing layers to reduce the redundant vibrations after activation. The transducers with backing layer are connected by polyimide coated copper electrodes. ACF, anisotropic conductive film; PI, polyimide; VIA, vertical interconnect access.



Supplementary Fig. 2 | Critical device–artery alignment in existing prototypes.

Top–down view illustrating the alignment between the existing prototype and **a**, the carotid artery, or **b**, the brachial/radial artery. The carotid artery has a generally larger diameter (4~7 mm)⁹⁷ compared to that of brachial/radial artery (2~4 mm)^{95,98}. The prototype's transducer array features a pitch of ~3 mm. The transducers (labeled by black dashed boundary) closest to the arterial center (labeled by white dashed line) are selected to measure the BP. **c**, Cross–sectional view of the alignment between the selected transducer element and carotid artery. The acoustic field covers the center of the target artery. Therefore, the arterial diameter can be accurately measured. This alignment ensures a high–accuracy carotid BP waveform. **d**, Cross–sectional view of the alignment between the selected transducer and brachial/radial artery. Here, the acoustic field doesn't align optimally with the artery's center, leading to inaccuracies in measuring arterial diameter, and consequently, a distorted brachial/radial BP waveform.



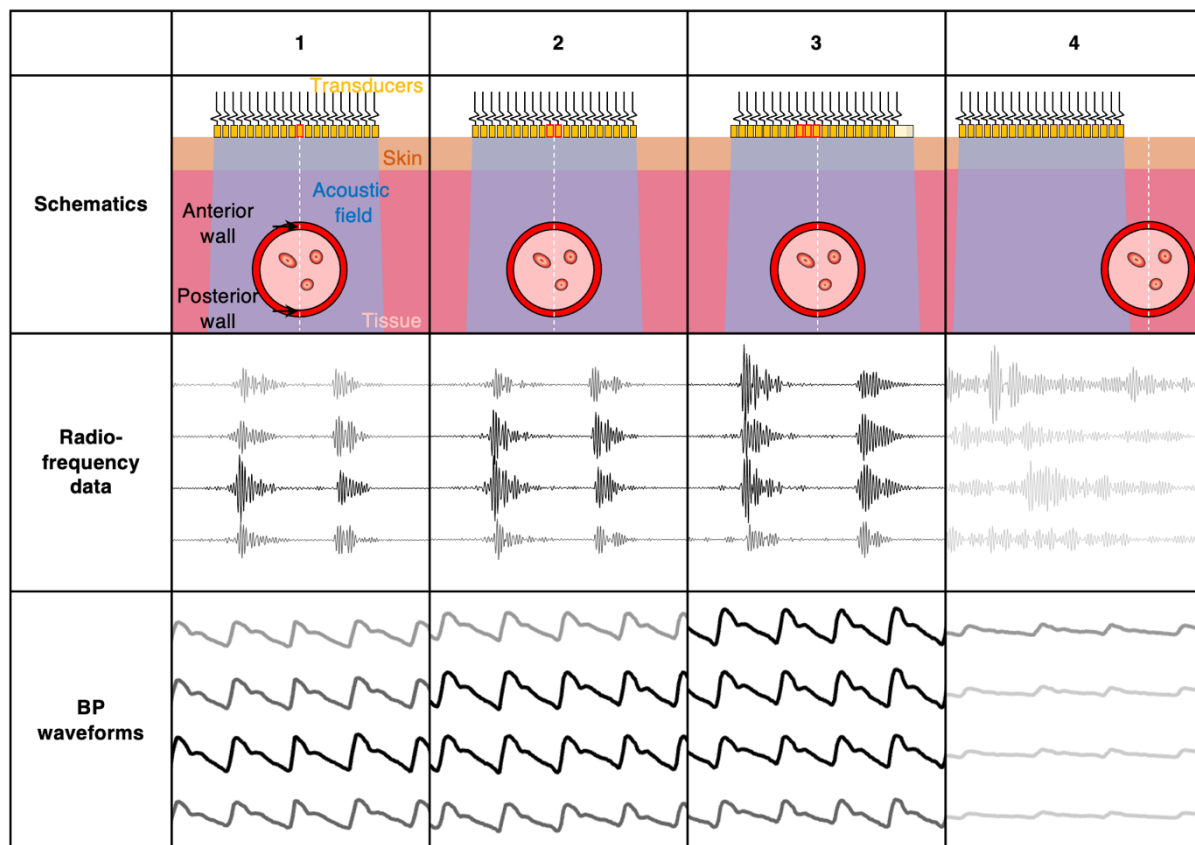
Supplementary Fig. 3 | Timeline of BP monitoring standards.

The development history of different standards is marked on the timeline. BHS 1993, ESH–IP 2010, IEEE Std 1708a–2019, and ISO 81060–2:2018 are the four standards that are widely used. AAMI, Association for the Advancement of Medical Instrumentation; Amd, amendment; ANSI, American National Standards Institute; BHS, British Hypertension Society; EN, European Committee for Standardization; ESH–IP, European Society of Hypertension International Protocol; GHL, German Hypertension League; IEEE, Institute of Electrical and Electronics Engineers; ISO, International Organization for Standardization; SP, Standard Proposal; Std, standard.

Standards	Sample size	Gender range	Age range	Blood pressure range												
BHS 1993	≥ 85	N/A	N/A	SBP 90 130 160 180 Size <table border="1" style="display: inline-table;"><tr><td>≥ 8</td><td>≥ 20</td><td>≥ 20</td><td>≥ 20</td><td>≥ 8</td></tr></table> DBP 60 80 100 110 Size <table border="1" style="display: inline-table;"><tr><td>≥ 8</td><td>≥ 20</td><td>≥ 20</td><td>≥ 20</td><td>≥ 8</td></tr></table>	≥ 8	≥ 20	≥ 20	≥ 20	≥ 8	≥ 8	≥ 20	≥ 20	≥ 20	≥ 8		
≥ 8	≥ 20	≥ 20	≥ 20	≥ 8												
≥ 8	≥ 20	≥ 20	≥ 20	≥ 8												
ESH-IP 2010	≥ 33	≥ 10 females and males	≥ 25 years old	SBP 90 130 160 180 Size <table border="1" style="display: inline-table;"><tr><td>10-12</td><td>10-12</td><td>10-12</td></tr></table> DBP 40 80 100 130 Size <table border="1" style="display: inline-table;"><tr><td>10-12</td><td>10-12</td><td>10-12</td></tr></table>	10-12	10-12	10-12	10-12	10-12	10-12						
10-12	10-12	10-12														
10-12	10-12	10-12														
AAMI/ESH/ISO, ISO 81060-2:2018	≥ 85 (for non-invasive reference method)	≥ 30% females and males	≥ 12 years old	SBP 100 140 160 Size <table border="1" style="display: inline-table;"><tr><td>≥ 5%</td><td></td><td>≥ 5%</td></tr><tr><td colspan="3" style="text-align: center;">≥20%</td></tr></table> DBP 60 85 100 Size <table border="1" style="display: inline-table;"><tr><td>≥ 5%</td><td></td><td>≥ 5%</td></tr><tr><td colspan="3" style="text-align: center;">≥20%</td></tr></table>	≥ 5%		≥ 5%	≥20%			≥ 5%		≥ 5%	≥20%		
	≥ 5%				≥ 5%											
≥20%																
≥ 5%		≥ 5%														
≥20%																
≥ 15 (for invasive reference method)	SBP 100 160 Size <table border="1" style="display: inline-table;"><tr><td>≥ 10%</td><td></td><td>≥ 10%</td></tr></table> DBP 70 85 Size <table border="1" style="display: inline-table;"><tr><td>≥ 10%</td><td></td><td>≥ 10%</td></tr></table>	≥ 10%		≥ 10%	≥ 10%		≥ 10%									
≥ 10%		≥ 10%														
≥ 10%		≥ 10%														
IEEE Std 1708a-2019	≥ 85	≥ 26 females and males	21-50 years old	BP Normal Prehypertension hypertension hypertension Size <table border="1" style="display: inline-table;"><tr><td>≥ 21</td><td>≥ 21</td><td>≥ 21</td><td>≥ 21</td></tr></table>	≥ 21	≥ 21	≥ 21	≥ 21								
≥ 21	≥ 21	≥ 21	≥ 21													

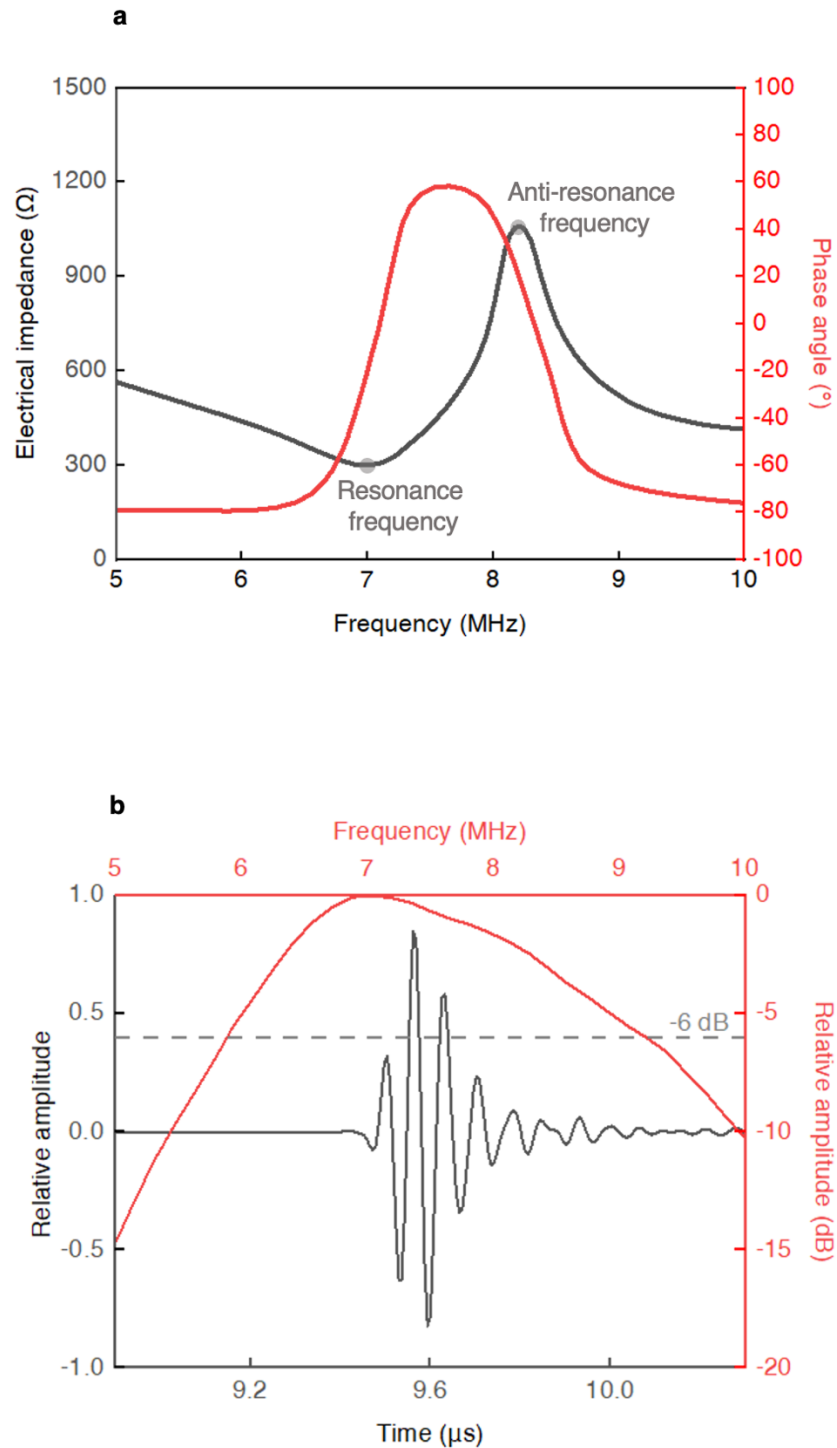
Supplementary Fig. 4 | Criteria for selecting participants of different standards.

The demographical requirements such as sample size, sex range, age range, and BP range are listed for different standards. Note that most standards require a large sample size, broad sex and BP distribution to ensure the reliability and validity of the findings. The normal BP range stands for SBP < 120 mmHg and DBP < 80 mmHg. The prehypertension BP range stands for 120 mmHg ≤ SBP < 139 mmHg and 80 mmHg ≤ SBP < 89 mmHg. The S1 hypertension BP range stands for 140 mmHg ≤ SBP < 159 mmHg and 90 mmHg ≤ SBP < 99 mmHg. The S2 hypertension BP range stands for SBP ≥ 160 mmHg and DBP ≥ 100 mmHg. AAMI, Association for the Advancement of Medical Instrumentation; BHS, British Hypertension Society; DBP, diastolic blood pressure; ESH-IP, European Society of Hypertension International Protocol; IEEE, Institute of Electrical and Electronics Engineers; ISO, International Organization for Standardization; N/A, not applicable; SBP, systolic blood pressure; Std, standard.



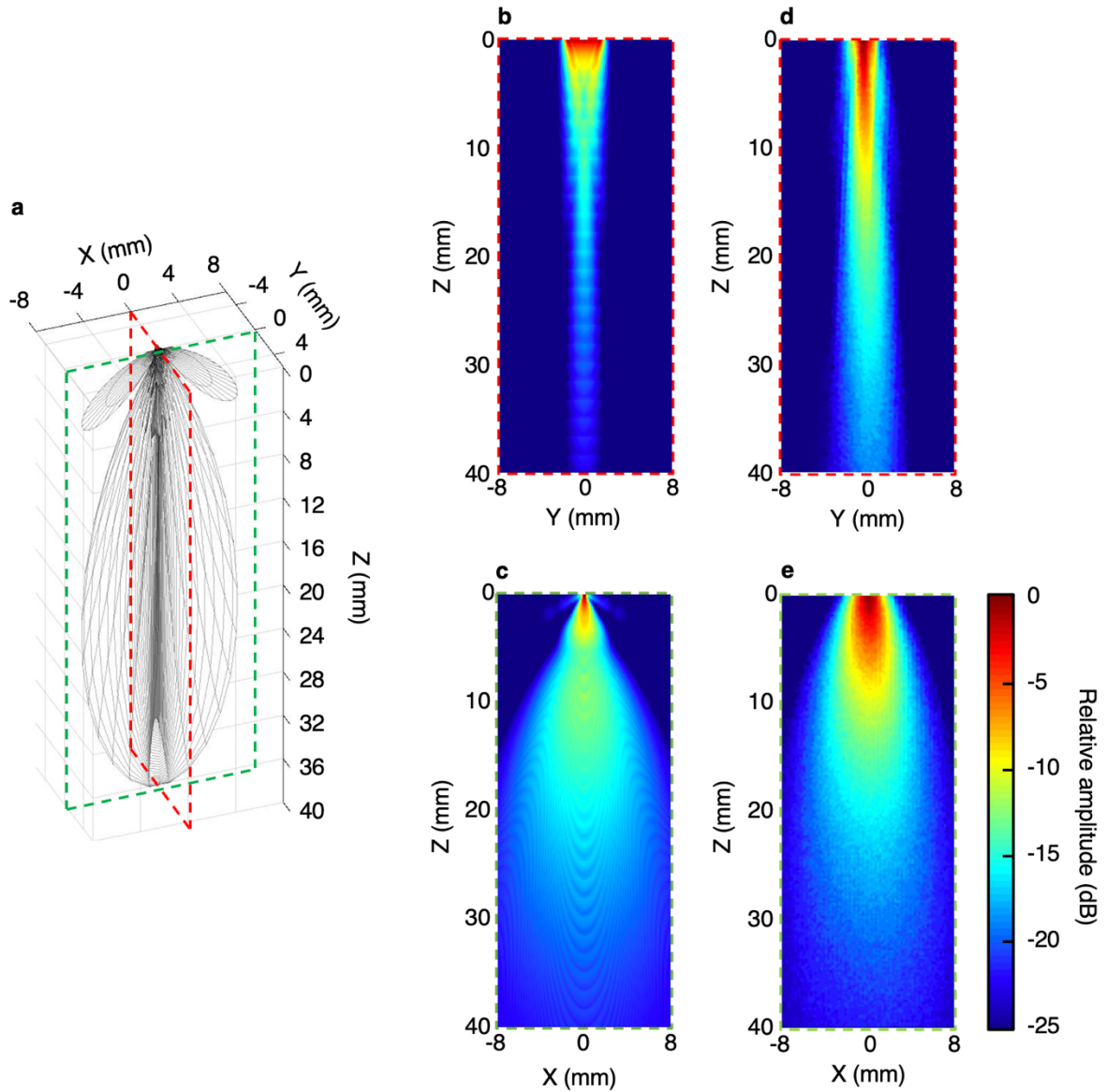
Supplementary Fig. 5 | Connected device–artery alignment in this work.

When the pitch is small, the acoustic windows of all transducer elements are connected, which makes it easier to align the device and artery. In this case, there are four device–artery alignment situations to consider when measuring BP using the re–engineered ultrasound sensor. Firstly, the linear array is orthogonal to the target artery, and only one of the transducers (labeled in red) is directly above the artery center. This provides the most accurate BP values. Secondly, the linear array is orthogonal to the target artery, but the arterial center is located between two transducers (labeled in red). Taking advantage of the minimal pitch (0.5 mm in this work), these two elements provide similar results, which are also comparable to the result in the first situation. Adopting the equations (20), (21), and (22), the largest error from the slight misalignment will be < 2 mmHg when measuring the brachial or radial artery (< 5 mm in diameter). Thirdly, the linear array crosses the target artery with a random ($0\sim 90^\circ$) angle. In this case, more than one transducer (labeled in red) is located above the arterial center. The ultrasound waves that propagate normally to the arterial center have an almost 90° incidence angle to the arterial wall surface, generating the largest reflection waves, which is attributed to the highest peak in received radiofrequency data. Therefore, the in–plane angle between the device and the artery does not interfere with BP measurement. Lastly, the arterial center is outside the ultrasound field, and the received signal only contains the movement from sidewalls or surrounding tissue. The peaks from anterior and posterior walls are invisible in received radiofrequency data, and a re–alignment of the device is needed.



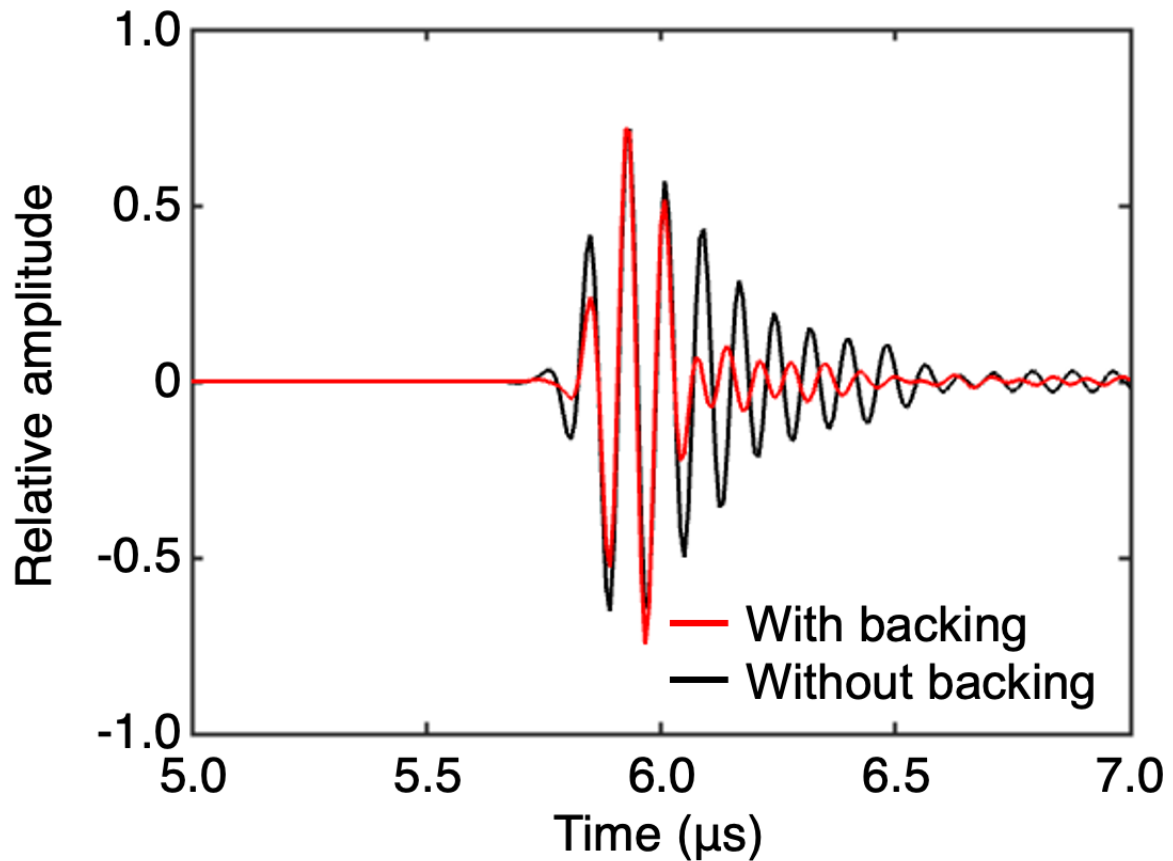
Supplementary Fig. 6 | Piezoelectric property characterizations.

a, Impedance and corresponding phase angle of the transducer elements as a function of frequency. The resonant (7.03 MHz) and anti-resonant (8.22 MHz) frequencies are labeled with shaded circles. **b**, Time and frequency domain characterizations of the signal in water. The -6 dB bandwidth is around 40%.



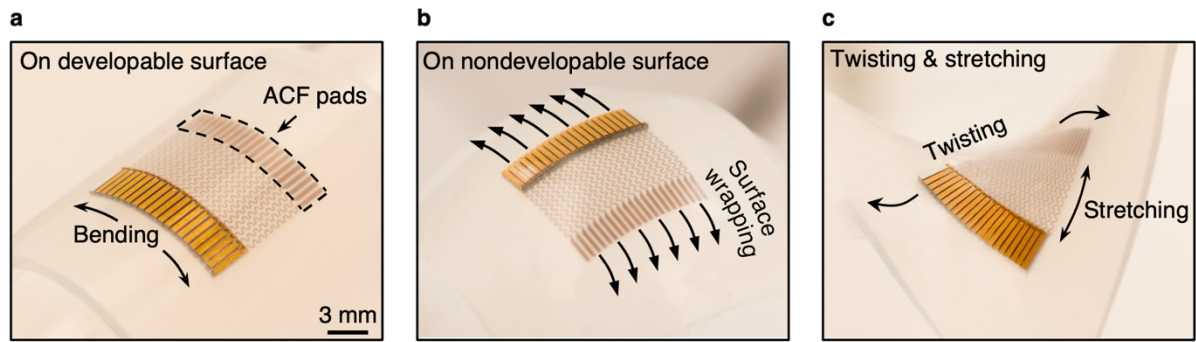
Supplementary Fig. 7 | Simulated and scanned device acoustic fields.

a, Simulated three-dimensional acoustic field. The red and green dashed boxes label the Y-Z plane and X-Z plane, respectively. **b,c**, Simulated two-dimensional acoustic fields at Y-Z and X-Z planes, respectively. The simulation was performed using an open-source Matlab toolbox (i.e., Field II). **d,e**, Scanned two-dimensional acoustic fields at Y-Z and X-Z planes, respectively. Both simulation and scanning results show around 25 mm penetration depth. The two-dimensional acoustic fields share the same scale bar.



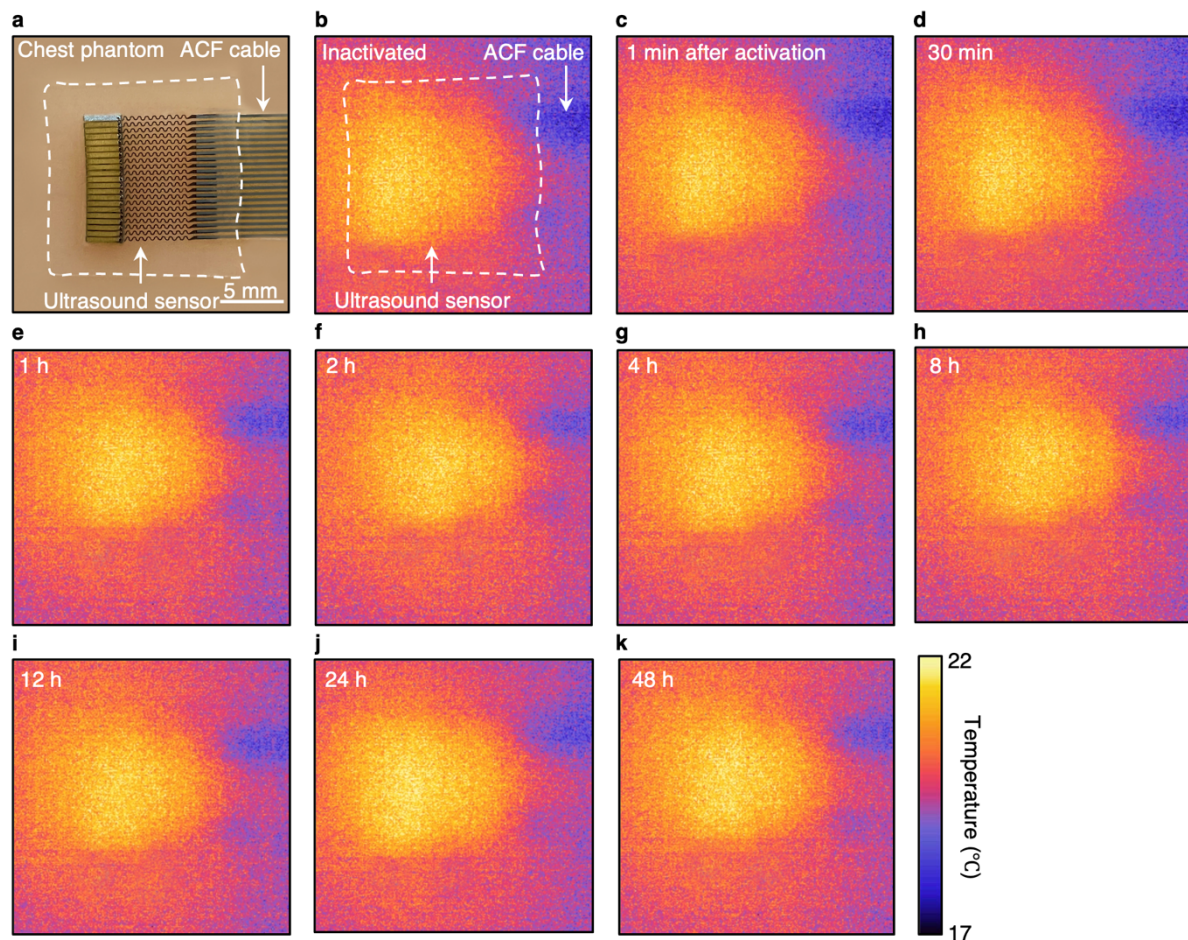
Supplementary Fig. 8 | Pulse-echo responses of a transducer element with and without a backing layer.

The transducer with a backing layer (red) demonstrates a shorter spatial pulse length, thus enhancing the spatial resolution and enabling more precise localization of arterial walls. In contrast, the transducer without the backing layer (black) shows a longer spatial pulse length, indicating less resolution.



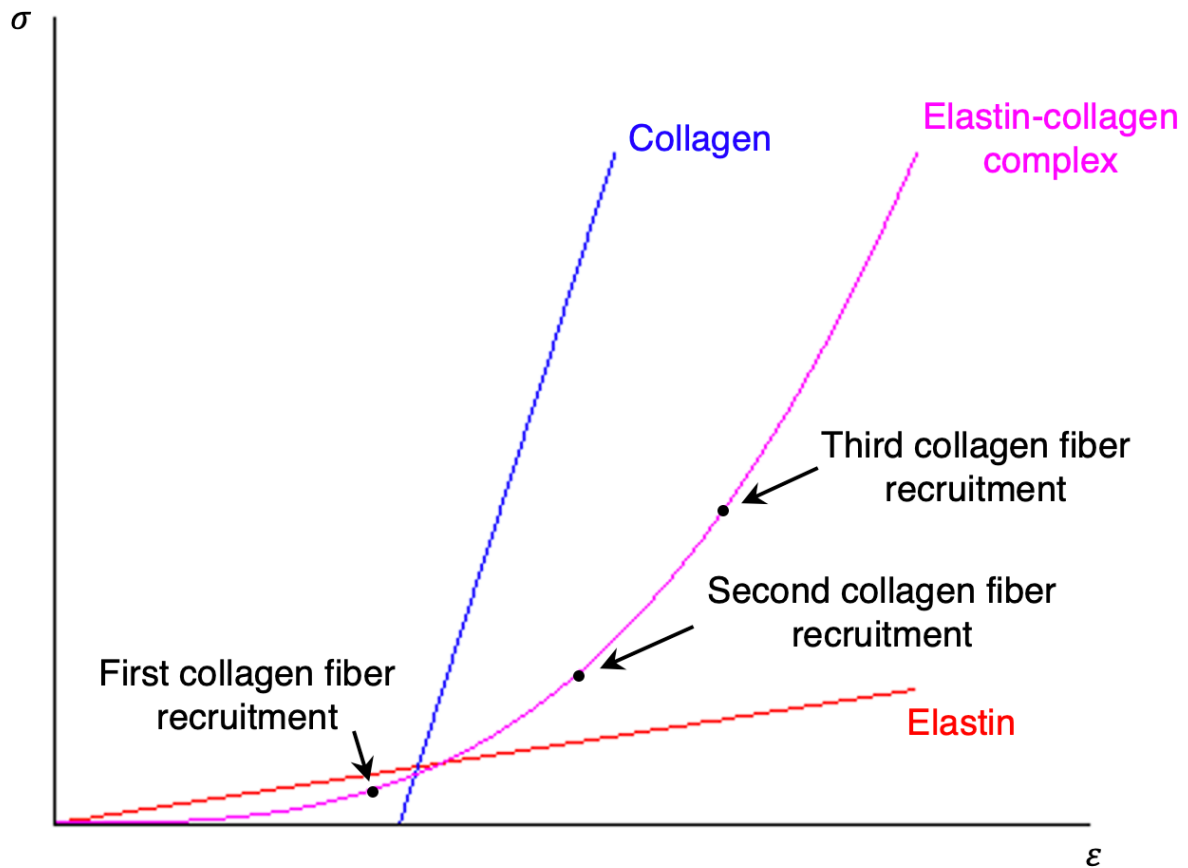
Supplementary Fig. 9 | Optical images of the re-engineered ultrasound sensor.

The ultrasound sensor under mixed deformation, including **a**, bending; **b**, wrapping; as well as **c**, twisting and stretching. The sensor maintains its integrity under these conditions, demonstrating its excellent mechanical compliance and robustness. The images share the same scale bar. ACF, anisotropic conductive film.



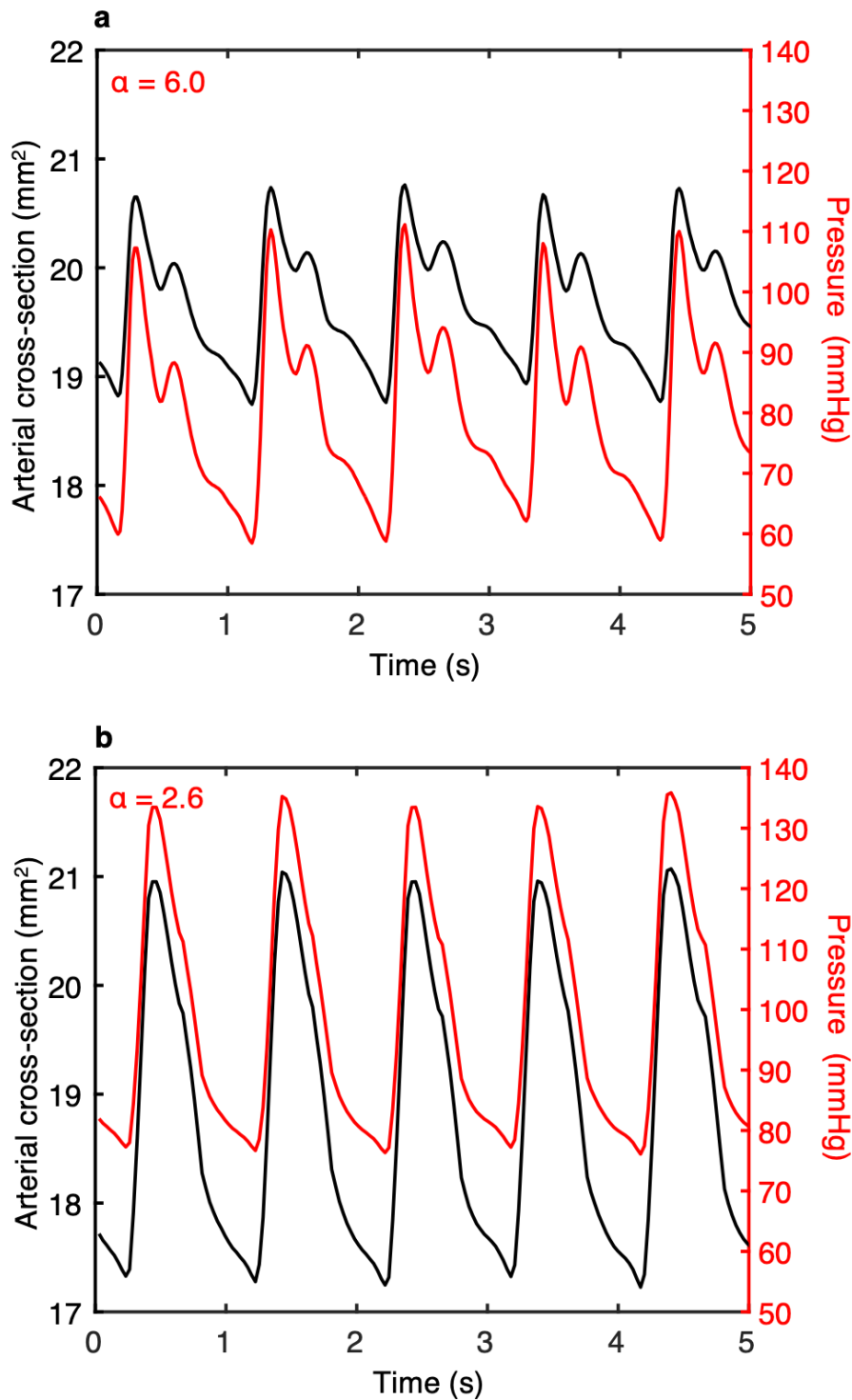
Supplementary Fig. 10 | Thermal characterization of the ultrasound sensor.

a, Optical image of the ultrasound sensor on a representative human chest phantom. **b–k**, A series of thermal images of inactivated and activated ultrasound sensor. The thermal emissivity of the thermal imaging camera (C5, FLIR) was set to be 0.95 to accurately measure the temperature of organic materials and the human skin. Throughout an activation period of 48 h with a pulse repetition frequency of 1000 Hz and a voltage of 20 V, the sensor exhibits impressive thermal stability, with the overall temperature rise < 1 °C, thus ensuring safe, long-term operation on the human body. The images share the same scale bar. ACF, anisotropic conductive film.



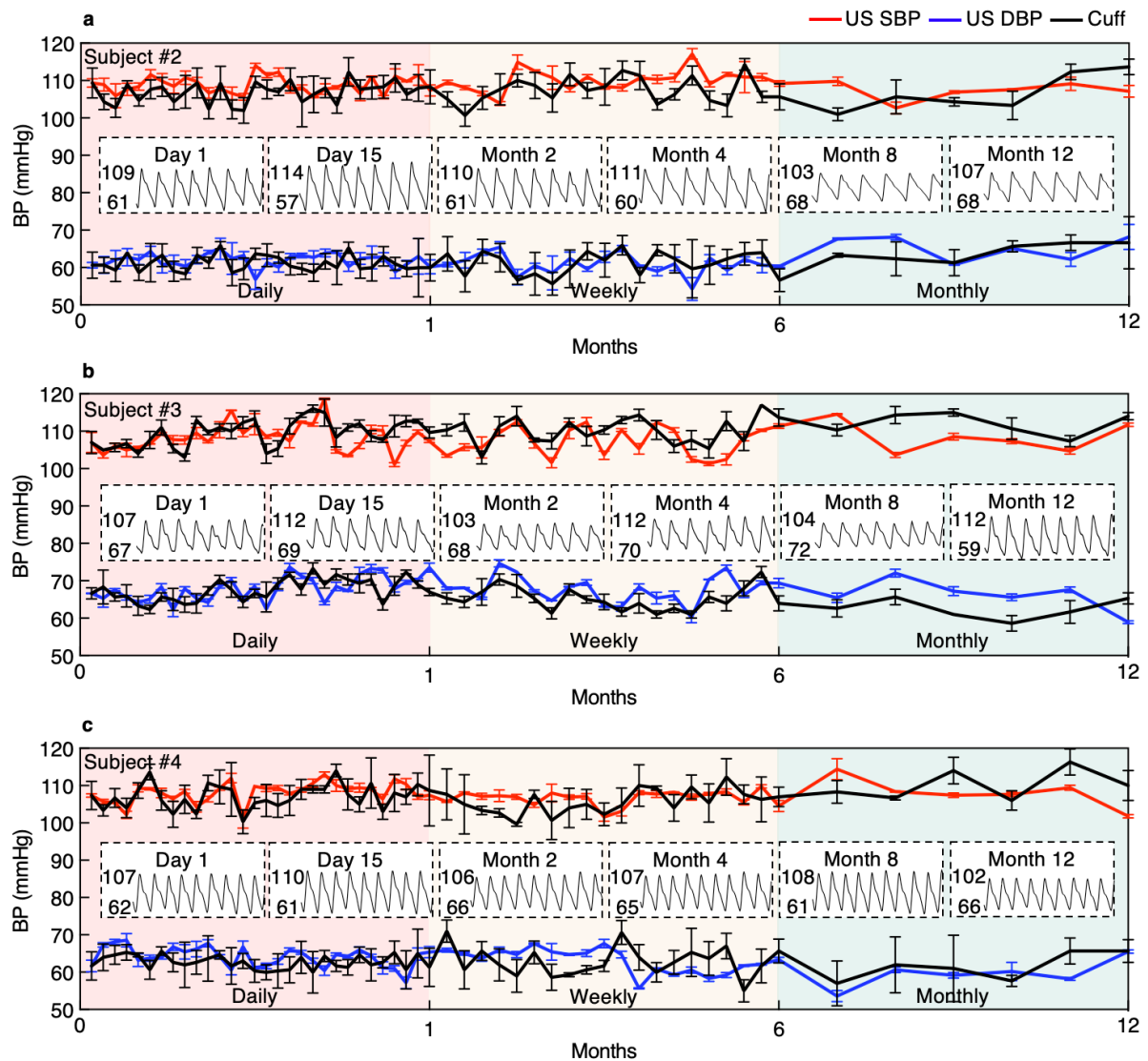
Supplementary Fig. 11 | Arterial wall distension mechanism.

The three curves are the stress–strain behavior of the elastin, collagen, and elastin–collagen complex. Elastin has a lower Young’s modulus than collagen. The stress–strain relationship in the elastin–collagen complex demonstrates an exponential nature, which can be attributed to the sequential recruitment of multiple collagen fibers during the deformation process⁵³. σ , stress. ϵ , strain.



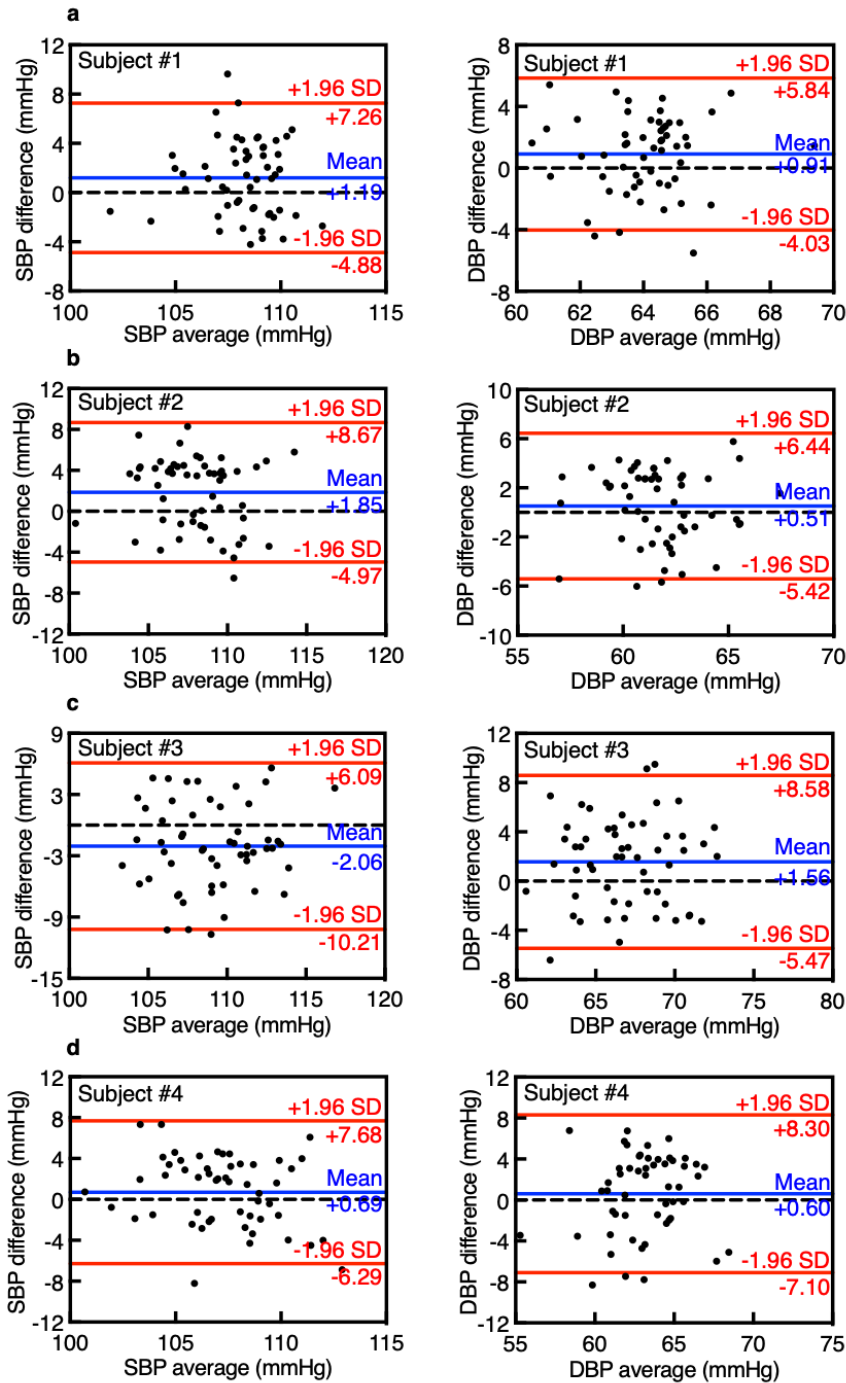
Supplementary Fig. 12 | Comparison of pressure waveforms and diameter waveforms.

a, A participant with a stiffness coefficient α of 6.0. **b**, A participant with a stiffness coefficient α of 2.6. In both panels, the pressure waveforms (red) are computed from the alterations in the arterial cross section (black). This demonstrates that pressure waveforms can be derived from dynamic arterial cross-sectional changes in individuals.



Supplementary Fig. 13 | Calibration duration of the ultrasound sensor for participants #2, #3, and #4.

a-c, Ultrasound sensor measurements for SBP (red) and DBP (blue) with its respected sphygmomanometer measurements (black) for 1 year in participants #2, #3, and #4, respectively. The measurements were repeated three times for each time point. Error bars indicate one standard deviation of the measurements. The insets show the exemplary BP waveforms of the ultrasound sensor on day 1, day 15, month 2, month 4, month 8, and month 12. After calibration, the ultrasound sensor, compared with the sphygmomanometer, exhibits minimal differences in SBP and DBP throughout the 1-year measurement, demonstrating its long-term accuracy. BP, blood pressure; DBP, diastolic blood pressure; SBP, systolic blood pressure; US, ultrasound.



Supplementary Fig. 14 | Bland–Altman plots of calibration results for each participant.

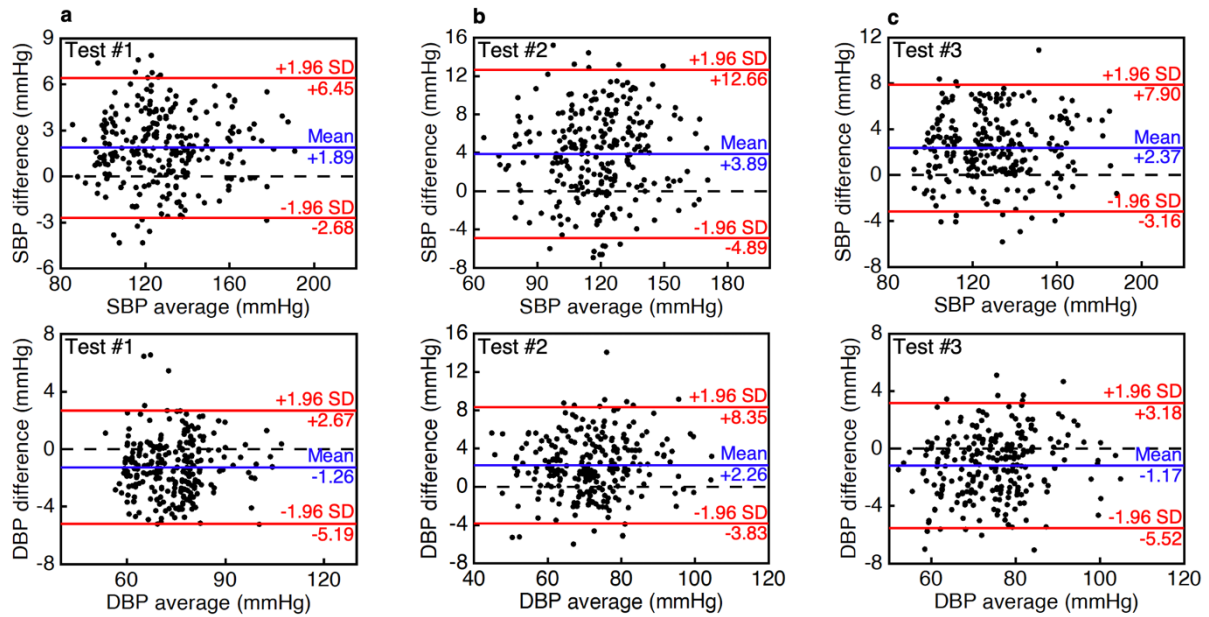
a–d, Bland–Altman plots of SBP (left column) and DBP (right column) from the ultrasound sensor and sphygmomanometer for participants #1, #2, #3, and #4, respectively. Solid blue lines represent the mean differences between the two measurements, solid red lines represent the 95% limits of agreement (i.e., 1.96 standard deviations above and below the mean differences), and dash black lines label the zero difference between the two devices. We observe high accuracy throughout the one–year measurement for all four healthy participants. DBP, diastolic blood pressure; SBP, systolic blood pressure; SD, standard deviation.

													
Cardiac Output	—	↑	↓	↓	—	↑	↑	↑	↑↑	↓	↓	↑	↑
Vascular Tone	—	—	—	—	—	↑	↑	↑↑	↑	↓	↓	↑	↑
Blood Volume	—	↓	↑	↑↑	↓	—	—	—	—	—	—	↑	—

 Sitting	 Hand raising	 Cycling	 BP increase  No change  BP decrease
 Standing	 Mental arithmetic	 Deep breath	
 Supine	 Ice bath	 Meditation	
 Passive leg raising	 Isometric handgrip	 Meal	
		 Caffeine	

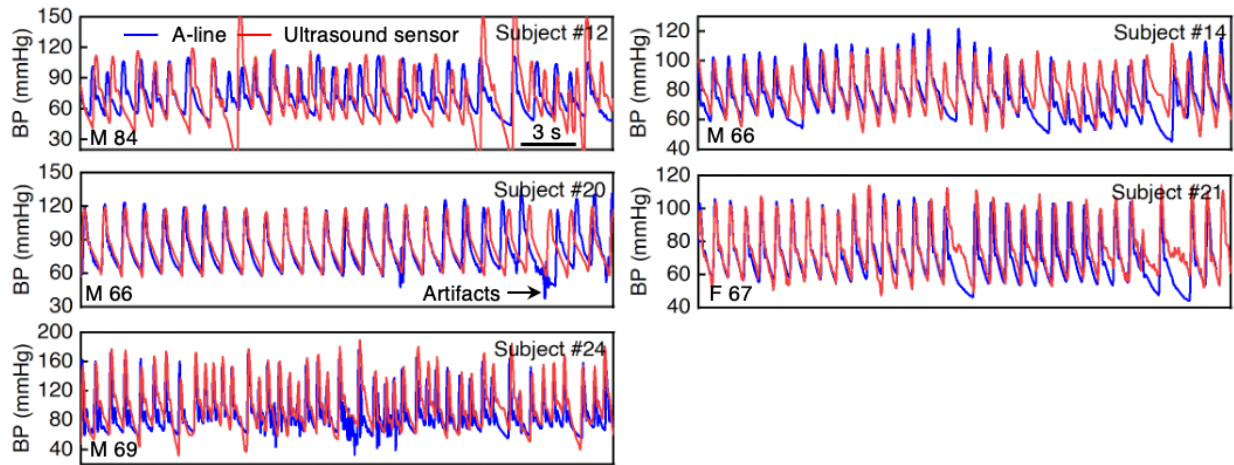
Supplementary Fig. 15 | Summarized effects of different daily activities on cardiovascular parameters.

The daily activities are categorized by their effects on three cardiovascular parameters, which are cardiac output, vascular tone, and blood volume. The upper arrow and downward arrow indicate the increase and decrease in BP, respectively, due to each cardiovascular parameter. Double arrows denote a particularly large influence. No substantial influence on BP through the cardiovascular parameter is indicated by a horizontal bar.



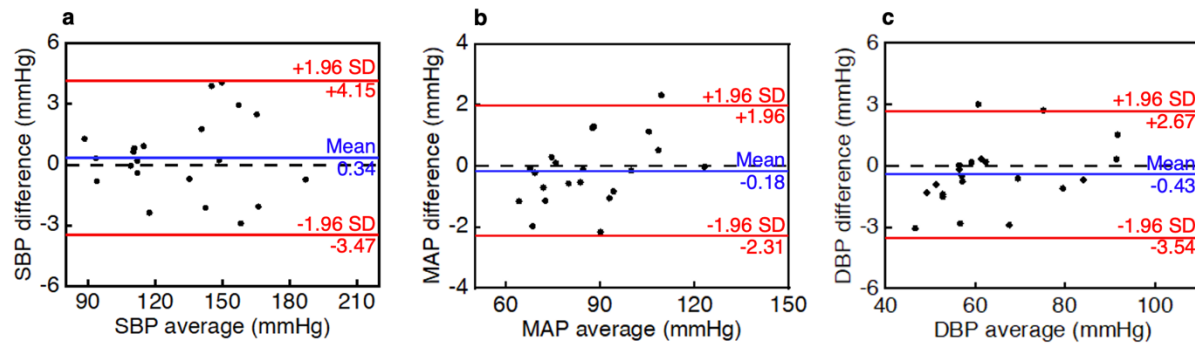
Supplementary Fig. 16 | Bland–Altman plots of repeated measurements in the outpatient clinic study.

a–c, Bland–Altman plots representing the differences between the two devices for repeated measurements of SBP and DBP in three tests against their averages⁷⁹. The standard deviations for the differences in SBP are 2.33, 4.48, and 2.82 mmHg in the three tests. The standard deviations for the differences in DBP are 2.01, 3.11, and 2.22 mmHg in the three tests. Solid blue lines label the mean differences between the two devices, solid red lines label the 95% limits of agreement (i.e., 1.96 standard deviations above and below the mean differences), and dashed black lines label the zero difference between the two devices. The 95% limits of agreements of SBP and DBP are similar compared to that of original Bland–Altman plots (Fig. 3f–h). DBP, diastolic blood pressure; SBP, systolic blood pressure; SD, standard deviation.



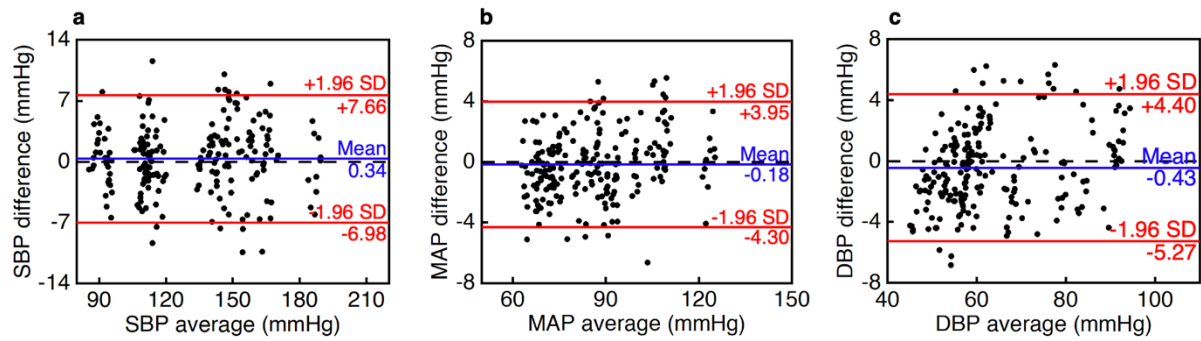
Supplementary Fig. 17 | Waveform comparison on excluded patients in the catheterization laboratory study.

30 s continuous BP waveform from each participant who had large BP fluctuations recorded by the A-line (blue) and ultrasound sensor (red). The gender and age of each patient were labeled accordingly. Per ISO 81060–2:2018, if the device is primarily designed for utilization during periods of large BP fluctuations, a special patient population should be selected for validation. If not, all data from a participant shall be excluded if the invasive reference SBP range is > 20 mmHg or if the invasive reference range is > 12 mmHg during or before the test (ISO 81060–2:2018 6.2.4.d.1)²⁵. The artifacts recorded from the A-line in participant #20 may have resulted from accidental pressure transducer movement. Participant #14 with a mild irregular heart rhythm exhibited missing pulses in the A-line readings, while these pulses were detected by the ultrasound sensor. The results from participants #21 and #24 display consistent BP waveforms from both the A-line and the ultrasound sensor, underscoring the sensor's capability to accurately track BP under these conditions. However, in severe cases like participant #12, comparative results are less satisfactory, with notable phase and amplitude differences between the two devices. Potential explanations for these discrepancies could be linked to arterial viscoelastic properties and possible distortion of the pressure–diameter curve during irregular rhythms. Despite these interferences, the BP waveform recorded by the ultrasound sensor remained largely unaffected. Consequently, the ultrasound sensor demonstrates its overall good performance on BP waveform recording even in the presence of irregular heart rhythms. The waveforms share the same scale bar. A-line, arterial line; BP, blood pressure; F, female; M, Male.



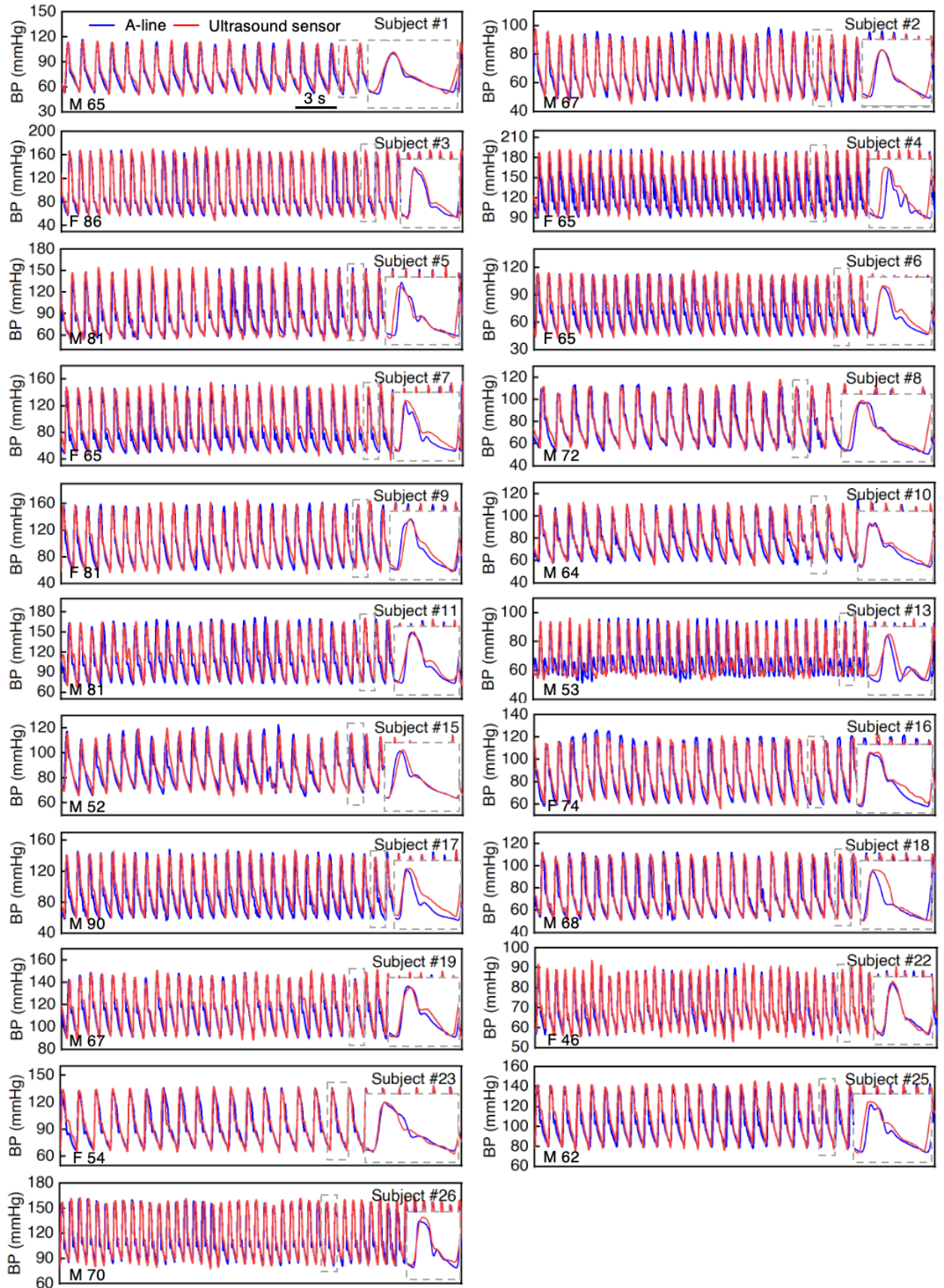
Supplementary Fig. 18 | Bland–Altman plots of BP distribution between participants in the cardiac catheterization laboratory study.

a–c, Bland–Altman plots of the measurement difference over the average of the two devices’ values between participants on SBP, MAP, and DBP, respectively. Each dot represents the mean of replicate measures within a participant. The standard deviations for the differences in SBP, MAP, and DBP are 1.94, 1.09, and 1.59 mmHg, respectively. These values fall considerably below the thresholds outlined by ISO 81060–2:2018 criteria 2 (Supplementary Fig. 18)⁶⁶, thereby suggesting a high degree of agreement between the measurements by both devices. Note that ISO 81060–2:2018 criteria 1 considers all repeat measurements independently while criteria 2 considers the average of the repeat measurement. Solid blue lines indicate the mean differences between the two devices, solid red lines label the 95% limits of agreement (i.e., 1.96 standard deviations above and below the mean differences), and dash black lines indicate the zero difference between the two devices. DBP, diastolic blood pressure; MAP, mean arterial pressure; SBP, systolic blood pressure; SD, standard deviation.



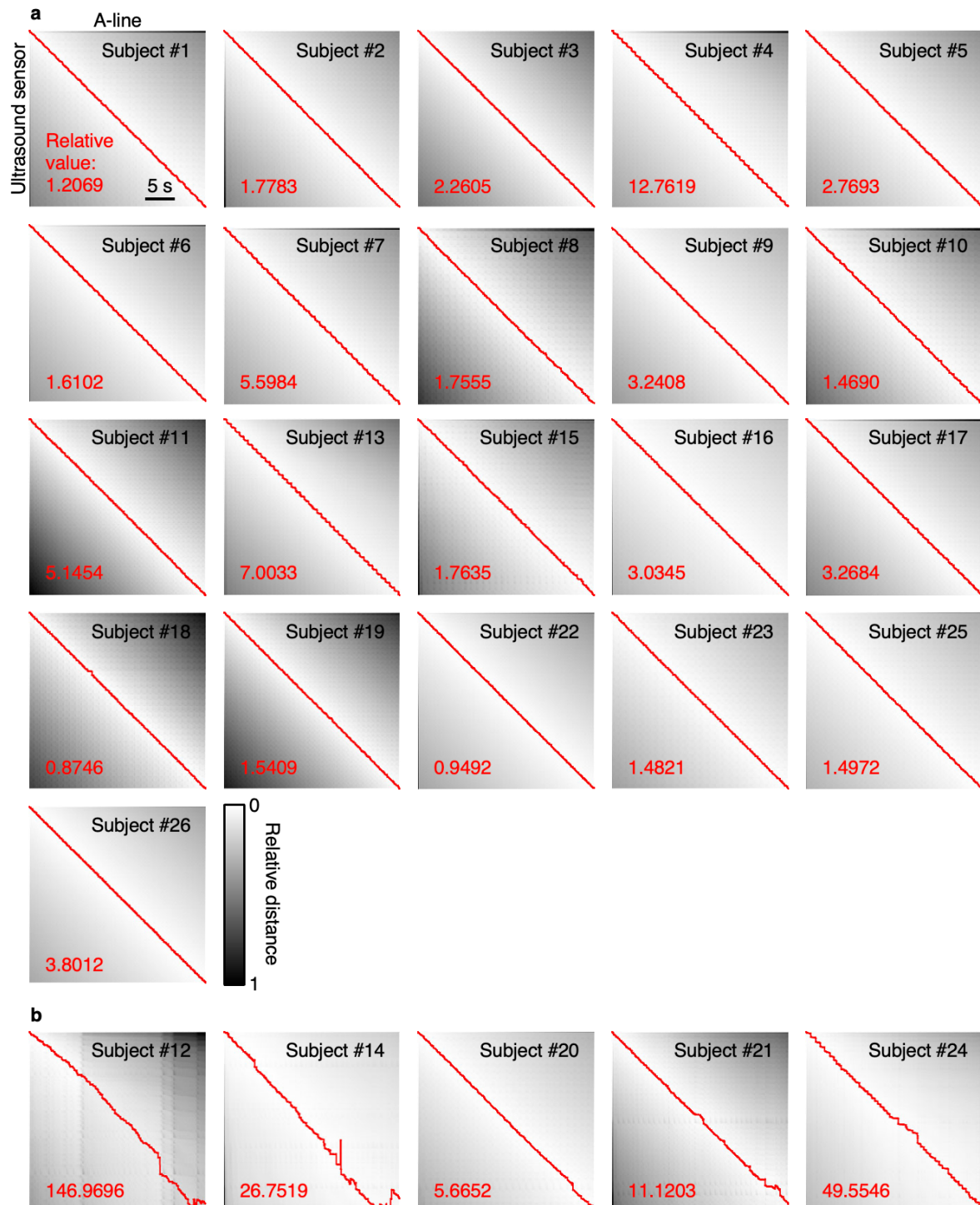
Supplementary Fig. 19 | Bland–Altman plots of repeated measurements in the cardiac catheterization laboratory study.

a–c, Bland–Altman plots representing the differences between the average of the two devices for repeated measurements of SBP, MAP, and DBP, respectively⁷⁹. The standard deviations for the differences in SBP, MAP, and DBP are 4.06, 2.32, and 2.88 mmHg, respectively. Solid blue lines label the mean differences between the two devices, solid red lines label the 95% limits of agreement (i.e., 1.96 standard deviations above and below the mean differences), and dash black lines label the zero difference between the two devices. The 95% limits of agreements of SBP, MAP, and DBP are narrower compared to that of original Bland–Altman plots (Fig. 4c). DBP, diastolic blood pressure; MAP, mean arterial pressure; SBP, systolic blood pressure; SD, standard deviation.



Supplementary Fig. 20 | Waveform comparison on included patients in the catheterization laboratory study.

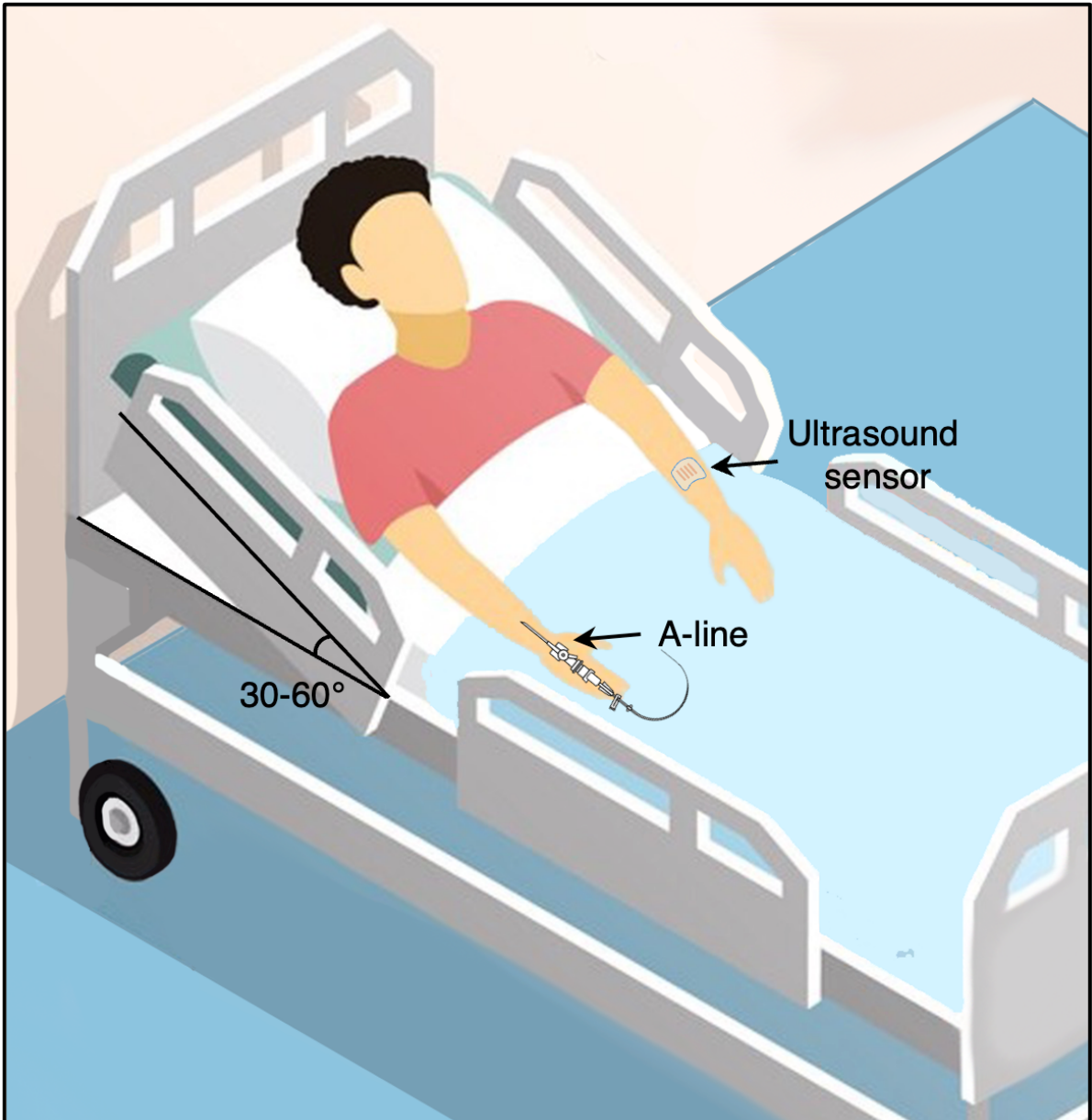
30 s continuous BP waveforms from each participant who maintained a stable BP range and participated in the clinical study in the cardiac catheterization laboratory were recorded by the A-line (blue) and ultrasound sensor (red). The gender and age of each patient were labeled accordingly. A single pulse from each plot, highlighted by a gray dashed box, is zoomed in for a more detailed illustration of a steeper slope during systole and an overall lower pressure during diastole as it moves from central to peripheral arteries. All waveforms from both devices show high consistency. The waveforms share the same scale bar. A-line, arterial line; BP, blood pressure; F, female; M, Male.



Supplementary Fig. 21 | Dynamic time warping analysis.

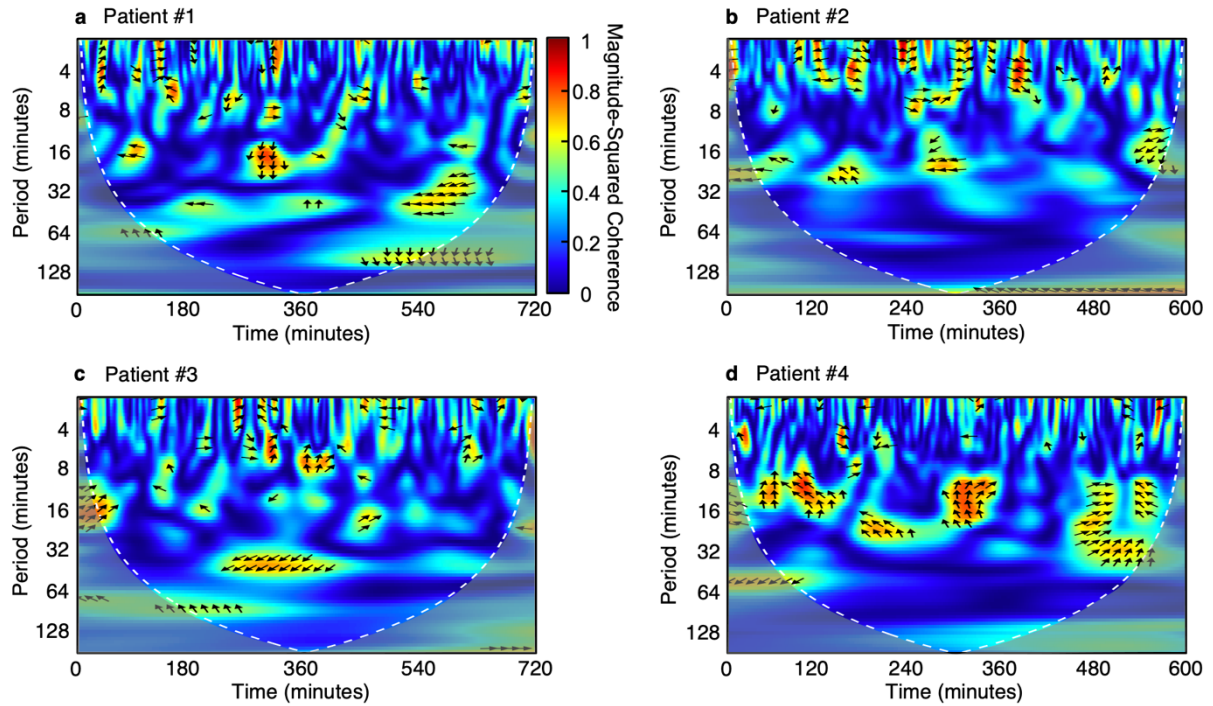
a, Dynamic time warping analysis of the BP waveforms of the participants included in the cardiac catheterization laboratory study. **b**, Dynamic time warping analysis of the BP waveforms of the participants excluded in the study because the BP variations of these participants were larger than what's allowed by the standard (ISO 81060–2:2018 6.2.4.d.1)²⁷. Each pixel denotes the distance between the pair of two points in the two time series data, with the darkness indicating the different distance between the two points. The red line shows the best match. The more skewing or curving this line, the more warped or shifted the two time

series data against one another. The larger the relative value of each plot, the larger generally the average distance between the two time series data. Compared to the Pearson correlation coefficient which only determines the strength of a linear relationship between two time series data, dynamic time wrapping is more appropriate for analyzing the morphological agreement between the data. The diagrams share the same scale bar.



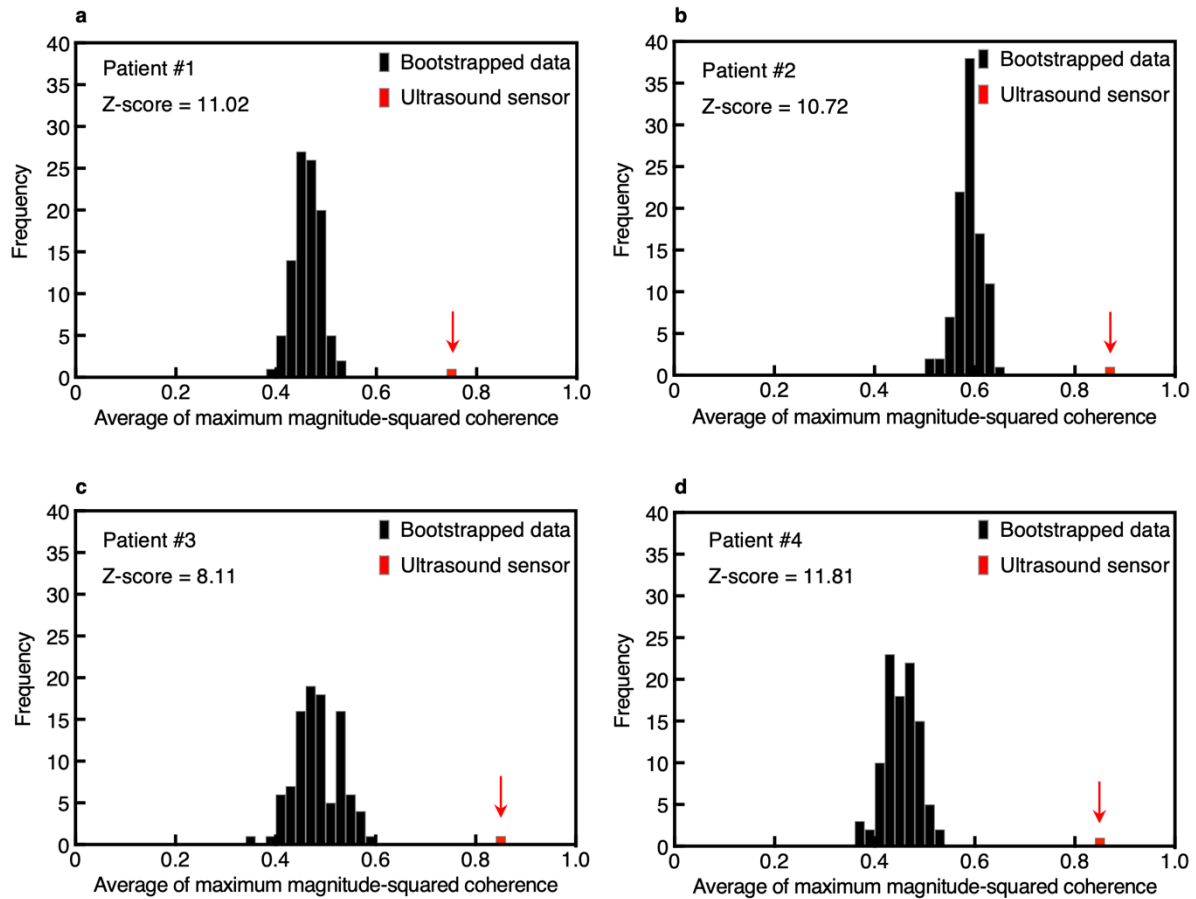
Supplementary Fig. 22 | Fowler's position.

Schematics illustrating the clinical testing setup in the intensive care unit. The patients were in Fowler's position, defined as a bed inclined 30 to 60°. Both the ultrasound sensor and the A-line were placed on the radial artery, but on contralateral arms.



Supplementary Fig. 23 | Wavelet coherence spectrogram between the bootstrapped dataset and A-line dataset.

a–d, Wavelet coherence spectrogram of MAP measurements between the bootstrapped dataset and A-line dataset of four patients. The color scale represents the magnitude-squared coherence, and the black arrows represent the phase difference between the two datasets, where rightward arrows indicate in-phase and leftward arrows indicate anti-phase. Compared to wavelet coherence spectrogram between the ultrasound sensor dataset and A-line dataset, the wavelet coherence spectrogram for the bootstrapped dataset shows low magnitude-squared coherence in the entire region with random phase arrows.



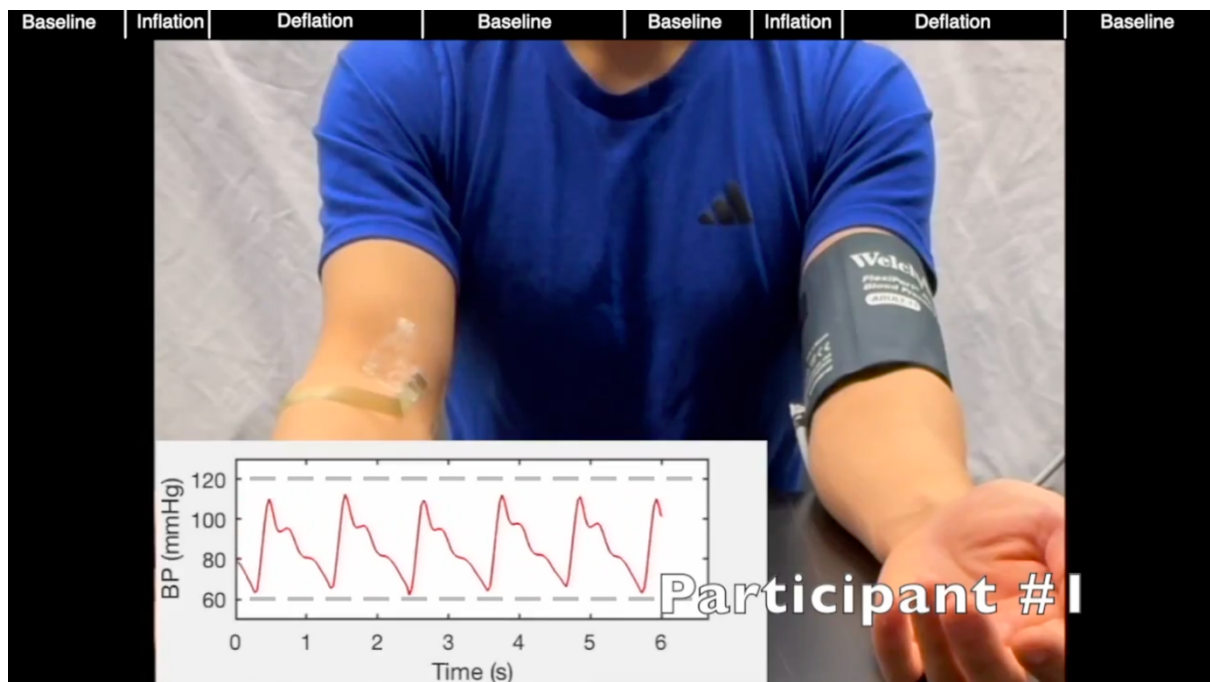
Supplementary Fig. 24 | Comparison of average of maximum magnitude-squared coherence for bootstrapped data and experimental data.

a–d, Histogram of bootstrapped data (black) and experimental data (red) of the average of the maximum magnitude-squared coherence throughout the entire measurement period for each patient. The histogram suggests a large difference between the bootstrapped data and experimental data with high z-score values, signifying the non-randomness of the coherence between ultrasound sensor and A-line data.

Supplementary Table 1 | Testing methods for each validation study.

Study	Reference device	Relative placement	Ultrasound sensor position	Reference device position	Measurement order
Calibration duration	Sphygmomanometer	Contralateral	Distal brachial artery	Brachial artery	Simultaneous
Daily activities	Sphygmomanometer	Ipsilateral	Distal brachial artery	Brachial artery	Sequential
Outpatient clinic	Sphygmomanometer	Contralateral	Distal brachial artery	Brachial artery	Simultaneous
Cardiac catheterization laboratory	Arterial line	Ipsilateral	Distal brachial artery	Radial artery	Simultaneous
Intensive care unit	Arterial line	Contralateral	Proximal radial artery	Proximal radial artery	Simultaneous

The reference BP device, relative placement of the ultrasound sensor in comparison to the reference device, position of the two devices, and measurement order of the different validation studies are compared. For the studies on calibration duration and in the outpatient clinic, BP was measured contralaterally for simultaneous measurement without the sphygmomanometer affecting BP measurements with the ultrasound sensor²⁶. Daily activities study required a single hand to perform hand raise, ice bath, and isometric handgrip based on established protocols, so BP measurements were obtained ipsilaterally^{99,100}. The cardiac catheterization laboratory study was performed ipsilaterally in accordance with the ISO 81060–2:2018 standard⁶⁶. The intensive care unit study positioned the sensors contralaterally due to practical limitations imposed by the secured indwelling A–line, other sensors, and wires (e.g., for electrocardiogram and pulse oximeter) with its associated taping.



Supplementary Video 1 | BP waveforms recorded during sphygmomanometer inflation and deflation.

The recording on each of the two participants includes ~30 s baseline, ~1 min sphygmomanometer inflation and deflation, and another ~30 s baseline after the deflation. The reference gray dashed lines help better illustrate the BP variation. The first participant showed ~4 mmHg BP increase while the second participant exhibited minimal changes in BP during the sphygmomanometer inflation and deflation.

References

- 1 Beevers, G., Lip, G. Y. & O'Brien, E. Blood pressure measurement: Part I—Sphygmomanometry: Factors common to all techniques. *BMJ* **322**, 981-985 (2001).
- 2 Ward, M. & Langton, J. A. Blood pressure measurement. *BJA Educ.* **7**, 122-126 (2007).
- 3 Beevers, G., Lip, G. Y. & O'Brien, E. Blood pressure measurement: Part II—Conventional sphygmomanometry: Technique of auscultatory blood pressure measurement. *BMJ* **322**, 1043-1047 (2001).
- 4 Elseed, A., Shinebourne, E. & Joseph, M. Assessment of techniques for measurement of blood pressure in infants and children. *Arch. Dis. Child.* **48**, 932 (1973).
- 5 Ogedegbe, G. & Pickering, T. Principles and techniques of blood pressure measurement. *Cardiol. Clin.* **28**, 571-586 (2010).
- 6 Ringrose, J. S. & Padwal, R. Automated blood pressure measuring devices: how are they clinically validated for accuracy? *J. Hum. Hypertens.* **37**, 101-107 (2023).
- 7 Tholl, U., Forstner, K. & Anlauf, M. Measuring blood pressure: pitfalls and recommendations. *Nephrol. Dial. Transplant.* **19**, 766-770 (2004).
- 8 Pickering, T. G. *et al.* How common is white coat hypertension? *JAMA* **259**, 225-228 (1988).
- 9 Ameloot, K., Palmers, P. J. & Malbrain, M. L. The accuracy of noninvasive cardiac output and pressure measurements with finger cuff: a concise review. *Curr. Opin. Crit. Care* **21**, 232-239 (2015).
- 10 Slogoff, S., Keats, A. S. & Arlund, C. On the safety of radial artery cannulation. *Anesthesiology* **59**, 42-47 (1983).
- 11 Hignett, R. & Stephens, R. Radial arterial lines. *Br. J. Hosp. Med.* **67**, M86-M88 (2006).
- 12 Saugel, B., Kouz, K., Meidert, A. S., Schulte-Uentrop, L. & Romagnoli, S. How to measure blood pressure using an arterial catheter: a systematic 5-step approach. *Crit. Care* **24**, 172 (2020).
- 13 Nuttall, G. *et al.* Surgical and patient risk factors for severe arterial line complications in adults. *Anesthesiology* **124**, 590-597 (2016).
- 14 Scheer, B. V., Perel, A. & Pfeiffer, U. J. Clinical review: complications and risk factors of peripheral arterial catheters used for haemodynamic monitoring in anaesthesia and intensive care medicine. *Crit. Care* **6**, 1-7 (2002).
- 15 Association for the Advancement of Medical Instrumentation. American national standards for electronic or automated sphygmomanometers. *ANSI/AAMI SP 10-1987* (1987).
- 16 O'Brien, E. *et al.* The British Hypertension Society protocol for the evaluation of automated and semi-automated blood pressure measuring devices with special reference to ambulatory systems. *J. Hypertens.* **8**, 607-619 (1990).
- 17 O'Brien, E. *et al.* The British Hypertension Society protocol for the evaluation of blood pressure measuring devices. *J. Hypertens.* **11**, S43-S62 (1993).
- 18 Tholl, U. *et al.* The German Hypertension League (Deutsche Hochdruckliga) Quality Seal Protocol for blood pressure-measuring devices: 15-year experience and results

- from 105 devices for home blood pressure control. *Blood Press. Monit.* **21**, 197-205 (2016).
- 19 <https://standards.iteh.ai/catalog/standards/cen/1a4903f1-d313-4d06-b63a-b32527654337/en-540-1993>.
- 20 O'Brien, E. *et al.* Working Group on Blood Pressure Monitoring of the European Society of Hypertension International Protocol for validation of blood pressure measuring devices in adults. *Blood Press. Monit.* **7**, 3-17 (2002).
- 21 O'Brien, E. *et al.* European Society of Hypertension International Protocol revision 2010 for the validation of blood pressure measuring devices in adults. *Blood Press. Monit.* **15**, 23-38 (2010).
- 22 <https://www.iso.org/standard/50814.html>.
- 23 Association for the Advancement of Medical Instrumentation. American national standard non-invasive sphygmomanometers—part 2: Clinical validation of automated measurement type iso 81060-2/ansi-aami. (2013).
- 24 Institute of Electrical and Electronics Engineers. IEEE standard for wearable cuffless blood pressure measuring devices. *IEEE Std*, 1708-2014 (2014).
- 25 Stergiou, G. S. *et al.* A Universal Standard for the Validation of Blood Pressure Measuring Devices: Association for the Advancement of Medical Instrumentation/European Society of Hypertension/International Organization for Standardization (AAMI/ESH/ISO) Collaboration Statement. *Hypertension* **71**, 368-374 (2018).
- 26 Institute of Electrical and Electronics Engineers. IEEE Standard for Wearable, Cuffless Blood Pressure Measuring Devices Amendment 1. (2019).
- 27 <https://www.iso.org/standard/71161.html>.
- 28 Food and Drug Administration. *Marketing clearance of diagnostic ultrasound systems and transducers: Guidance for industry and food and drug administration staff*. Report No. FDA-2017-D-5372 (Food and Drug Administration, 2023).
- 29 [https://www.aium.org/resources/official-statements/view/recommended-maximum-scanning-times-for-displayed-thermal-index-\(ti\)-values](https://www.aium.org/resources/official-statements/view/recommended-maximum-scanning-times-for-displayed-thermal-index-(ti)-values).
- 30 International Electrotechnical Commission. IEC 62127-2 “Ultrasonics – Hydrophones – Part 2: Calibration for ultrasonic fields up to 40 MHz”. *International Electrotechnical Commission, Geneva, Switzerland*, Ed. 2.1 (2013).
- 31 International Electrotechnical Commission. IEC 62359:2010/AMD1:2017 “Ultrasonics – Field Characterization – Test methods for the determination of thermal and mechanical indices related to medical diagnostic ultrasonic fields”. *International Electrotechnical Commission, Geneva, Switzerland*, Ed. 2.1 (2017).
- 32 International Electrotechnical Commission. IEC 62127-1:2022 “Ultrasonics – Hydrophones – Part 1: Measurement and characterization of medical ultrasonic fields”. *International Electrotechnical Commission, Geneva, Switzerland*, Ed. 2.0 (2022).
- 33 Duck, F. A. Medical and non-medical protection standards for ultrasound and infrasound. *Prog. Biophys. Mol. Biol.* **93**, 176-191 (2007).

- 34 Nelson, T. R., Fowlkes, J. B., Abramowicz, J. S. & Church, C. C. Ultrasound biosafety considerations for the practicing sonographer and sonologist. *J. Ultrasound Med.* (2009).
- 35 Bigelow, T. A. *et al.* The thermal index: its strengths, weaknesses, and proposed improvements. *J. Med. Ultrasound* **30**, 714-734 (2011).
- 36 Kelly, R. & Fitchett, D. Noninvasive determination of aortic input impedance and external left ventricular power output: a validation and repeatability study of a new technique. *JACC* **20**, 952-963 (1992).
- 37 Van Bortel, L. M. *et al.* Non-invasive assessment of local arterial pulse pressure: comparison of applanation tonometry and echo-tracking. *J. Hypertens.* **19**, 1037-1044 (2001).
- 38 Goncalves Seabra, A. C., Silva, A. F. d., Stieglitz, T. & Amado-Rey, A. B. In Silico Blood Pressure Models Comparison. *IEEE Sens. J.* **22**, 23486-23493 (2022).
- 39 Sugawara, M., Niki, K., Furuhashi, H., Ohnishi, S. & Suzuki, S. Relationship between the pressure and diameter of the carotid artery in humans. *Heart Vessels* **15**, 49-51 (2000).
- 40 O'Rourke, M. F. & Gallagher, D. E. Pulse wave analysis. *J. Hypertens.* **14**, S147-157 (1996).
- 41 Vlachopoulos, C., O'Rourke, M. & Nichols, W. W. *McDonald's blood flow in arteries: theoretical, experimental and clinical principles.* (CRC press, 2011).
- 42 O'Rourke, M. F., Pauca, A. & Jiang, X.-J. Pulse wave analysis. *Br. J. Clin. Pharmacol.* **51**, 507 (2001).
- 43 Davies, J. I. & Struthers, A. D. Pulse wave analysis and pulse wave velocity: a critical review of their strengths and weaknesses. *J. Hypertens.* **21**, 463-472 (2003).
- 44 Boutouyrie, P., Briet, M., Collin, C., Vermeersch, S. & Pannier, B. Assessment of pulse wave velocity. *Artery Res.* **3**, 3-8 (2009).
- 45 Solà, J. & Delgado-Gonzalo, R. *The Handbook of Cuffless Blood Pressure Monitoring.* (Springer, 2019).
- 46 Ma, Y. *et al.* Relation between blood pressure and pulse wave velocity for human arteries. *Proc. Natl. Acad. Sci.* **115**, 11144-11149 (2018).
- 47 Mukkamala, R. *et al.* Toward Ubiquitous Blood Pressure Monitoring via Pulse Transit Time: Theory and Practice. *IEEE Trans. Biomed. Eng.* **62**, 1879-1901 (2015).
- 48 Wong, M. Y., Poon, C. C. & Zhang, Y. T. An evaluation of the cuffless blood pressure estimation based on pulse transit time technique: a half year study on normotensive subjects. *Cardiovasc. Eng.* **9**, 32-38 (2009).
- 49 Pereira, T., Correia, C. & Cardoso, J. Novel Methods for Pulse Wave Velocity Measurement. *J. Med. Biol. Eng.* **35**, 555-565 (2015).
- 50 Meinders, J. M. & Hoeks, A. P. Simultaneous assessment of diameter and pressure waveforms in the carotid artery. *Ultrasound Med. Biol.* **30**, 147-154 (2004).
- 51 Powalowski, T. & Peńsko, B. A noninvasive ultrasonic method for the elasticity evaluation of the carotid arteries and its application in the diagnosis of the cerebrovascular system. *Arch. Acoust.* **13**, 109-126 (1988).

- 52 Hoeks, A., Brands, P., Smeets, F. & Reneman, R. Assessment of the distensibility of superficial arteries. *Ultrasound Med. Biol.* **16**, 121-128 (1990).
- 53 Chandran, K. B., Rittgers, S. E. & Yoganathan, A. P. *Biofluid mechanics: the human circulation*. (CRC press, 2012).
- 54 Joyner, M. J., Charkoudian, N. & Wallin, B. G. Sympathetic nervous system and blood pressure in humans: individualized patterns of regulation and their implications. *Hypertension* **56**, 10-16 (2010).
- 55 Nava, E. & Llorens, S. The Local Regulation of Vascular Function: From an Inside-Outside to an Outside-Inside Model. *Front. Physiol.* **10**, 729 (2019).
- 56 Lehoux, S., Castier, Y. & Tedgui, A. Molecular mechanisms of the vascular responses to haemodynamic forces. *J. Intern. Med.* **259**, 381-392 (2006).
- 57 Fantuzzi, G. & Mazzone, T. Adipose tissue and atherosclerosis: exploring the connection. *Arterioscler. Thromb. Vasc. Biol.* **27**, 996-1003 (2007).
- 58 Lin, M. *et al.* A fully integrated wearable ultrasound system to monitor deep tissues in moving subjects. *Nat. Biotechnol.* **42**, 448–457 (2023).
- 59 Vazquez, B. Y. Blood pressure and blood viscosity are not correlated in normal healthy subjects. *Vasc. Health Risk Manag.* **8**, 1-6 (2012).
- 60 Kohn, J. C., Lampi, M. C. & Reinhart-King, C. A. Age-related vascular stiffening: causes and consequences. *Front. Genet.* **6**, 112 (2015).
- 61 Kamenskiy, A. V., MacTaggart, J. N., Pipinos, II, Bikhchandani, J. & Dzenis, Y. A. Three-dimensional geometry of the human carotid artery. *J. Biomech. Eng.* **134**, 064502 (2012).
- 62 Daly, L. & Bourke, G. J. *Interpretation and uses of medical statistics*. (John Wiley & Sons, 2008).
- 63 Altman, D. G. & Bland, J. M. Measurement in medicine: the analysis of method comparison studies. *J. R. Stat. Soc. Ser. D Stat. Soc.* **32**, 307-317 (1983).
- 64 Bland, J. & Altman, D. A note on the use of the intraclass correlation coefficient in the evaluation of agreement between two methods of measurement. *Comput. Biol. Med.* **20**, 337-340 (1990).
- 65 Bland, J. M. & Altman, D. Statistical methods for assessing agreement between two methods of clinical measurement. *Lancet* **327**, 307-310 (1986).
- 66 <https://www.iso.org/standard/73339.html>.
- 67 Sun, J. X., Reisner, A. T., Saeed, M., Heldt, T. & Mark, R. G. The cardiac output from blood pressure algorithms trial. *Crit. Care Med.* **37**, 72 (2009).
- 68 McCorry, L. K. Physiology of the autonomic nervous system. *Am. J. Pharm. Educ.* **71** (2007).
- 69 Geddes, L. A. *Handbook of blood pressure measurement*. (Springer Science & Business Media, 2013).
- 70 Fountain, J. H., Kaur, J. & Lappin, S. L. *Physiology, renin angiotensin system*. (StatPearls Publishing, 2023).
- 71 Muntner, P. *et al.* Measurement of blood pressure in humans: a scientific statement from the American Heart Association. *Hypertension* **73**, e35-e66 (2019).

- 72 Lavi, S., Egbarya, R., Lavi, R. & Jacob, G. Role of nitric oxide in the regulation of cerebral blood flow in humans: chemoregulation versus mechanoregulation. *Circulation* **107**, 1901-1905 (2003).
- 73 Olufsen, M. S. *et al.* Blood pressure and blood flow variation during postural change from sitting to standing: model development and validation. *J. Appl. Physiol.* **99**, 1523-1537 (2005).
- 74 Guyenet, P. G. The sympathetic control of blood pressure. *Nat. Rev. Neurosci.* **7**, 335-346 (2006).
- 75 Husain, K., Ansari, R. A. & Ferder, L. Alcohol-induced hypertension: Mechanism and prevention. *World J. Cardiol.* **6**, 245 (2014).
- 76 Tasnim, S., Tang, C., Musini, V. M. & Wright, J. M. Effect of alcohol on blood pressure. *Cochrane Database Syst. Rev.* (2020).
- 77 Saugel, B., Grothe, O. & Wagner, J. Y. Tracking Changes in Cardiac Output: Statistical Considerations on the 4-Quadrant Plot and the Polar Plot Methodology. *Anesth. Analg.* **121**, 514-524 (2015).
- 78 Nachman, D. *et al.* Wireless, non-invasive, wearable device for continuous remote monitoring of hemodynamic parameters in a swine model of controlled hemorrhagic shock. *Sci. Rep.* **10**, 17684 (2020).
- 79 Bland, J. M. & Altman, D. G. Measuring agreement in method comparison studies. *Stat. Methods Med. Res.* **8**, 135-160 (1999).
- 80 Su, H. & Guo, Z. Accuracy of non-invasive blood pressure measurement in patients with atrial fibrillation. *J. Hum. Hypertens.* **36**, 229-234 (2022).
- 81 Antzelevitch, C. & Burashnikov, A. Overview of Basic Mechanisms of Cardiac Arrhythmia. *Card. Electrophysiol. Clin.* **3**, 23-45 (2011).
- 82 Alpert, B. S., Quinn, D. & Gallick, D. Oscillometric blood pressure: a review for clinicians. *Am. J. Hypertens.* **8**, 930-938 (2014).
- 83 Gonçalves Seabra, A. C., Ferreira da Silva, A., Stieglitz, T. & Amado Rey, A. B. Blood Pressure Models for Wearable Sensors. *TechRxiv. Preprint.* (2021).
- 84 Papaioannou, T. G. & Stefanadis, C. Vascular wall shear stress: basic principles and methods. *Hellenic. J. Cardiol.* **46**, 9-15 (2005).
- 85 O'Rourke, M. F. & Nichols, W. W. Aortic diameter, aortic stiffness, and wave reflection increase with age and isolated systolic hypertension. *Hypertension* **45**, 652-658 (2005).
- 86 Grinsted, A., Moore, J. C. & Jevrejeva, S. Application of the cross wavelet transform and wavelet coherence to geophysical time series. *Nonlin. Process. Geophys.* **11**, 561-566 (2004).
- 87 Tian, F., Tarumi, T., Liu, H., Zhang, R. & Chalak, L. Wavelet coherence analysis of dynamic cerebral autoregulation in neonatal hypoxic-ischemic encephalopathy. *NeuroImage Clin.* **11**, 124-132 (2016).
- 88 Addison, P. S. Wavelet transforms and the ECG: a review. *Physiol. Meas.* **26**, R155-199 (2005).

- 89 Chavez, M. & Cazelles, B. Detecting dynamic spatial correlation patterns with generalized wavelet coherence and non-stationary surrogate data. *Sci. Rep.* **9**, 7389 (2019).
- 90 Gonçalves, S. & Politis, D. Discussion: Bootstrap methods for dependent data: A review. *J. Korean Stat. Soc.* **40**, 383-386 (2011).
- 91 Curtis, A. E., Smith, T. A., Ziganshin, B. A. & Elefteriades, J. A. The mystery of the Z-score. *Aorta* **4**, 124-130 (2016).
- 92 Huang, H., Wu, R. S., Lin, M. & Xu, S. Emerging Wearable Ultrasound Technology. *IEEE Trans. Ultrason. Ferroelectr. Freq. Control* **PP** (2023).
- 93 Hu, H. *et al.* A wearable cardiac ultrasound imager. *Nature* **613**, 667-675 (2023).
- 94 Arnold, J. *et al.* Large artery function in patients with chronic heart failure. Studies of brachial artery diameter and hemodynamics. *Circulation* **84**, 2418-2425 (1991).
- 95 Madssen, E., Haere, P. & Wiseth, R. Radial artery diameter and vasodilatory properties after transradial coronary angiography. *Ann. Thorac. Surg.* **82**, 1698-1702 (2006).
- 96 Wang, C. *et al.* Monitoring of the central blood pressure waveform via a conformal ultrasonic device. *Nat. Biomed. Eng.* **2**, 687-695 (2018).
- 97 Krejza, J. *et al.* Carotid artery diameter in men and women and the relation to body and neck size. *Stroke* **37**, 1103-1105 (2006).
- 98 Teragawa, H. *et al.* Endothelial dysfunction is an independent factor responsible for vasospastic angina. *Clin. Sci.* **101**, 707-713 (2001).
- 99 Mouro, L., Bouhaddi, M. & Regnard, J. Effects of the cold pressor test on cardiac autonomic control in normal subjects. *Physiol. Res.* **58** (2009).
- 100 Mortimer, J. & McKune, A. J. Effect of short-term isometric handgrip training on blood pressure in middle-aged females. *Cardiovasc. J. Afr.* **22**, 257-260 (2011).